TR-O-0075

49

Design of Millimetre Wave Personal Radio Systems Using Fibre Optic Links

Howard Thomas

1994. 6. 13

ATR光電波通信研究所

Final Report
May 18th 1992 December 1st 1993
Project Theme: Design of Millimetre Wave Personal Radio Systems Using Fibre Optic Links
Project Subtheme: Mobile Communication Systems

Howard Thomas
ATR 光電波研究所
無線第二研究室

April 7, 1994

Overview

My research theme at ATR was Design of MMW Personal Radio Systems Using Fibre Optic Links. Within that theme I had two main objectives; construction of a demonstration system and identification of new fibre optic architectures and techniques with potential for reducing system cost.

Figure 1 outlines the main themes of the research I undertook at ATR; the principle goals achieved are summarized and the direction which future development could take is indicated.

The emphasis in the report is on aspects of my research not fully dealt with in published papers and reference is made to those publications when appropriate.

TITLE: Design of MMW personal radio systems using fibre optic links

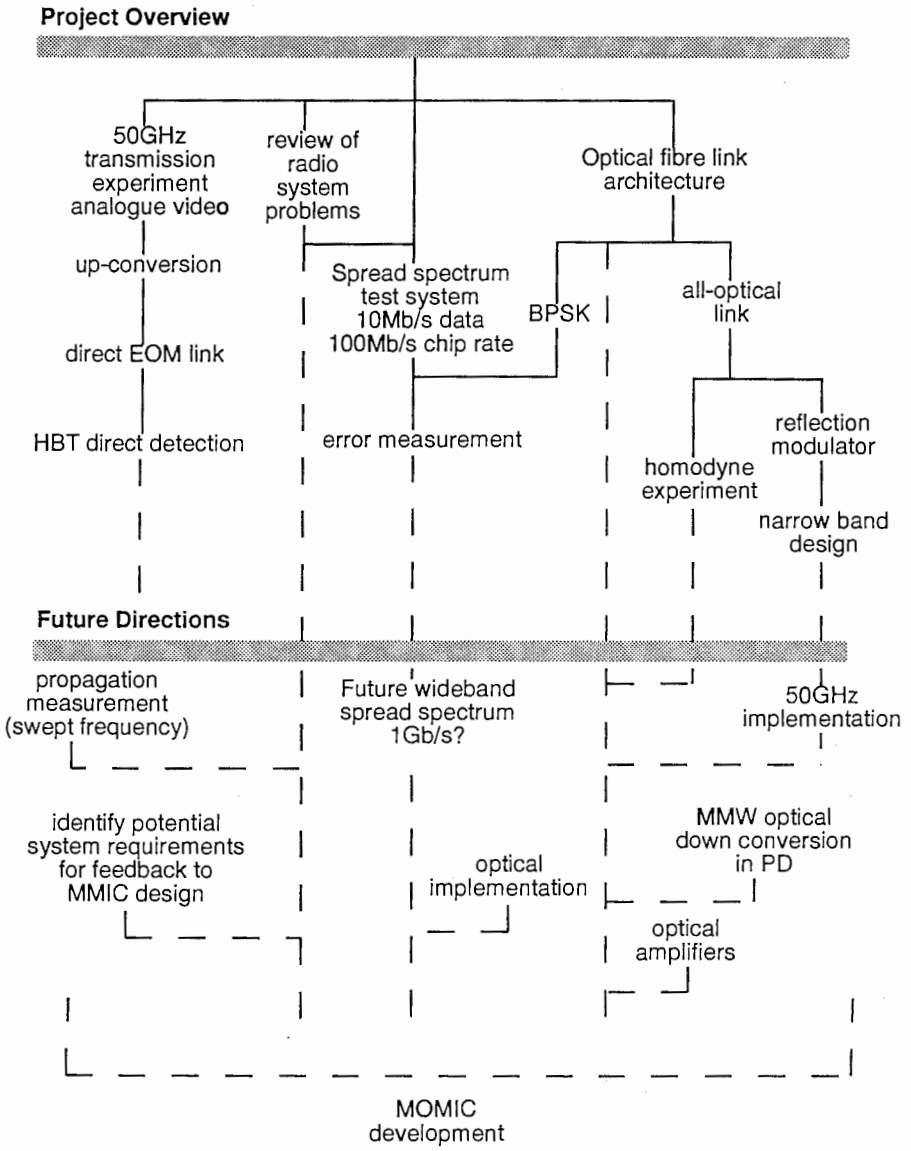

Figure 1: Overview of my research activity at ATR

Contents

List of Figures

List of Tables

Part I

Research background

1 Personal communications

The trend in mobile communication is towards higher frequencies, wider bandwidths, and smaller denser cell structures. Exemplifying this trend is the concept of a "Dick Tracy" wristwatch telephone supplying high quality video.

In a"tetherless" situation where mobile unit power and size are restricted by use of hand-held terminals or where user density or bandwidth per user are high, the preferred solution is a micro or pico-cellular structure. Currently, much work is being done on development of "personal radio systems" for supply voice and low rate data (about 8kb/s) to small cheap terminals in 1-2GHz frequency bands [1], [2]. Additionally, work is being conducted to identify requirements for future land mobile personal telephone systems (FLMPTS) for suppling data at rates from 100kb/s to 1Mb/s.

2 Millimetre wave personal radio

The directive of ATR is development of enabling technology for future communications systems. Thus, looking beyond systems currently under consideration, ATR is investigating use of the millimetre waveband for wideband personal radio and at the application of optical fibre distribution of signals within such systems [3], [8]. Figure 2 illustrates the concept of millimetre wave personal communications.

The baseline from which to predict bandwidth requirements for millimetre wave band personal communications is unclear. However, the future land mobile personal telephone system project (FLMPTS) is considering offering bandwidth up to 1Mb/s and some radio LAN systems offering 10Mb/s. Thus, 10Mb/s seems a reasonable lower limit for a millimetre wave system. Additionally, fixed telecommunication systems (ATM and B-ISDN) may provide per user bandwidths exceeding 100Mb/s, so a requirement for mobile compatibility with these systems would give an upper bandwidth limit of about 100Mb/s.

In order to make the concept feasible, the cost, size and complexity of the system, particularly the base-station sites, must be minimized. The distribution of radio signals over fibre optic cables is being investigated as a means to achieve this [5], [3]. Additionally, the problems of multi-path fading and channel distortion need to be addressed, particularly as the expected channel data rate exceeds the coherent bandwidth of the mobile radio channel, implementation of spread spectrum modulation has been considered as one possible means to address this [8].

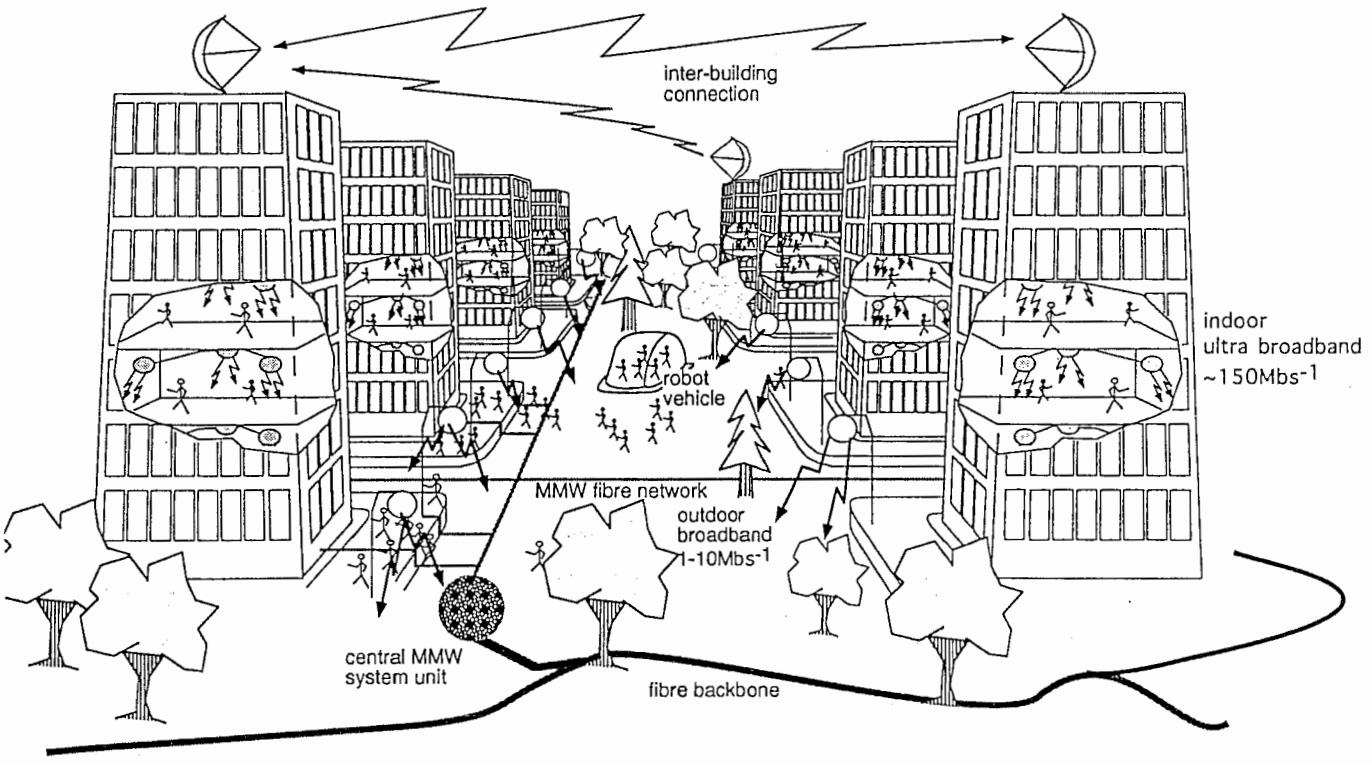

Figure 2: Millimetre wave personal communications scenario

3 Fibre optic links

Fibre optic links distribute millimetre wave signals by using the optical signal as a carrier waveform and a photo-detector to recover the signal at the far end of the link. In direct analogy with radio transmission, links can use AM, FM and PM based modulation techniques.

Intensity modulation is the technique we use as it is the most simple to detect which is very important when signals must be distributed to a multiplicity of remote base-stations. FM and PM are more complex, particularly PM with its requirement for a coherent reference.

There are three basic ways to realize high frequency intensity modulation of light; **direct** modulation of the light source, **external modulation** of a CW light source and **indirect transmission**, that is, sending IF and reference signals over the link and using a remote local oscillator. Current laser sources are limited to about 30GHz for direct modulation, high performance external modulators are commercially available to 50GHz and in laboratories to 75GHz, and there is no limit to the operation frequency in the case of indirect transmission. Polifko and Ogawa presented a comparative review [5] of 12 different fibre link architectures contrasting millimetre wave potential, dynamic range, complexity, and relative cost. In this report, the main emphasis is on external modulation based links directly transmitting millimetre wave signals over fibre as these have the greatest potential for simplifying the structure of the base-station in a micro-cellular network.

In this report we consider means to realize "all optical" base-station to central node up-links as a possible means to reduce component count in the base-stations. Also, we considered novel ways to increase the functionality of a Mach Zehnder external modulator by using it to impress digital modulation on an optical sub-carrier.

Optical fibre is also subject to limitations, particularly, chromatic dispersion polarization mode dispersion and at high powers, stimulated scattering. Although these effects are small in a micro-cell application due to the short path lengths it would be instructive to quantify them as they might pose a limit to the maximum extent of a fibre distributed millimetre wave network.

Part II

Mach Zehnder modulators

4 Overview

Since some specific details of EOM operation are important in the following, I shall present a brief overview of integrated optic Mach Zehnder operation and define a few terms.

A Mach Zehnder modulator uses interference between two optical paths to convert differential phase modulation into intensity modulation. Typically, light is split into two paths, a differential phase change effected, and the two paths recombined to produce interference.

The device may be implemented as a travelling wave structure on a planar integrated optical circuit on $LiNb0_3$ by using Titanium diffusion to form waveguides and Y-junctions on the substrate surface. Electrodes are then formed over these waveguides which make use of the electro-optic effect to cause the required differential phase change. The goal in EOM design is to realize the lowest possible drive voltage over the desired range of operating frequencies. Sub

goals to achieve this aim are to achieve an impedance match to 50Ω to ease drive requirements.

Theoretically, the response of the integrated optic modulator to an applied voltage is;

$$P_{out} = \frac{P_{in}}{2}\left\{\frac{\left(1-\sqrt{r}_p\right)^2}{1+r_p} + \frac{4\sqrt{r}_p}{1+r_p}\left\{\frac{1}{2} + \left[\left[\frac{\cos(\pi[V_{RF}/V_\pi + V_{bias}/V_\pi + \phi)}{2}\right]\right]\right\}\right\} \quad (1)$$

where P_{out}, P_{in} are the respective optical input and output powers, r_p is the power division ratio between the two arms of the Mach Zehnder, ϕ is the zero voltage phase offset between the Mach Zehnder arms [1], V the applied voltage and V_π the voltage required to induce π phase change between the modulator arms.

The core of Equation 1 is shown in square brackets. If an RF voltage $V_{rf}\cos\omega t$ substituted into the core, where $V_{rf} = \pi V_{RF}/V_\pi$ and $\phi(V_{bias}) = \pi V_{bias}/V_p i + \phi$, we get

$$P_{out} \propto \cos\left(V_{rf}\cos\omega t + \phi(V_{bias})\right) \quad (2)$$

If we want to use the device as a linear modulator then V_{bias} should be adjusted so that $\phi(V_{bias}) = \pi/2$. So, Equation (2) appears as a sine curve to the applied RF voltage, ie approximately linear about 0 or multiples of π

4.1 Optical Index

Typically, modulators are designed to exploit the largest electro-optic coefficient available in the $LiNb0_3$ crystal, n_e which occurs along the optical (extraordinary) axis of the crystal. Thus, it is the dielectric constant along this axis which is important here. This is 2.16 at $1.3\mu m$ according to my information from Sumitomo[2] [6], [7].

4.2 Microwave index

This is subject to greater control that the optical index. Control may be effected by reducing the amount of the microwave field which enters the $LiNb0_3$ substrate. As the microwave index is higher than the optical index, the microwaves travel slower than the optical signal which results in a velocity mis-match and the so called "phase walk off" [3] which limits the frequency of operation of travelling wave modulators with straight electrodes. With no particular precautions the microwave index can be about 4 Simons [6, page 64]. With Sumitomo technology the microwave index can be reduced by inserting a (lower dielectric index) buffer layer between the co-planar waveguide and the substrate; typically SiO_2 is used. Additionally, this prevents excess optical attenuation resulting when electrodes are formed directly on the optical guide. Secondly, by increasing the thickness of the co-planar electrode metalization.

[1] In practice, the two arms of the modulator are not identical due, for example, to fabrication tolerances or different stress induced by the co-planar centre conductor and the co-planar ground electrodes, and a phase offset should be introduced into the cosine term

[2] There is a wavelength dependence and N_o is 2.15 $1.55\mu m$

[3] 0r "phase locking terms" for phase reversal designs

Both these methods have some drawbacks as there is now less electric field concentrated in the optical guide and available to effect changes in dielectric constant. Moreover, these adjustments also affect the waveguide impedance.

4.3 Impedance

Sumitomo Cement fix the separation of the optical waveguides as $32\mu m$ [4] which dictates the gap width of the coplanar electrode at $25\mu m$ [5]. The impedance of the co-planar electrode to a first order approximation is proportional to $Z_0 \propto b/a/\sqrt{(1+\epsilon_r)}$ where a is the width of the centre strip, b is the separation of the ground plane electrodes and ϵ_r is the relative dielectric constant. For design purposes we use the extended spectral domain method to calculate the impedance and N_m taking into account the buffer layer and metalization thickness.

In order to maximize power transfer into the modulator, we usually The design the waveguide to achieve a 50Ω match. Other approaches are possible, for example, using impedance transformers or, in the case of HP, designing a custom driving circuit with 25Ω impedance.

4.4 Loss mechanisms

Typically, the microwave loss at high frequencies increases due to the skin effect Gopinath [8]. Thus, the loss term has a $\sqrt{f}$ dependency. The basic relationship at high frequencies is

$$R_s \approx \sqrt{\frac{\pi \mu f}{\sigma}} \tag{3}$$

Where R_s is the sheet resistance of the electrode in Ω/square, σ is the conductivity of the metal, μ is the permeability of the metal. Surface roughness effects, compounded by the skin effect, usually reduce the conductivity σ and result in higher losses. At low frequencies, where skin depth is large compared with electrode thickness, a good approximation is,

$$R_s \approx \frac{2}{\sigma T} \tag{4}$$

In our case $1.3\sqrt{\text{GHz}}$ dB/cm approximates to measured data by Polifko on coplanar waveguide test structures on $LiNb0_3$ upto 40GHz.

4.5 Some equations and definitions

The relationship between applied voltage and phase shift caused by the device can be expressed as

[4] This degree of separation is necessary to stop optical coupling between the waveguides when the waveguides are 4cm long. However, for shorter waveguides it would be possible to reduce the waveguide separation

[5] The central electrode is placed directly over one of the optical guides, while the other optical guide falls slightly inside the electrode region where the strength of the vertical component of the electric field is greater

$$\Delta\phi = \frac{2\Gamma n_e^3 r_{33}}{\lambda G} VL = \kappa VL, \qquad \kappa = \frac{2\Gamma n_e^3 r_{33}}{\lambda G} \tag{5}$$

where, λ is the free space optical wavelength, G is the width of the gap between the co-planar electrodes, Γ is the overlap integral which expresses the change in index induced in the waveguide by the overlap of the external electric field and the optical field of the E_{pq}^z mode, n_e is the index of the optical axis of the crystal, r_{33} is the electro-optic coefficient along the optical axis of the crystal and L is the length of the device. The Equation indicates that the phase shift is proportional to the applied voltage and device length multiplied by some constant.

However, when a microwave signal propagates through the device the mis-match between the velocity of the optical and microwave signals introduces a sinusoidal variation in the amplitude and sign of the microwave electric field as "seen" by a photon propagating along the device.

The result of the **velocity mismatch** is to impose a $sin[x]/x$ frequency response characteristic on the device, Alferness [9],

$$\Delta\phi(t_0) = \kappa V_0 L \frac{\sin[\pi f/2f_d]}{[\pi f/2f_d]} e^{-j2\pi f t_0} \tag{6}$$

Distance for π phase change: If we want to design a phase reversal electrode structure for operation at a single frequency[6] then we will want to swap the electrodes over when the microwave signal has changed by π with respect to the optical phase front[7]. This condition occurs when

$$\begin{aligned} &2\pi f L/c(N_m - N_o) = \pi \\ &\Rightarrow L = c/(2f(N_m - N_o) \end{aligned} \tag{7}$$

Design frequency f_d: Alternatively, for a fixed length of device, we can view the frequency at which this phase condition occurs as an indication of device bandwidth. At this point, for a straight electrode design, the phase response will have fallen, with respect to the DC response, by factor $2/\pi$ and the electrical response, after detection of the optical output, will have fallen by the square of this, that is, $3.9dB$[8]. Additionally, for a periodic phase reversal electrode, this will be the designed frequency of operation. Thus, we get the definition of f_d,

$$f_d = c/(2L(N_m - N_o) \tag{8}$$

Phase reversal modulator bandwidth estimation Velocity mis-match limits the frequency response of Mach Zehnder modulators. However, as alluded to above, velocity matching can be artificially created over a limited frequency range by using phase reversal electrodes [9]. The response of a periodic phase reversal electrode modulator is given by the

[6] non-periodic electrode structures can be used to give a very broadband frequency response

[7] After this point cancellation of the accumulated phase shift starts to occur

[8] the ratio of the integral of $\cos x$ over the integral of dx from $0 \rightarrow \pi$

sum of the phase contribution of a single element accounting for the change in phase along the device;

$$\Delta\phi(t_0) = \kappa V_0 e^{-j2\pi f t_0} \sum_{p=1}^{N} (-1)^p \int_{(p-1)L_i}^{pL_i} e^{j2\pi f x/c(N_m - N_o)} 10^{-\alpha[f]Lx} dx \tag{9}$$

where $\alpha[f]$ is the frequency dependent loss. However, neglecting the loss, Alferness [9] developed an expression for the phase shift generated by a phase reversal modulator of N sections which is useful for analyzing the expected response

$$\Delta\phi(t_0) = \kappa V_0 L \frac{\sin[\pi f/2f_d]}{[\pi f/2f_d]} \left\{ \frac{\sin\left[\frac{N}{2}(\pi f/f_d + \pi)\right]}{\cos[\pi f/2f_d]} \right\} e^{-j2\pi f t_0} \tag{10}$$

The first term is describes the response of a single element and determines the envelope of the response, the second term is the so called "phase locking term" and determines how sharply the response peaks around f_d and its harmonics. Looking just at the phase locking term, and solving for when its amplitude falls by $1/\sqrt{2}$ from its peak value of N, we get the following approximate expression for the 3dB bandwidth of the electrical response;

$$\Delta f = \frac{1.76 f_d}{N} \tag{11}$$

Part III

Research on optical modulators

5 Overview

Research was conducted in two areas. Firstly, techniques to realize "all-optical" up-links from the base-station to the central node. The aim being to eliminate the need for a light source, local oscillator, or millimetre wave mixer in the base-station. Here, dual EOM mixing and reflection modulators were studied. Secondly, techniques to increase functionality of EOM devices, here direct sub-carrier bi-phase modulation using bias switching was studied.
Figure 3, shows the concept of "all-optical" signal distribution employing series connected EOM's and Figure 4 shows an alternative configuration employing photo-detector non-linearity to perform photo-detection and down conversion. The first of these two configurations is described here, however, the second is potentially more advantageous.

6 Dual EOM mixing

The possibility of using dual EOM mixing as a means for producing an optically fed radio base-station containing no active components is investigated. Details of this work can be found in reference [3] and [4].

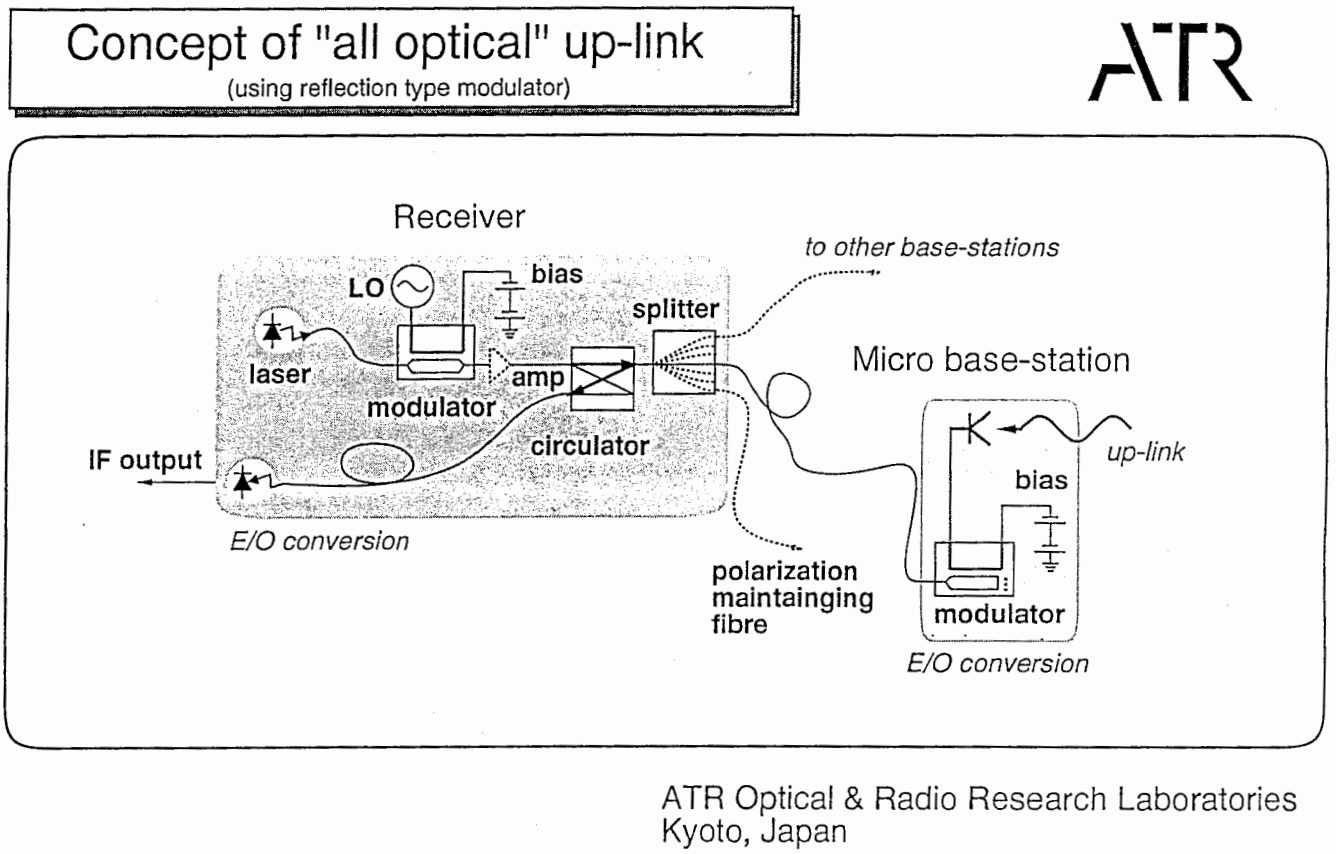

Figure 3: Concept of "all optical" up-link employing series connected EOM's

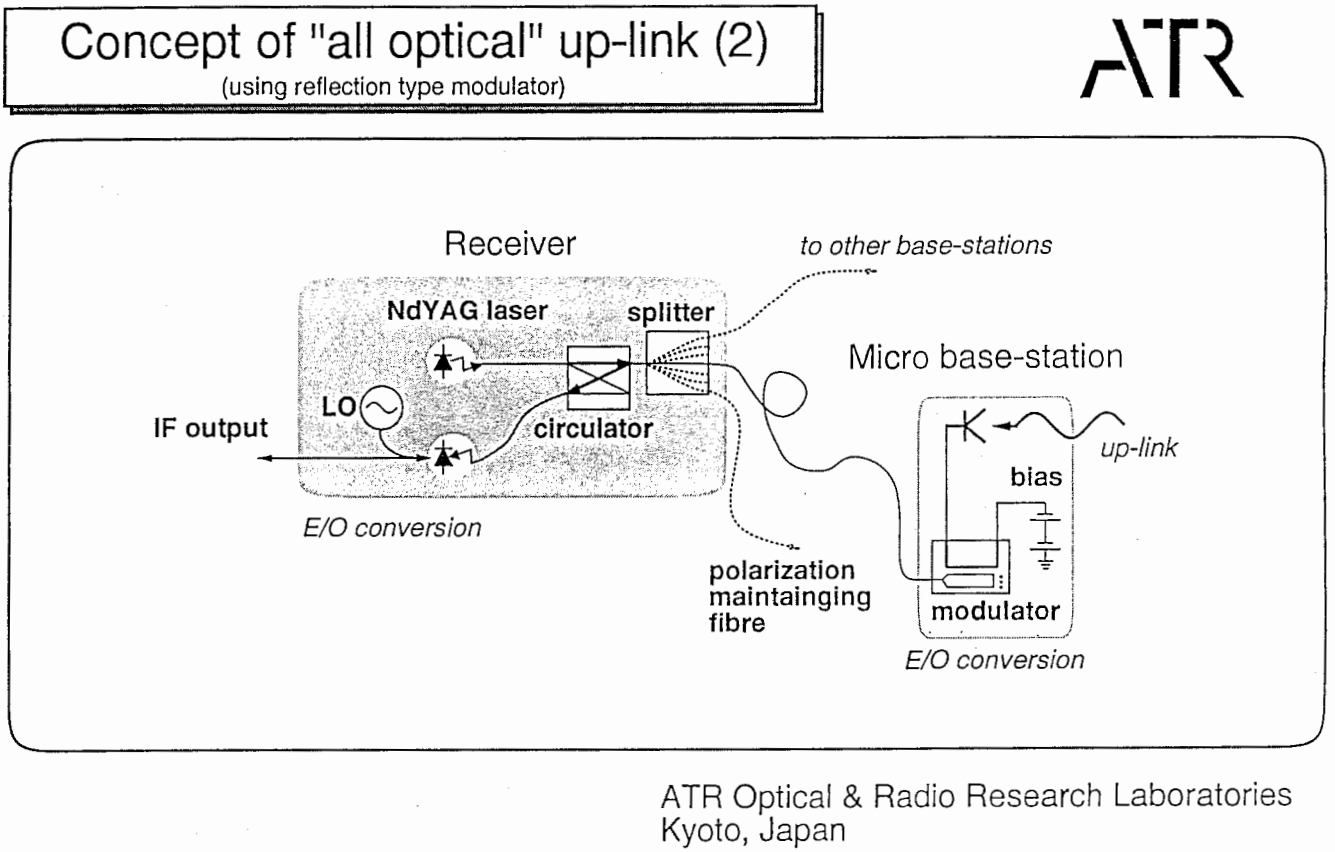

Figure 4: Concept of "all optical" up-link employing photo-diode non-linearity

6.1 Principle

The idea behind the configuration is to use one EOM to generate an optical LO signal which is then sent over optical fibre to the remote base-station site. The optical LO is then multiplied by the transfer function of the second EOM, producing sum and difference frequency components. These are sent back to the central station over a second fibre and detected by a photo-detector. The optical fibre link to the base-station will be by polarization maintaining fibre as the EOM used in the base-station is polarization sensitive. However, a polarization independent modulator could be employed at the remote base-station to avoid this restriction. For example, X-cut $LiNb0_3$ can yield a polarization independent modulator at the expense of a using a lower electro-optic coefficient of the crystal [7].

Although in this paper we are interested primarily in dual-EOM down conversion for an "all optical" up-link, dual-EOM mixing is equally capable of up-conversion and essentially, the performance is identical. However, for down conversion it is possible to use a lower frequency photo-diode with correspondingly greater responsivity; alternatively, a HBT structure with trans-impedance gain could be employed [12].

6.2 Conclusion

The technique of series connected EOM's can be used to perform "all-optical" down conversion as we define it here 3. However, the conversion loss of the technique is high and it is likely that it would be difficult to implement in a practical system as the counter measures to overcome the high conversion loss will themselves be expensive to implement. A more attractive alternative would perhaps be to distribute un-modulated light from the central node of the network and, then after its modulation at the remote site, down convert using photo-detector non-linearity by injecting the optical signal and the local oscillator signal directly in to the photo-diode 4.

7 Reflection modulator

7.1 principle

The motivation for investigating reflection type modulators is to eliminate the need for a light source in a base-station whilst maintaining connection with a single fibre.

A reflection modulator is just a standard modulator folded in half by placing a mirror at the end of the two optical paths. In this way, splitting and recombination occur at the same point and light enters and leaves through the same port (fibre). Figure 5 shows the structure of the reflection EOM designed as part of this project and illustrates details of the waveguide.

As we are concerned with travelling wave type integrated optical modulators we much consider the regions of co- and counter propagation of the optical and microwave signals separately.

7.2 Co- and counter propagation

Equation (7) gives an expression for the propagation distance L, after which the microwave phase lags by π with respect to its initial value as "seen" by a photon entering the modulator

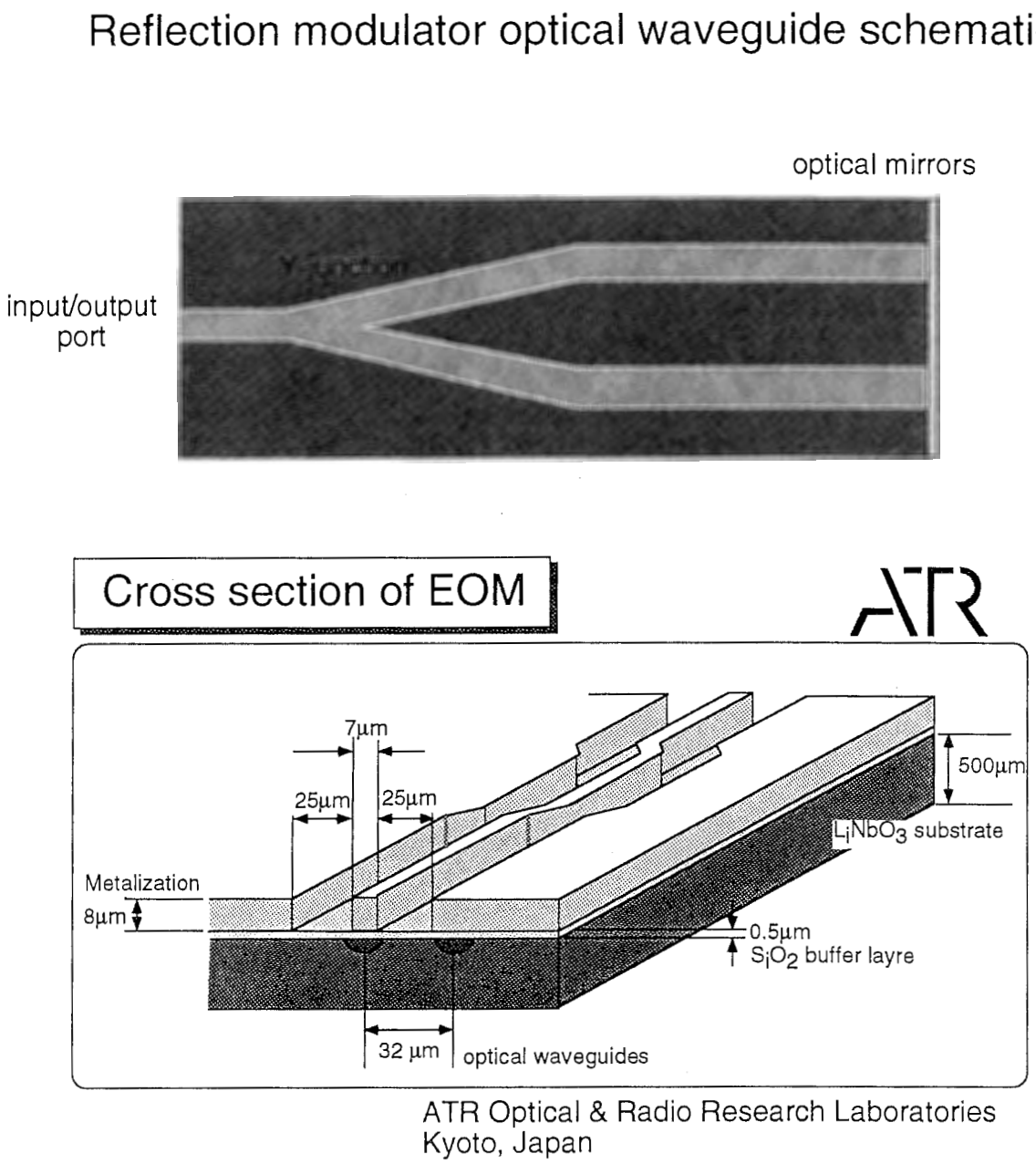

Figure 5: Reflection modulator schematic and detail of EOM waveguides structure

at time t_0 and propagating through the device. Related to this length L, Equation (7) gives an expression for f_d the frequency at which this π phase lag occurs for a device of length L. f_d has two uses, it is the approximate 3dB bandwidth of a straight electrode modulator, and it is the design frequency for a modulator with periodic phase reversal electrode structure;

$$L = c/(2f(N_m - N_o); \qquad f_d = c/(2L(Nm - No) \tag{12}$$

In the case of counter propagating signals, these expression change to

$$L = c/(2f(N_m + N_o); \qquad f_d = c/(2L(Nm + No) \tag{13}$$

Thus, we can view the reflection modulator as having two separate design frequencies f_d and we can choose to design for either or both of them at the same time.

For a straight electrode modulator the required phase operating point is obtained by applying DC bias to the coplanar electrode. However, in the case of a phase reversal structure with even numbers of sections the DC response is cancelled and a separate bias electrode should be constructed, additionally, even for an odd number of sections, if the number of sections is large, the net (un-cancelled) DC response may be small.

The reflection modulator can help in this case because, at zero frequency, the co- and counter-propagation contributions add-up to double the DC response.

7.3 The effect of losses

Microwave loss in the co-planar electrodes degrades the efficiency of the modulator because the effective interaction length is reduced. On the other hand, the Sin(x)/x frequency response of the modulator is spread out. In the case of frequency independent loss, this results in a larger 3dB bandwidth. However, when the loss is frequency dependent, the reduction in output with frequency can offset this producing a reduction in 3dB bandwidth. Figure 6 illustrates the cases of a lossless electrode, an electrode with a frequency independent loss of 3dB/cm, and an electrode with a frequency dependent loss of $1.3\sqrt{GHz}$dB/cm (similar to our measured data), also shown is the $\sqrt{2}$ level which marks the 3dB electrical bandwidth.

The respective increase and decrease in the 3dB bandwidth for the frequency independent and dependent lossy electrode compared with the lossless case is apparent in the Figure. Also apparent is the suppression of the Sin(x)/x null in the case of the electrode with frequency dependent loss; the first null in this case occurs at 1500GHz.

In terms of a phase reversal modulator, the phase reversal period is the same, so f_d is the same. However, the shorter effective length and reduction in effectiveness of successive sections broadens the response about each peak.

As a numerical example, consider a modulator with periodic phase reversal electrodes optimized for counter propagation where the electrodes have 10 2mm sections and where the modulator parameters are as in Table 1. f_d is 14.9GHz.

Directly evaluating Equation (10) for zero loss yields a 3dB electrical bandwidth of 15.6%, whilst the approximation of Equation (11) yields 17.6%. If Equation (10) is re-evaluated

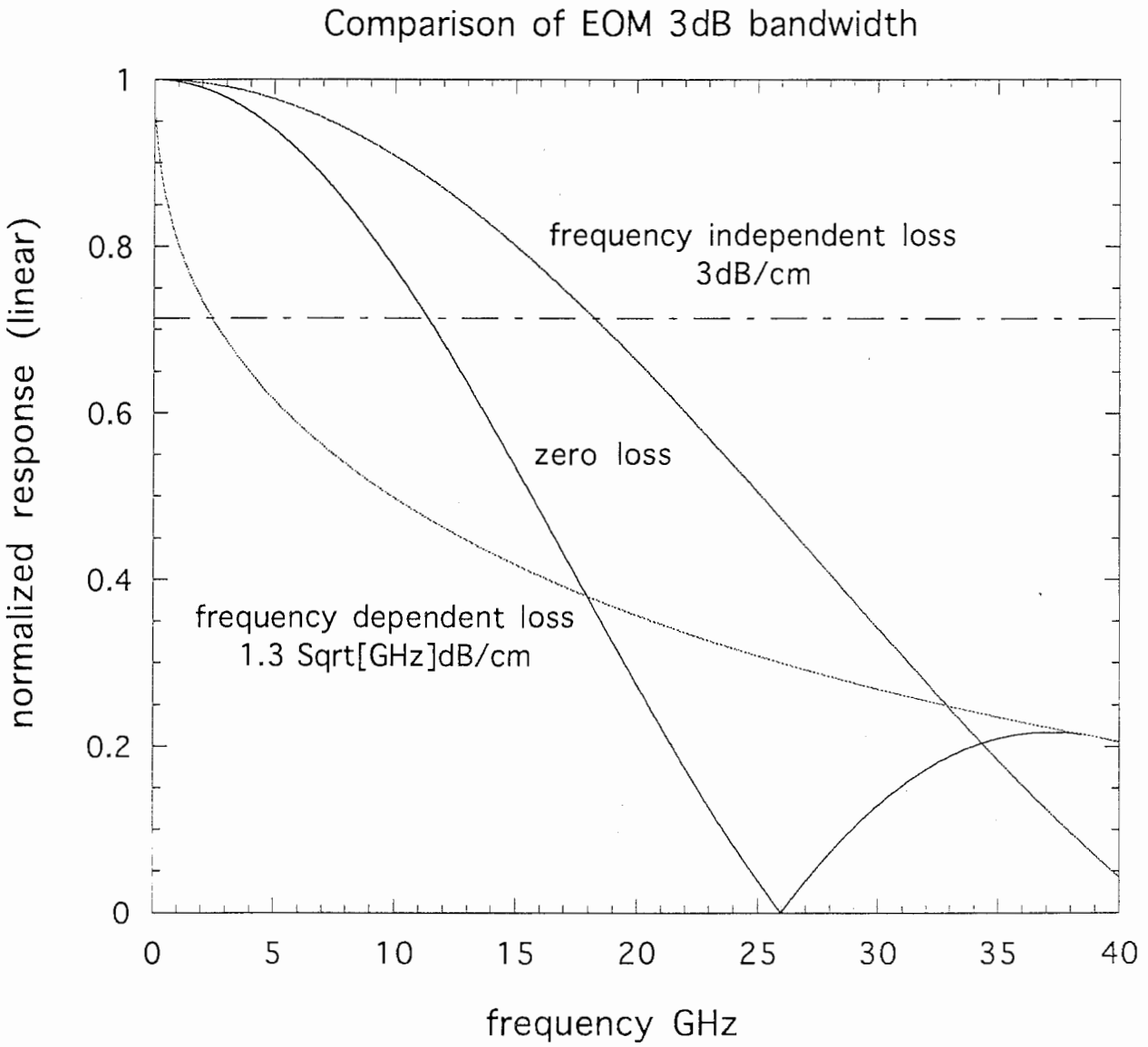

Figure 6: Comparison of EOM 3dB bandwidth for three different loss assumptions. The scale is linear and is normalized to the zero frequency response.

Substrate characteristics		
$\varepsilon \parallel$	$= 28$	$LiNb0_3$ dielectric constant
$\varepsilon \perp$	$= 43$	$LiNb0_3$ relative dielectric constant
ε	$= 4$	SiO_2 relative dielectric constant
	$= 500\mu m$	$LiNb0_3$ substrate thickness
$n_e^3 r_{33}$	$= 320 \times 10^{-12}$m/v	$LiNb0_3$ substrate thickness
Optical waveguide characteristics		
	$= 7\mu m$	waveguide width
	$= 32\mu m$	waveguide separation
N_o	$= 2.14$	refractive index $1.3\mu m$
Microwave waveguide characteristics		
G	$= 25\mu m$	coplanar gap width
W	$= 7\mu m$	coplanar centre conductor width
	$= 8\mu m$	electrode metalization
	$= 0.5\mu m$	SiO_2 buffer layer
N_m	$= 2.91$	microwave index
Z_0	$= 50$	microwave impedance
ε_{eff}	$= 8.46$	microwave impedance
α	$= 1.23\sqrt{GHz/cm}$	microwave loss dB (expt fit)
ρ	$= 0.7$	reflection coefficient

Table 1: Collected design parameters

including a loss term [9] of 8dB/cm, the bandwidth increases to 21% and the peak amplitude response falls by 11.5dB.

7.4 Design example

The fabrication process of Sumitomo sets certain parameters for us in the fabrication of our EOM's. However, we are free to set the thickness of the $Si0_2$ buffer layer and the electrode metalization. Table 1 summarizes the EOM design parameters.

Professor Kitazawa of Ibaraki University calculated the microwave refractive index N_m and waveguide impedance for a variety of buffer thicknesses and electrode thicknesses. Subject to fabrication constraints, a buffer layer thickness and metalization thickness of, $0.5\mu m$ and $8\mu m$ were chosen, yielding an impedance of 50Ω and microwave refractive of 2.91.

The optical refractive index is determined by the optical frequency and the relative orientation of the $LiNb0_3$ crystal. For a Z-cut substrate at $1.3\mu m$, N_o was 2.14; Titanium doping in the optical guides changes this by only about 0.5%.

As Sumitomo was uncertain of the fabrication technique for the optical mirror, we chose to keep our electrode designs simple so analysis would not be too difficult were there to be a problem with mirror fabrication. A straight electrode design and a three element phase reversal design were chosen.

Straight electrode design:

The maximum length of integrated-optic waveguides on our $LiNbO_3$ wafer, as determined by

[9] this is about the maximum we measure on our devices at 40GHz so is a worst case

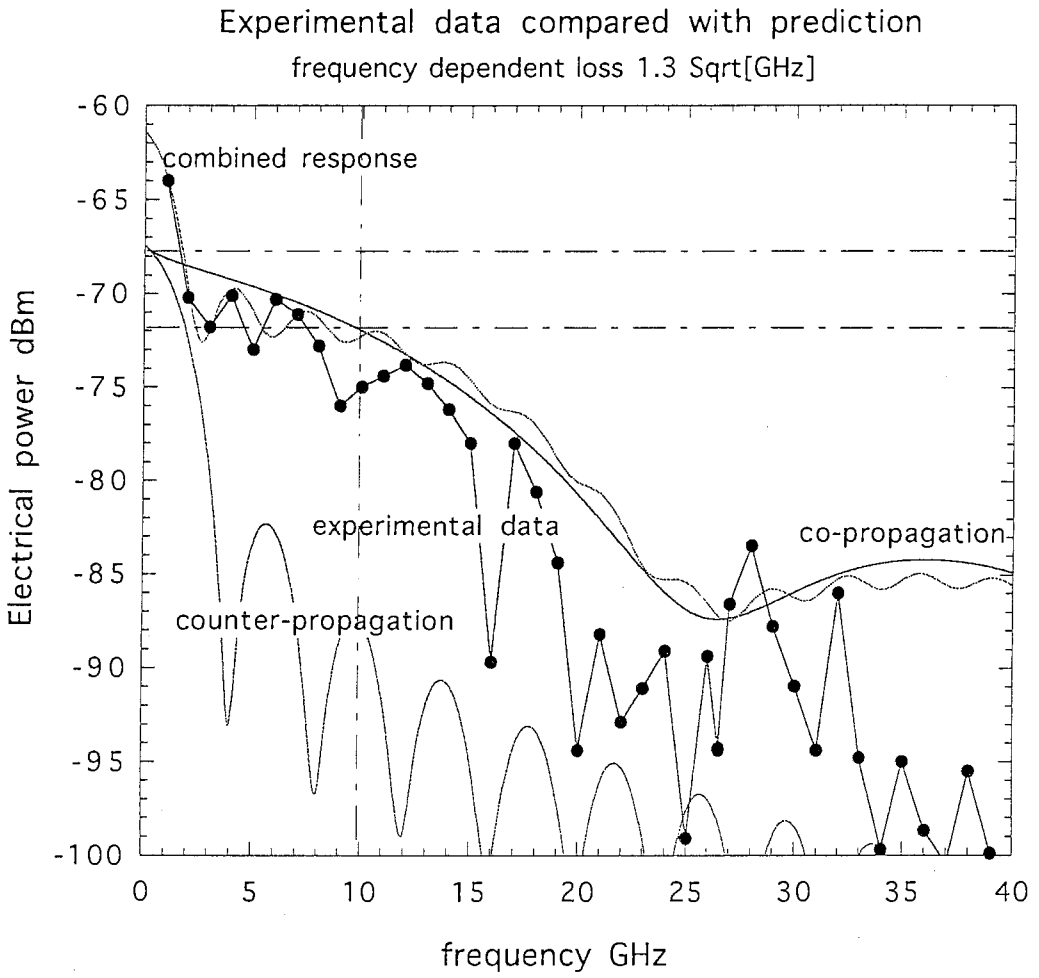

Figure 7: Straight electrode modulator; comparison of experimental data and theoretical model. Model includes frequency dependent loss. The predicted co- and counter-propagation terms are also indicated

our fabrication process, was 4cm. For the reflection modulators the wafer was split into two, reducing the length to 2cm. This was further reduced to leave a 2mm gap between the waveguide metalization and the edge of the diced substrate. Thus, the length of the modulator was set to 1.5cm. Evaluating Equations (12), and (13) for this length and using the parameters in Table 1 gives f_d as 13GHz for co-propagation and 2GHz for counter propagation.

Figure 7 shows the predicted response of the EOM compared with the measured performance. Also shown on the curve are the individual responses for forward and reverse propagation. At low frequencies the addition of the co- and counter-propagation terms causes a 6dB, enhancement in the combined response.

To make a comparison between our predicted value of f_d for co-propagation and the measured performance we must neglect the initial peak and look at the fall in the envelope. Estimation of f_d from the Figure is difficult because of ripples and a dip in the response near our expected value. However, the value is about 8–10GHz compared with a modelled value of 10GHz and a simple lossless estimation of 13GHz.

The dip at 9GHz coincides with a peak in the return loss Figure 8 so it is probably due to fabrication error rather than a fundamental cause; peaks due to surface wave coupling would not be expected to occur till 25GHz when the co-planar and surface wave phase velocities become equal for a $500\mu m$ thick substrate.

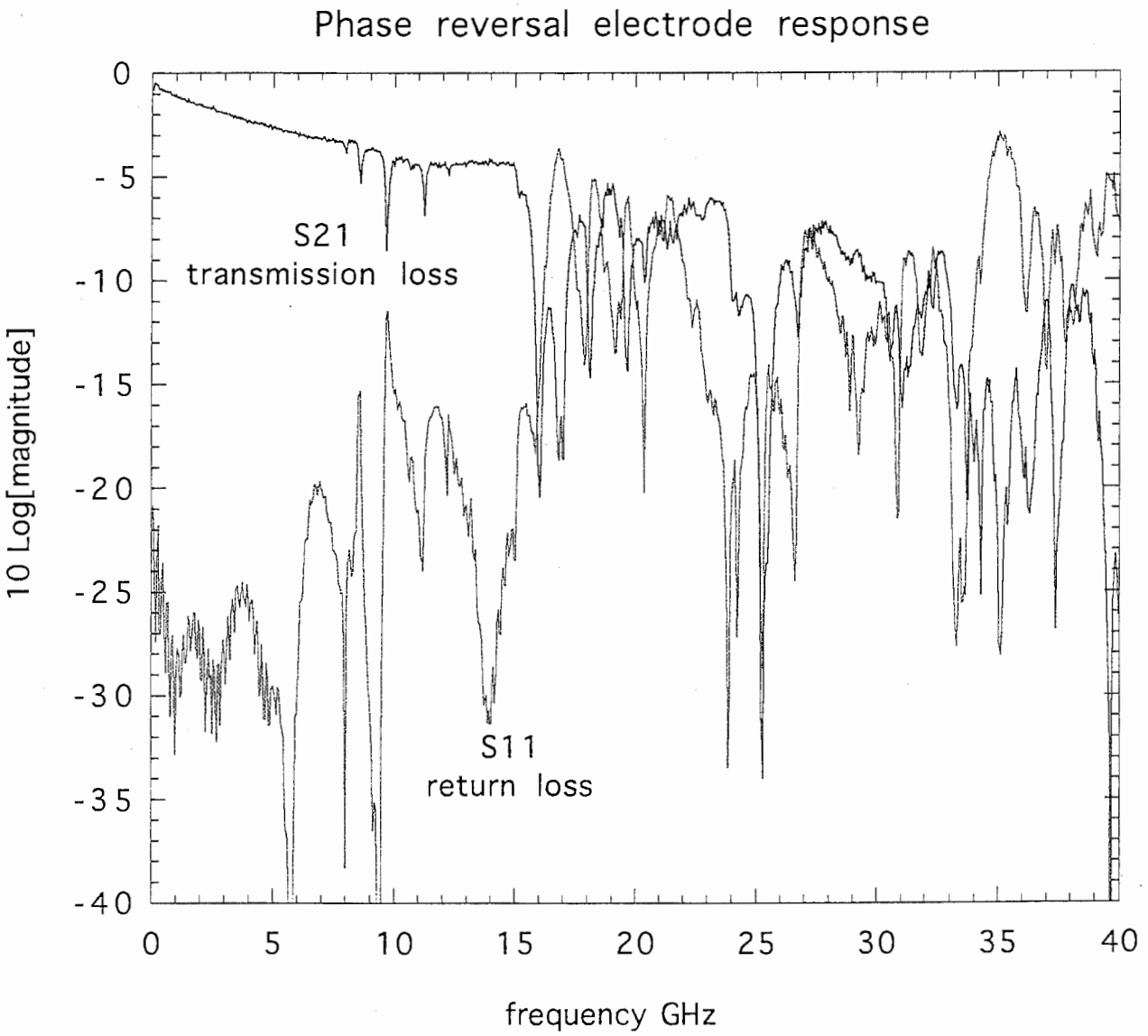

Figure 8: Experimental S21 and S11 for phase reversal electrode structure

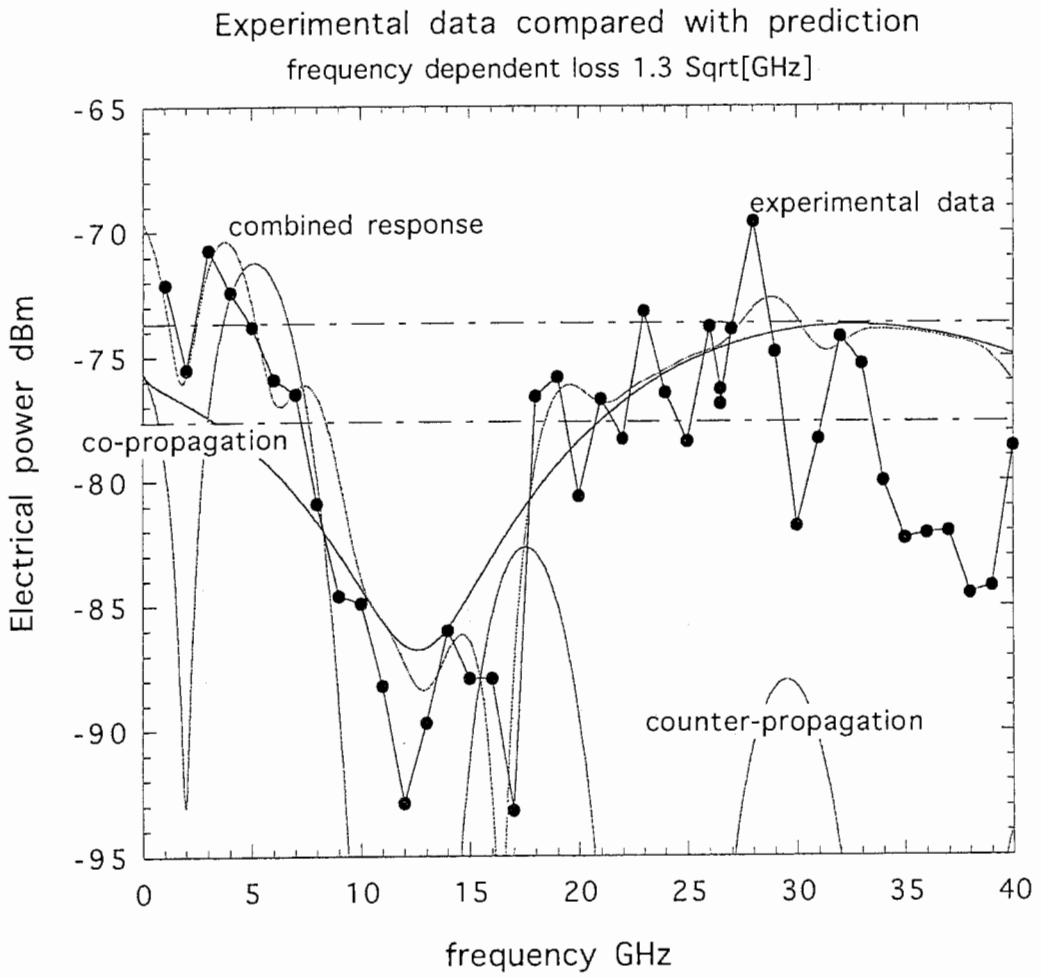

Figure 9: Three element phase reversal modulator; comparison of experimental data and theoretical model. Model includes frequency dependent loss. The predicted co- and counter-propagation terms are also indicated

In the case of counter propagation the f_d estimated from the Figure is about 1.5GHz compared with a simple lossless estimation of 2GHz.

Phase-reversal electrode design: A three element phase reversal electrode design was chosen to give a millimetre wave response in the 30–40GHz region whilst retaining a large enough DC response that biasing without a separate electrode is not a problem.

Keeping the electrode length the same as for the straight electrode case to maximize response gave 5mm long elements. Evaluating Equations (12), and (13) for this length using the parameters in Table 1 gives f_d as 39GHz for co-propagation and 6GHz for counter propagation.

Figure 9 shows same curves as Figure 7 for the case of our three section phase reversal electrode modulator. The measured and modelled responses fit well at low frequencies. At higher frequencies the experimental response has a large ripple and a fall in response above 30GHz compared with prediction. The likely cause of the problem is deterioration of the electrode return loss response at high frequencies Figures 8.

The device is quite broadband, the simple lossless estimation of 3dB bandwidth is 23GHz, however, the spiky-ness of the data make it difficult to give a good estimate of the bandwidth. Again, it is thought that the electrode return loss response is the major factor. However, at the higher frequencies, surface wave coupling would also be expected.

Improvement of modeling: Incorporation of the measured transmission loss data into an

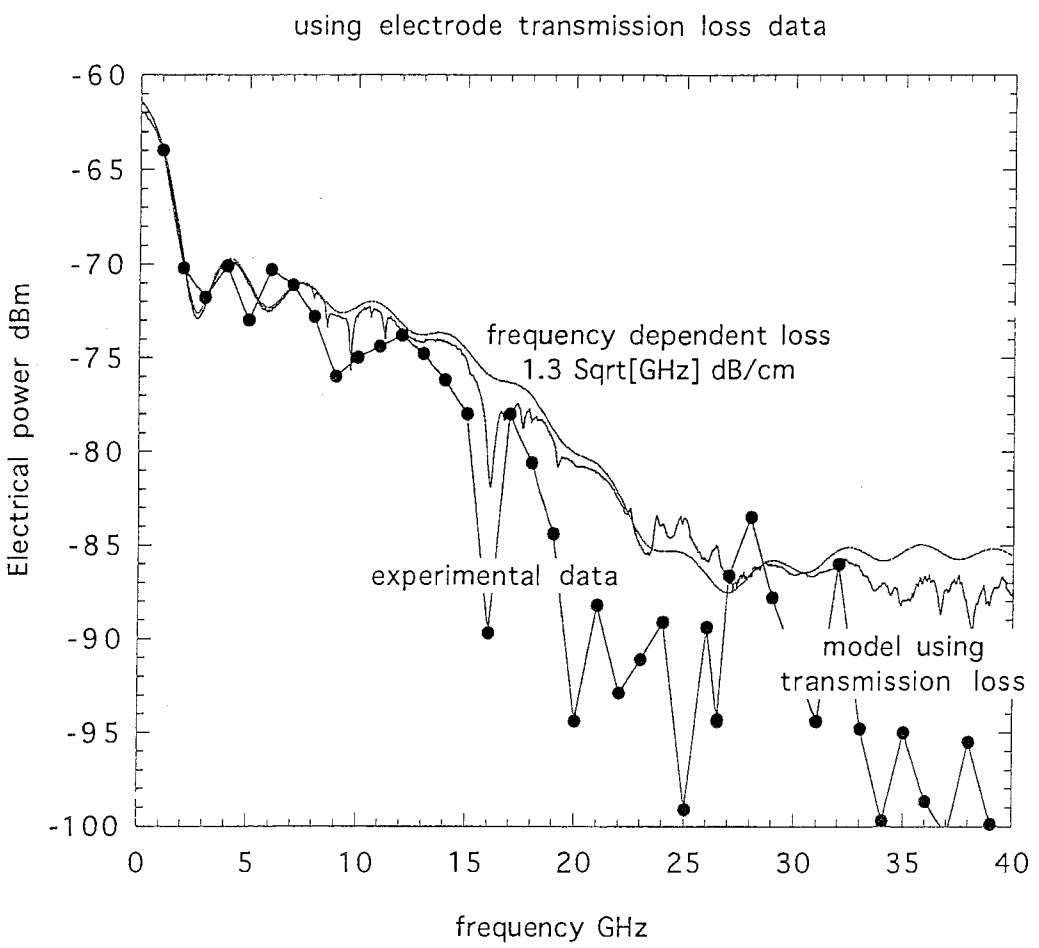

Figure 10: Straight electrode modulator; comparison of experimental data and model incorporating measured transmission loss data.

improved model of modulator response has been investigated. The loss was assumed to be distributed along the length of the device and, according to this assumption, the measured frequency dependent loss loss was substituted into equation Equation (9) and the result evaluated numerically. Figures 10 and 11 show the new predictions compared with measurement. It is clear that the nulls appear where they ought, however, the experimental ones are bigger. It is likely that this could be due to our assumption of uniform distribution of loss through the device when, for example, much power could be reflected from the input port or co-planar/co-axial transition and never enter the device. If this was the case, nulls, particularly high frequency ones, would become deeper. A time domain analysis of the transmission loss and return loss could be used to get a more realistic distribution of loss in the device.

7.5 Conclusion

Realization of a reflection-type with millimetre wave capabilities permits new fibre link architectures to be implemented. It is possible that the advantage of eliminating the light source and local oscillator from the far site will attractive for developing millimetre wave communications systems. The relatively high conversion loss realized with the link can be improved by replacing the 3dB coupler presently used to couple optical power into and out of the modulator with an optical circulator, this would yield 4dB improvement in optical performance which is equal to 8dB in the electrical domain. Additionally, the two design

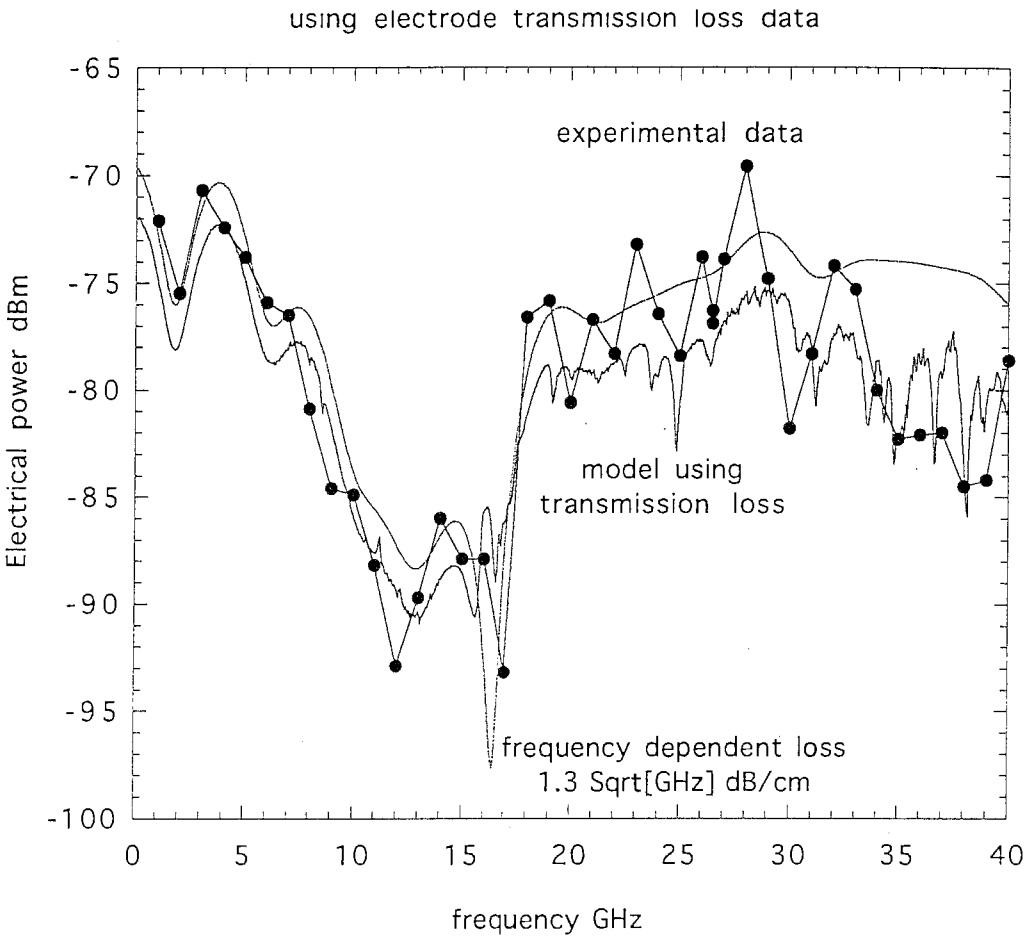

Figure 11: Three element phase reversal modulator; comparison of experimental data and model incorporating measured transmission loss data.

frequencies inherent in the device could possibly used to increase device functionality for some particular applications.

8 EOM bi-phase modulation

8.1 Linear case

It is possible to use a Mach Zehnder EOM achieve direct bi-phase modulation of an optical sub-carrier by switching the bias point with a binary data voltage [7]. We can see this if we insert a term into Equation (2) to represent the phase change caused by the data voltage,

$$P_{out} \propto \cos\left(V_{rf}\cos\omega t \pm \frac{\pi V_{data}}{V_\pi} + \phi(V_{bias})\right) \tag{14}$$

If $\phi(V_{bias})$ is set to zero and $\pi V_{data}/V_\pi = \pi/2$, then Equation (14) will switch between $\pm\sin(V_{rf}\cos\omega t)$ and we will achieve bi-phase modulation of the sub-carrier signal so long as $V_{rf} \ll \pi$. Figure 12 illustrates the most simple form of EOM direct BSPK modulation.

8.2 General case

In the general case, when V_{rf} has some arbitrary value, Equation (14) is more correctly represented as an expansion of Bessel functions. When $\phi(V_{bias})$ is set to zero and $\pi V_{data}/V_\pi = \pi/2$, we obtain,

$$P_{out} \propto \pm[J_1(V_{rf})\cos\omega t + J_3(V_{rf})\cos 3\omega t + \ldots] \tag{15}$$

whilst when If $\phi(V_{bias})$ is set to $\pi/2$ and $\pi V_{data}/V_\pi = \pi/2$, we obtain,

$$P_{out} \propto \pm[J_0(V_{rf}) + J_2(V_{rf})\cos 2\omega t + J_4(V_{rf})\cos 4\omega t + \ldots] \tag{16}$$

From Equation (15) and (16) we can see that by careful setting of the bias point and control of the magnitude of the RF signal, that it is possible to produce bi-phase modulation at any odd or even multiple of the applied radio frequency signal.

References [8], [7], [5], [3] and [2] describe the details of the experimental procedure and present experimental results.

Essentially, the bandwidth limit of the technique is defined by the 3dB bandwidth of the Mach Zehnder modulator and is typically many GHz. One demonstration experiment was conducted using a 1.4Gb/s data generator, this result is presented in reference [2].

8.3 Conclusion

A simple model of the Mach-Zehnder EOM is developed to show how it can be operated as a bi-phase modulator. Experimental results confirm the predictions of the model [7].

observed spectra
(PRBS input)

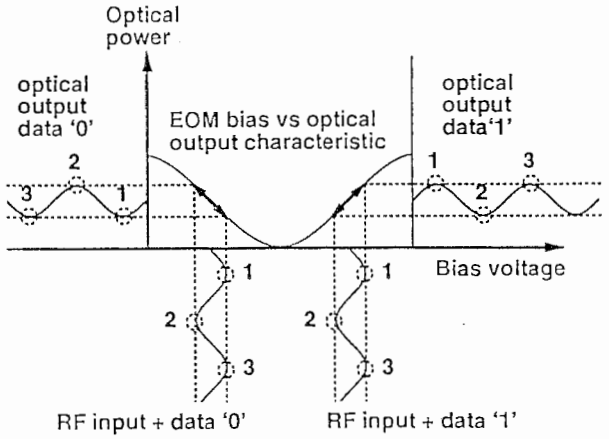

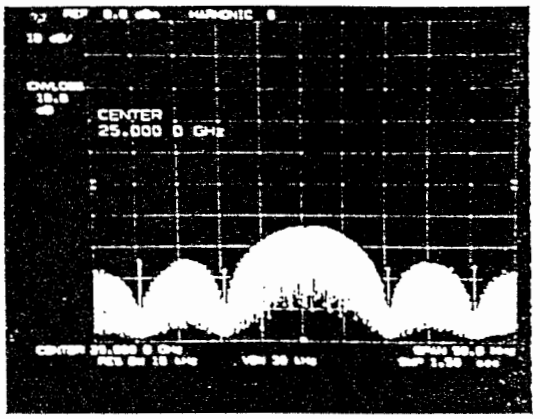

operational principle

Figure 12: Mach Zehnder EOM BPSK modulation

Suppression of the carrier component in the output is of the order of 35–34dB [7]. The variation of the suppression is due to drift in the bias characteristics of the EOM which could be compensated for by adaptively changing the bias point.

Bi-phase of an optical sub-carrier by switching of the DC bias with a data signal modulation has been demonstrated for a number of cases. The technique can certainly simplify the structure of the transmitter at the expense of a loss in flexibility as it now becomes difficult to have more than one user use the same EOM simultaneously. However, in applications where simplicity is paramount and users few it would be an attractive proposition.

Part IV

Overview of the radio channel

9 Multi-path and channel coherence bandwidth

Multi-Path propagation arises when there is more than one path between transmitter and receiver in a communication link. This is always occurs in the case of mobile communication. Multi-path propagation is characterized by **Multi-Path fading**, which arises as the result of interference between the delayed waves as their phases at the receiver change at different rates, and by **Delay spread** which arises as the lengths of the various paths are different.

Multi-path propagation, and the inter-symbol interference it produces, results in a limitation to wideband transmission of data. Here wideband is defined as

$$W \gg \frac{1}{2\pi T_m} = \Delta f_c \tag{17}$$

where, W is the transmission bandwidth T_m is the delay spread and Δf_c is the coherent bandwidth [16] pp714.

The delay statistics depend mainly on the geometry of the illuminated area. For example, delay spreads are much larger outside buildings than inside and in mountainous areas than in urban areas. Therefore, it is more difficult to transmit high data rates in open areas, unless propagation is point-to-point, than in an indoor area. In the indoor environment, path delays are relatively short, several metres or less, and delay spreads are of the order 50—100ns [17]. However, hand-held terminals move slowly, and computer fixed ones not at all, so duration of fades can be quite large.

There has not been very much published on wideband characterization of multi-path in the indoor environment at millimetre wave frequencies but, indications are that delay spread is not very sensitive to frequency and results will be similar to those at lower frequencies [18]. Additionally, the scope for using absorbing materials and directive antennas at millimetre wave frequencies is much greater than at lower frequencies due to the shorter wavelengths. Thus, ability to control multi-path may make a significant impact on system design.

The case which we are considering is for data rates in the range 10–100Mb/s. Thus, the bit duration is shorter than the delay spread, or alternatively, the signaling bandwidth exceeds the coherence bandwidth of the channel.

Some work has suggested that multi-path propagation is less of a problem at optical wavelengths as most scattering is diffused and not specular so the interference at the receiver is not so strong [19].

10 Anti-multi path techniques

Proakis [16] details many techniques which may be employed to reduce the effect of multi-path propagation. Basically, the aim is to provide diversity in some way shape or form. This can be seen directly in the case of frequency or antenna diversity and more indirectly in the case of spread spectrum RAKE reception or signal coding.

Investigation of the multi-path propagation problem and means to approach its solution was just one aspect of the project which had as its aim realization of a demonstration system within the first year of my stay at ATR. Therefore, emphasis was on a means to develop a practical system, whilst keeping in mind potential for future development.

Spread spectrum modulation was identified as a good candidate for addressing the problem of multi-path propagation and, moreover, it is useful as a means for testing the wideband performance of the fibre optic link. Other approaches could also be investigated, for example, multi-carrier transmission, adaptive equalization, and RAKE reception directly on the received signal when the transmission bandwidth W exceeds $1/2\pi T_m$ [16, pages 729–741], but these are not dealt with here.

10.1 Spread spectrum modulation

Spread spectrum modulation has the ability to resolve delayed multi-path components and either eliminate or use them to provide diversity. Moreover, it supports code division multiple access (CDMA) and facilitates "soft hand-over" between cells and base-station macro-diversity to suppress shadow fading [20], [21], [22]. Measurements at 2.6GHz indicate that such capabilities would be required for indoor communication when data rates are greater than a few Mbs^{-1} [17]. This requirement is expected to be similar at millimetre wave frequencies as experimental results show that delay spread is relatively insensitive to frequency [18]. For outdoor communication delay spreads are larger and there is an even greater need for anti-multi-path techniques to support wideband transmission.

Spectral spreading may be effected in a number of different ways. In direct sequence spread spectrum modulation the data signal is multiplied by a wideband coded signal, whereas, in frequency hopping, the signal steps over a number of different transmission frequencies in a coded pseudo random way. However, resolution of delay components requires direct sequence spread spectrum as—slow—frequency hopping (many bits per hop) cannot provide bit-by-bit diversity.

11 System concept

Our proposed system is based on direct sequence spread spectrum modulation of millimetre wave carriers using an EOM. These millimetre wave signals are then distributed to multiple remote base-station sites over a radial network of fibre optic cables. Figure 13 shows an outline of the system concept. The Figure illustrates macro-diversity as the mobile user receives two

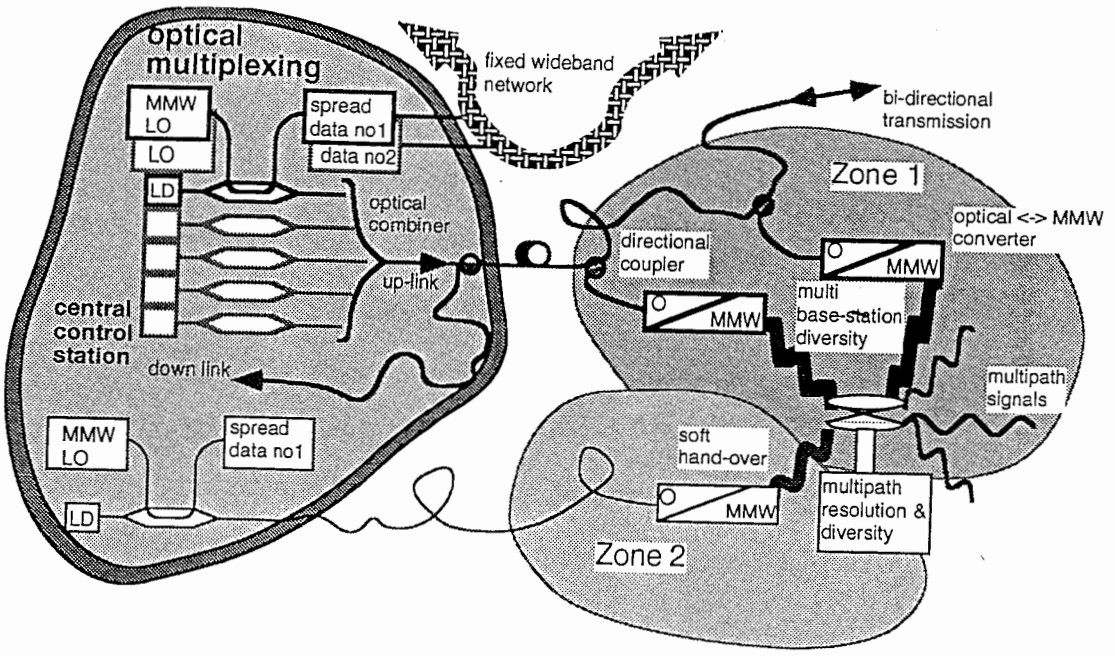

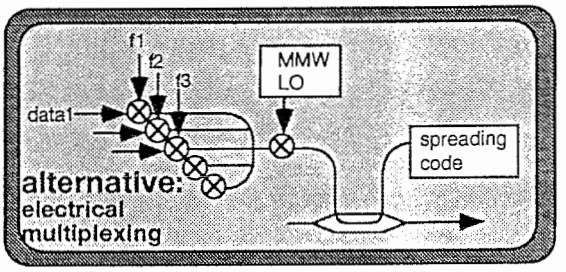

Figure 13: System concept

signals, (heavy lines), from different base-stations. In addition, soft hand-over is illustrated, (heavy dotted line), as the user simultaneously receives signals from cell 1 and cell 2 prior to hand-over.

11.1 Estimate of CDMA Capacity

In this section we make use of the results of Pickholtz, who derived an approximate estimate of the number of users who could simultaneously access a CDMA system in a Rayleigh fading environment. In indoor propagation fading is typically Rician so the Rayleigh assumption should be conservative.

In CDMA there is no fixed number of frequency slots or time slots as in FDMA or TDMA. Simply, the channel quality that each user "sees" gradually degrades as the number of actively transmitting users increases. Also, in CDMA, every cell uses all available frequencies, a re-use factor of 1. This cannot be done with FDMA or TDMA as excessive interference would result. The net increase in capacity of a CDMA system due to the above factors has been reported to be of the order of 4–6 [20], [21].

Pickholtz [22] provides an approximate lower bound on the maximum number of users able to simultaneously access a CDMA cell in a Rayleigh fading environment:

$$\hat{m} \leq \left\lfloor \frac{3}{2\alpha(1+K)} \frac{N}{r\lambda_{req}} \left(1 - \frac{\lambda_{req}}{\lambda_0}\right) \right\rfloor \tag{18}$$

Defining the terms and giving them reasonable values λ_0 is the thermal SNR=$30dB$, λ_{req} is the required SNR=$8dB$(providing a "channel" BER of 10^{-4} for DPSK, coding could be used to improve this), r is FEC code rate=1/2, N is the processing gain, K is adjacent channel overspill factor=1/2 and α is user activity factor=1/10. Then for a data rate of 10Mbs^{-1} and respective chip rates of 100Mbs^{-1}, 1Gs^{-1}, and 10Gbs^{-1} user capacity per cell is respectively 8, 80 and 800. Pickholtz describes (18) as a conservative estimate which would probably be exceeded in practice [22].

11.2 Novel spread spectrum ideas

Spread spectrum signals can be generated optically [23] which could allow very wide bandwidth and would also be suited to all optical LAN systems. Spreading codes can be generated by chaotic sequences and application of this technique is under investigation in several places [24].

11.3 Multi-level modulation

If multi-level modulation is used the symbol rate is reduced and the problem of ISI diminished. However, at the same time, the modulation becomes more sensitive to phase and amplitude distortion. Thus, a careful trade off between modulation level and complexity must be made. This is a problem for system simulation. For example, QPSK reduces the symbol rate by a factor of 2, 16QAM by 4, 64QAM by 6 and 256QAM by a factor of 8.

If we choose a data rate of 150Mb/s, for compatibility with with B-ISDN, the symbol duration for BPSK modulation is 7ns, QPSK reduces the symbol rate by a factor of 2, 16QAM by 4,

64QAM by 6 and 256QAM by a factor of 8, and the symbol durations become, respectively, 14ns, 28ns, 42ns and 56ns.

If spread spectrum is used the problem becomes the required spreading factor [10]. A practical factor is about 128 times the symbol rate [25]. Thus, the required chip rates for the spreading codes are 19.2Gb/s, 9.6Gb/s, 4.8Gb/s, 3.2Gb/s and 2.4Gb/s. Very high chip rates present a power consumption problem as power consumption increases with switching rate. However, 15GHz signal sources are commercially available. Spread spectrum also has the advantage that it is relatively easy to use multi-site diversity. Thus, line-of-sight transmission can be more nearly ensured and the receiver structure can be relatively simple.

Part V

Wideband test system

12 Overview

There are five key elements to the wideband test system; optical modulation, optical detection, millimetre wave transmission, millimetre wave detection and signal decoding. Each of these aspects is dealt with briefly here and details of the system construction and simulation of the digital receiver are described and directions for development are suggested. Several papers have been published concerning the system layout and performance particularly [8], [7], so we concentrate here on design and layout information outside the scope of those papers. Here we concentrate on Layout and design information not included in those papers.

One theme of the wideband experiments was a comparison of the theoretical BER performance of differential bi-phase shift keying (DPSK) with linear optical modulation, optical modulation using the EOM as a bi-phase modulator, and a back-to-back electrical connection. The main difference between ideal performance and experimental arose from the use of a digital receiver with limited A/D resolution. We simulated the effect using the DSPW software package for 3-bit and 4-bit resolution. A second theme was analysis of the performance of the system in an optically simulated multi-path environment. Only limited free space trials could be accomplished because of the limited Tx power available[11].

12.1 Choices in design of the system

A number of choices were made to facilitate system design.

A data rate of 10Mbs^{-1} and nominal chipping rate of 100Mbs^{-1} were chosen. This enabled fast TTL logic to be used in the transmitter circuitry, rather than faster ECL logic. This simplified circuit design at the expense of limiting the maximum chip rate.

DPSK modulation was adopted to avoid the need for carrier phase recovery in the receiver.

[10] for a multiple carrier system is used the problem is the required number of carriers and concomitant system complexity; assuming a 2Mb/s unequalized data rate is achievable, the required number of carriers for PSK, QPSK, 16QAM, 64QAM and 256QAM is of the order of 75, 38, 19, 13, and 10

[11] Amplifiers now purchased would enable these experiments to be done an MMIC amplifier is also being developed to enable this to be done

Digital detection was employed to allow simplification of implementation and to avoid the need for an IF delay line; using an IF delay line would make changing the data rate difficult, also it is a relatively difficult component to procure, whereas in digital circuitry, making a one-bit delay is a simple matter. The compromise made in construction was choice of a 4kb ROM device as the look-up table for digital detection which limited resolution to 3-bits. Results of a computer simulation to investigate this effect are detailed here.

Matched filtering was carried out at IF using a narrowband filter as this was the most simple means available to us. It did not cause an appreciable difference from the optimum solution of implementation of integrate and dump filters at baseband.

12.2 System details

Figure 14 shows the block diagram of the experimental system which is described below

Spread Spectrum and Data Generation Section:

Both the data input and spreading code are non-return-to-zero (NRZ) pseudo-random binary sequences (PRBS) obtained from error rate test sets. The input data is a 2^{23}-1 pseudo random binary sequence (PRBS) at 10Mbs^{-1} bit rate and the spreading code is a 2^{23}-1 PRBS with a nominal clock rate of 100Mbs^{-1}.

The two signals are fed into a circuit I constructed. The circuit has the function of converting the input levels to TTL, synchronizing the two waveforms, differentially encoding the data input, multiplying the signals using an XOR gate and buffering the output into a high power amplifier. TTL logic was used in the circuit as high speed devices (> 110MHz) were immediately available in the laboratory. The choice not to use ECL logic was a compromise which allowed rapid development of the experimental hardware at the expense of limiting the maximum data rate to about 110MHz.

The functional description is as follows: the ECL levels from the two generators are converted to TTL; the data signal is differentially encoded using an XOR gate and a flip-flop; the data and spreading code are buffered by a second flip-flop clocked by spreading code clock; the data and code are multiplied in a second XOR gate; the resultant signal is buffered by a second flip-flop; converted to ECL levels; finally the DC level is blocked and a variable DC offset introduced. Also generated, at the same time, is a delayed version of the spreading code for use in de-spreading. The delay is selectable (up to one data clock period) in units of the chip clock period and is realized by switching between the outputs of a an array of flip-flops through which the code signal is daisy-chained.

The two outputs from the circuit, the spread data signal and the delayed code, are then buffered by two wideband amplifiers for driving either microwave mixers or for bias switching on Mach Zehnder modulators.

Millimetre Wave/Optical Section: The optical section of the link consists of a $Nd:YAG$ laser, optical attenuator, EOM and a 40GHz 1.3μm 0.48mW/mA responsivity photo-detector. The EOM is a $LiNbO_3$ Mach-Zehnder device constructed on a Z-cut $LiNbO_3$ crystal with coplanar waveguide electrodes, optical insertion loss is 6.8dB and $V\pi$ is 5V at DC. At 40GHz, the effective $V\pi$ is increased to about 11V, that is, a much higher voltage need be applied at 40GHz than at DC to introduce π phase change in the device.

The millimetre wave carrier is either applied directly to the EOM as shown in the Figure or it

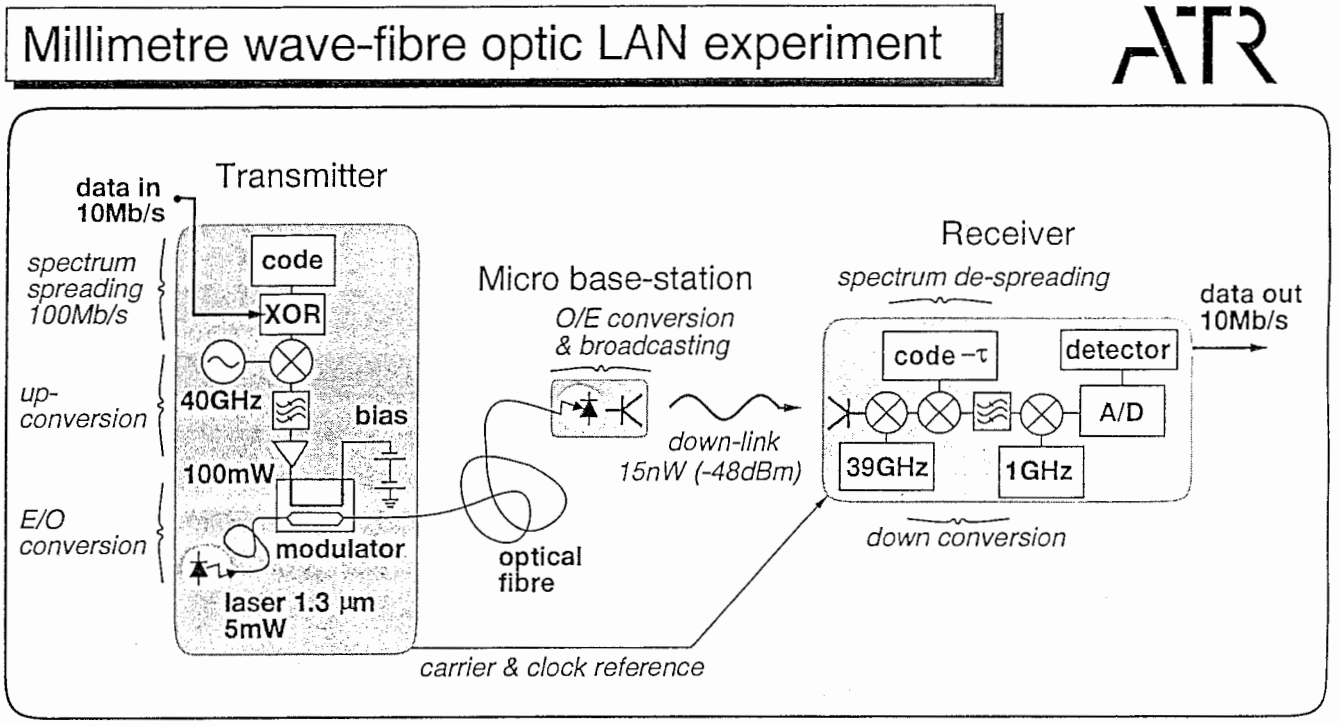

Figure 14: System block diagram employing EOM as 40GHz optical sub-carrier bi-phase modulator

can be modulated in a conventional way using a microwave mixer, filtered, amplified and then applied to the modulator. In the first case the modulator is used as a sub-carrier bi-phase modulator and in the second as a linear modulator.

Reception and Down Conversion Section The signal is down converted to 1GHz and an AGC is used to keep a constant signal level (the AGC voltage is derived from the signal after de-spreading) and de-spread using the delayed spreading code. The delay is selected by switching the code in 1 chip intervals and fine adjustment made by altering the chip clock rate. The de-spread signal passes through a 20MHz bandwidth filter, which approximates an IF matched filter for the $10Mbs^{-1}$ data, and is down converted to baseband I and Q signals.

Digital Detection Error Rate Measurement Section: The main compromise in the design of the digital receiver was the choice of a 3-bit resolution. This was determined by the use of a 4kb ROM look-up table. In a practical design a higher resolution would be used. However, 4-bit resolution would require a high speed 64kb (2^16) ROM device and one was not available at the time of construction. The alternative would have been to use a number of 4kb devices, however, a compromise was made of performance for ease of construction.

Figure 15 shows the circuit diagram for the digital receiver. The I and Q signals are filtered to suppress out of band components by a simple RC filter; the signals are buffered to have a voltage swing between 1V and 2V; analogue to digital (A/D) converted with 6-bit resolution (the signals are sampled at the clock rate); the 3 most significant bits are taken from each channel and delayed by one data clock period; the 3-bits and delayed 3-bits from each channel (altogether 12-bits), are fed to a the 12 inputs of a 4kb ROM device. Figure 16 shows the timing diagram of the A/D sampling, delay, and ROM look-up process. The ROM device contains a table of all the possible input combinations and the resultant output value of 0 or 1. The values were calculated by computer then written into the ROM device using a DATA I/0 chip programmer. The operation of the ROM device and the table of values were checked by computer simulation.

The error rate of the recovered signal was then measured using a standard error rate test set.

13 System simulator

13.1 A few words on DSPW

The computer software package DSPW was used to conduct simulations of the system performance. The package has a graphical interface which allows a block diagram of the system under simulation to be constructed; connections with the same labels are automatically connected together.

The package contains a large number of library elements, so, in a large part, the system can be constructed by simply connecting pre-defined elements into sub-systems and then connecting those sub-systems. However, it is also possible to write a custom C-code description of a desired element and then create a new element.

Simulation is carried out on the complex envelope of the signal rather than in a less computationally efficient way by sampling a modulated RF signal.

Simulation of BER performance at low error rates is always time consuming because of the number of errors, typically at least 100, which must be counted to provide a reasonable

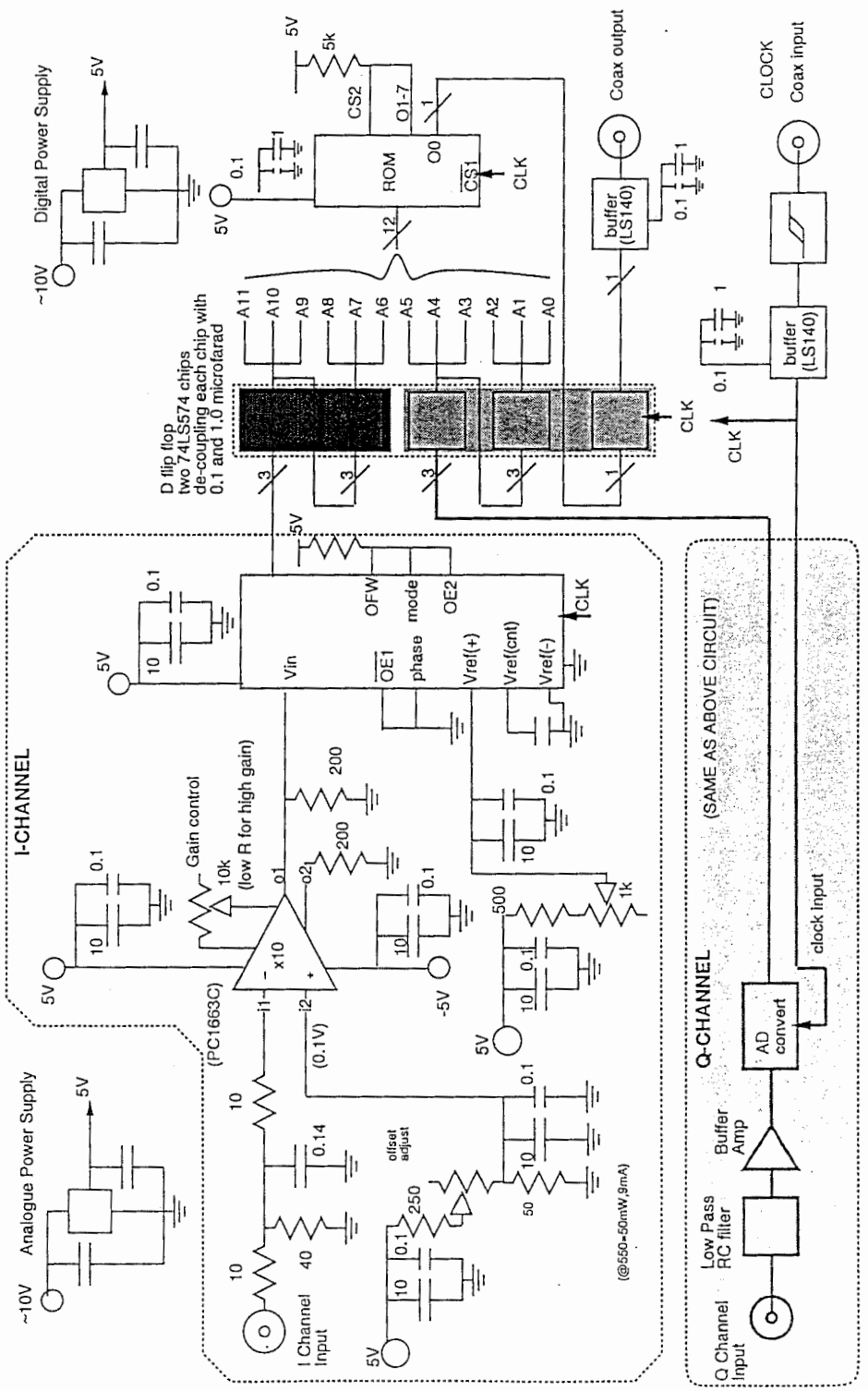

Figure 15: Schematic diagram of the digital receiver

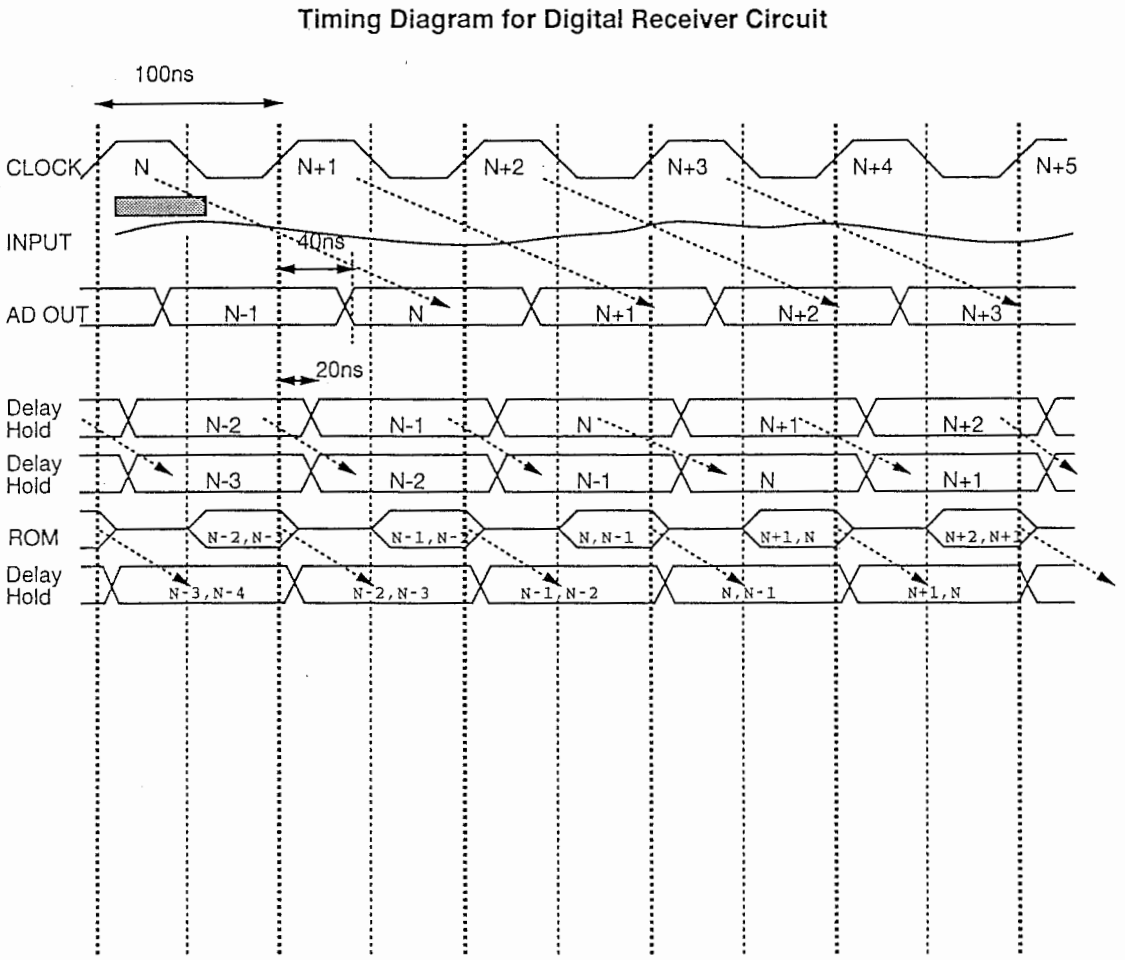

Figure 16: Timing diagram of the digital receiver

estimate. Thus, at a rate of 10^-6, 10^8 bits must be evaluated. To limit the complexity of the system and reduce calculating time, we chose to simulate just the effect of the limited error rate and neglect the effect of spectrum spreading and de-spreading.

13.2 Simulation of finite A/D resolution

The files created exist in the directory "thomas-ss" on rs25. They can be viewed by starting DSPW (running DSPW shell file) and looking in that directory using the DSPW environment.

Figure 17 shows the functional block diagram of the system. Data is generated, differentially encoded, and modulated and transmitted through a "channel". The channel is a two ray model but for evaluation of the A/D resolution effect, only one ray is used. The channel measures the signal level and introduces noise to give a specified SNR. The signal then passes to the receiver.

Figure 18 shows the detail of the receiver structure for the case of 3-bit resolution. The input is filtered separated into real and imaginary parts, A/D converted, delayed, the address corresponding to the A B C D values is calculated, and the corresponding value in the ROM device is output. The ROM device is a custom coded block containing a string of 1 and 0's corresponding to the input address. In the case of 4-bit or greater simulation, the A/D blocks and the decoder were custom coded as it was more efficient than constructing the devices from library blocks.

Looking back to Figure 17, the decoded data signal is input to an error counter where it is compared with a delayed version of the original input signal. When a specified number of errors is counted then the error rate value is written to a file and the SNR is incremented. The process continues until the system had stepped through its range of SNR values. The process also detects if some minimum minimum error rate has been exceeded. The results of the system simulation are shown in Figure 19 where it can be seen that the 3-bit resolutioncauses a 2dB reduction in performence at an error rate of 10^{-6} compared with ideal DPSK, whereas the 4-bit resolution data is within 1dB of ideal DPSK at 10^{-6}.

14 Some experimental Results

14.1 BER performance in noise

Figure 20 shows the SNR vs BER performance of the system using the EOM as a bi-phase modulator compared with that of an all electrical configuration using a standard MMW mixer as the PSK modulator. Also, in the figure is the simulated performance of the receiver, assuming a 3-bit A/D accuracy and as a standard for comparison, the performance of ideal DPSK. The experimental curves are very close to the simulated result. The all electrical system is identical (within experimental error approximately $\pm 0.2dB$ SNR) to the simulated prediction and, at a BER of 10^{-6}, the optical system is within $1dB$ of the simulation.

14.2 BER performance in simulated multi-path

In addition to the evaluation of BER performance in noise performance was evaluated in a simulated multi-path environment [8], [7]. This was effected in the optical domain by splitting the optical path into two, introducing an extra length of fibre into one arm (about 5m) then

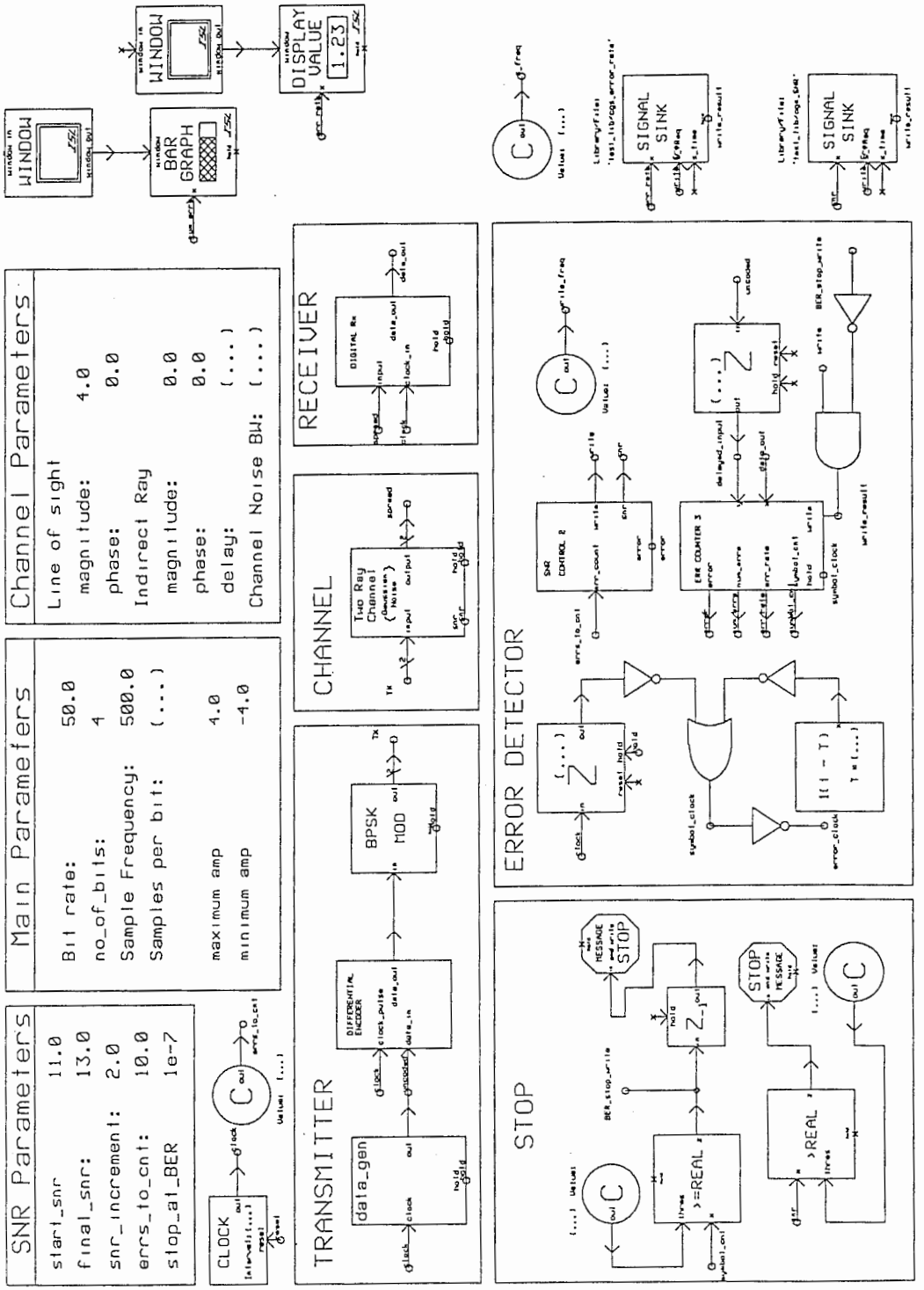

Figure 17: Simulation system

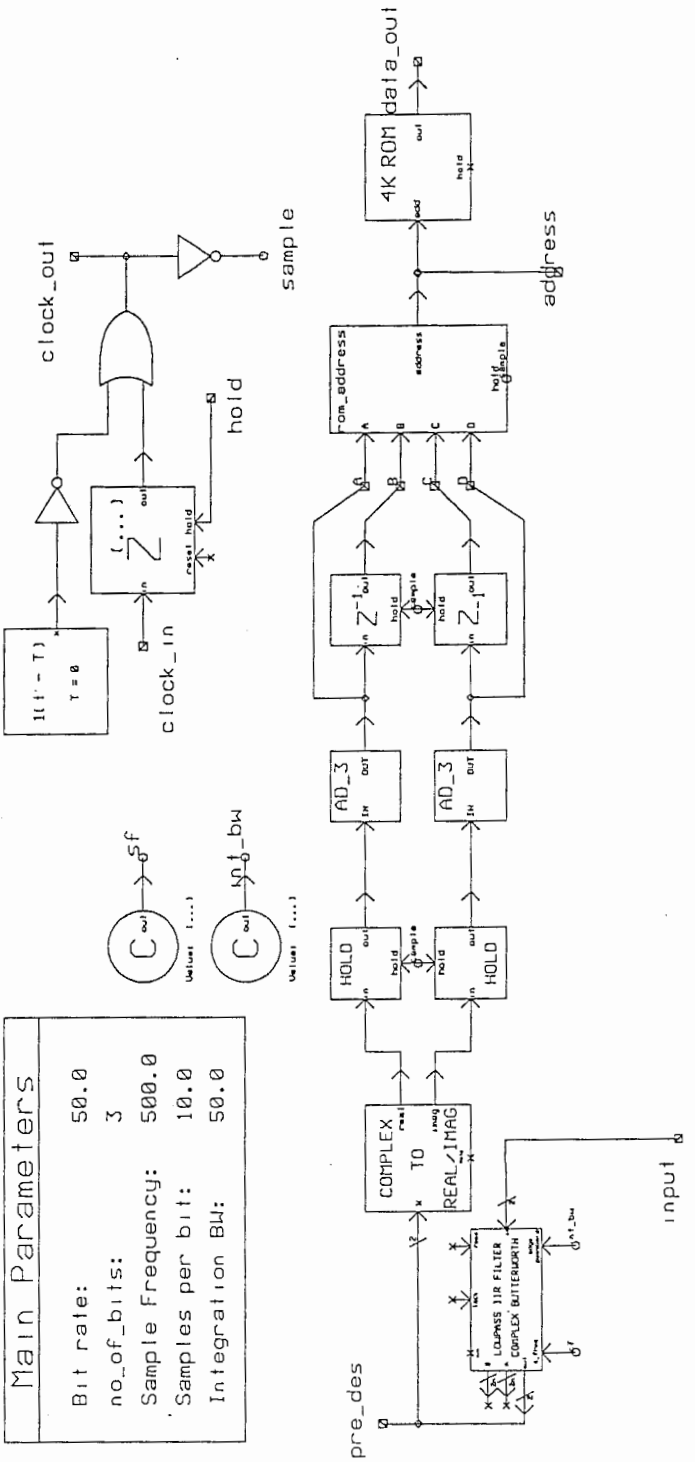

Figure 18: Receiver detail

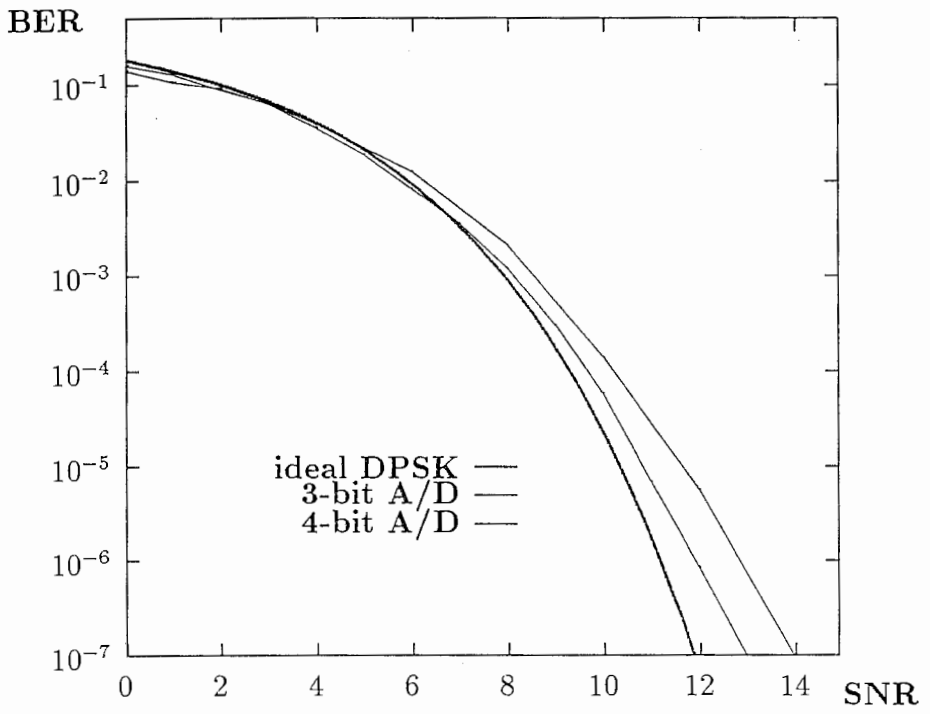

Figure 19: Comparison of experimental BER vs SNR for ideal DPSK 3-bit A/D simulation and 4-bit A/D simulation

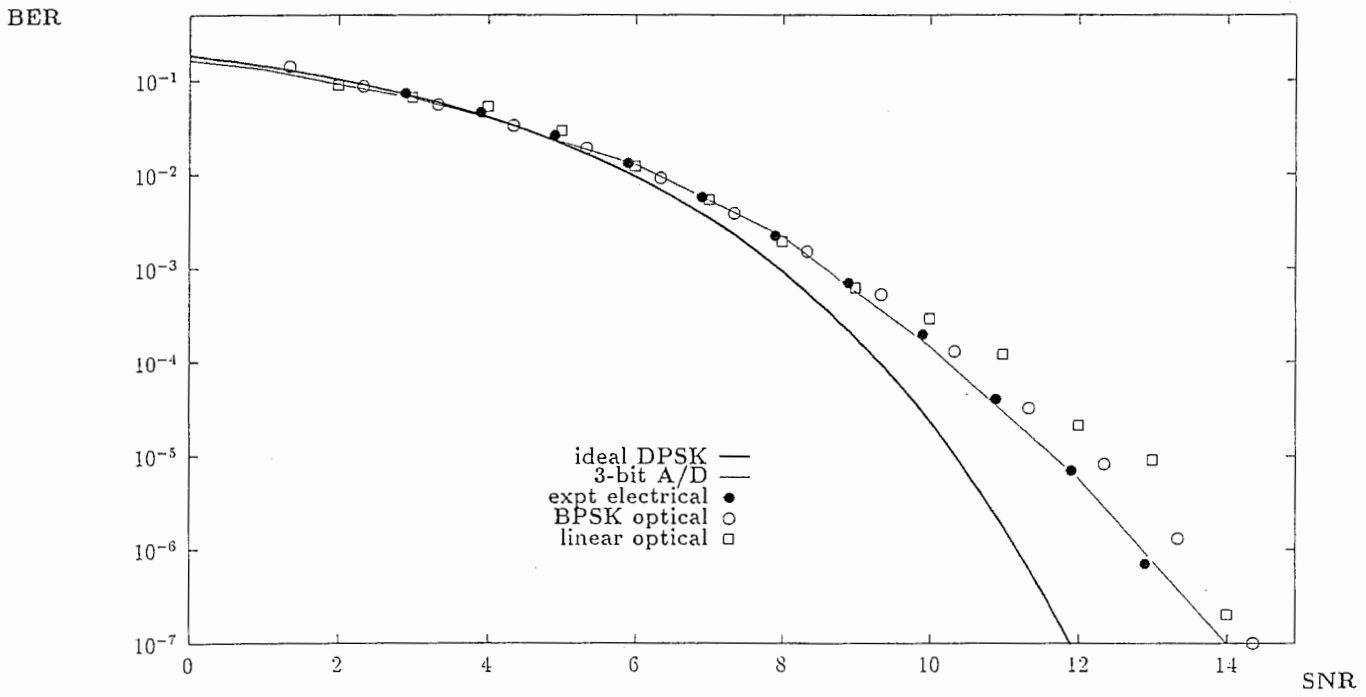

Figure 20: Comparison of experimental BER vs SNR for optical link and all-electrical link, compared with ideal 3-bit A/D simulation

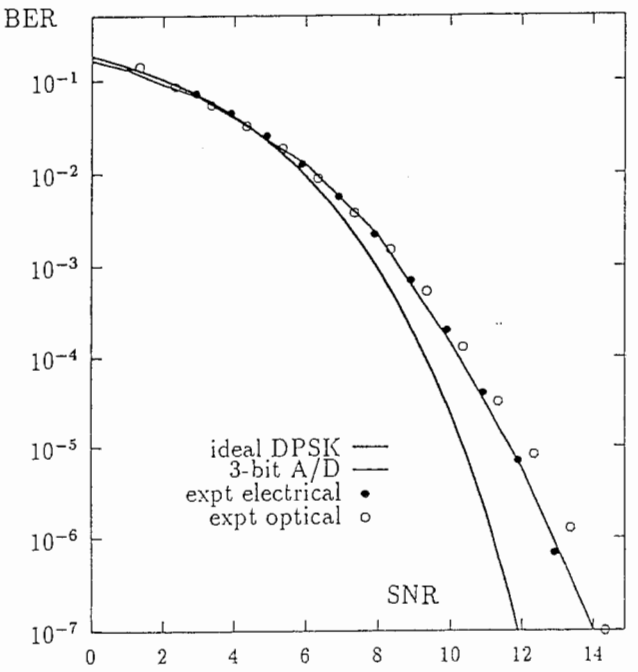

Figure 21: Comparison of experimental BER vs S/I(dB), compared with ideal and 3-bit A/D simulation

recombining the signals in the electrical domain after detection. An additional $4.5dB$ optical loss resulted on the main path. The relative amplitude of the direct and line of sight signals was altered using an attenuator.

Figure 21 shows the ratio of the desired signal to the interfering (delayed) signal, S/I in dB, versus the measured BER. Also on the Figure is the theoretical performance for ideal DPSK and the simulated performance. The curve is within 1dB of the simulated result at a BER of 10^{-6}. This indicates that the interference caused by the signal on the delayed path is comparable with that which would be caused by Gaussian noise.

15 Conclusion

The wideband system was successfully used to demonstrate the the concept of fibre distributed millimetre wave transmission based on spread modulation. Comparison of measured data with theory and with simulation showed good agreement.

Experimental results where the EOM is used as the key component in a direct sequence spread spectrum link are presented. The measured performance of the system is almost identical to that of an all micro-wave system and is within $1dB$ of the predicted performance. Results of a test of the multi-path suppression ability of the system show that performance is within $2dB$ of simulation at a BER of 10^{-5}. The main difference between measured and ideal receiver

performance is due to use of 3-bit A/D conversion, 4-bit resolution would give about 1dB improvement

Acknowledgment

I should like to thank Dr K Habara, Dr Inomata, Dr E Ogawa, Mr Imai for their support of this work and Mr T Ohgane, Mr T Aida and Mr W Matsui for their suggestions regarding design of the spread spectrum system. Furthermore, I should like to express my thanks to Dr Y Furuhama and Dr H Ogawa for their support of this work while they were at ATR and for their continuing interest in it now they have returned to their home institutions.

References

[1] D Cox. Portable digital radio communications—an approach to tetherless access. *IEEE Communications Magazine*, pages 30–40, November 1989.

[2] D Cox. Personal communications—a viewpoint. *IEEE Communications Magazine*, pages 8–20, November 1990.

[3] H Ogawa and D Polifko. Fibre optic millimetre-wave subcarrier transmission links for personal radio communication systems. In *IEEE MTT-S International Microwave Symposium Digest*, June 1992.

[4] Howard Thomas and Hiroyo Ogawa. Indoor millimetre wave PCN/LAN experiment based on direct MMW distribution over optical fibre and multi-path robust spread spectrum modulation. In *Proceedings of 43th IEEE Vehicular Technology Conference*, pages 236–240. IEEE Vehicular Technology Society, May 1993.

[5] D Polifko and H Ogawa. Fibre optic link architectural comparison for millimetre wave transmission. In *Proceedings SPIE Vol 1703*. The International Society for Optical Engineering, 1992.

[6] R Simons. *Optical Control of Microwave Devices*. Artech House, 1990.

[7] T Ishikawa. Polarization independent $linbo_3$ waveguide optical modulator for bidirectional transmission. *Electronics Letters*, 28(6), March 1992.

[8] Gopinath A. Losses in coplanar waveguides. *IEEE Transactions on Microwave Theory and Techniques*, 30(78):1101–1104, July 1982.

[9] Rod C Alferness, Steven K Korotky, and Enrique A J Marcatili. Velocity-matching techniques for integrated optic travelling wave switch/modulators. *IEEE Journal of Quantum Electronics*, 20(3):301–309, March 1984.

[10] Howard Thomas. All optical base-stations for MMW micro-cell radio. In *IEICE Technical Report Vol93, No 237, OQE93-87*, pages 33–38. IEICE Optics and Quantum Electronics Section, September 1993.

[11] Howard Thomas. Optical distribution of millimetre waves for mobile communications. In *PIMRC'93 Personal and Indoor Mobile Radio Conference*. IEICE in co-operation with IEEE, September 1993.

[12] Eiji Suematsu, Seiichi Banaba, Hiroyo Ogawa, and Nobuaki Imai. Fiber optic micro/millimetre wave sub-carrier transmission links using HBT's as photo-detectors. In *IEICE Technical Report OQE93-29*. IEICE Optics and Quantum Electronics Section, June 1993.

[13] Howard Thomas. Fibre optic link using an optical modulator as a millimetre wave sub-carrier bi-phase modulator. In *IEICE Technical Report Vol 93 No 78, MW93-29-38*, pages 13–20. IEICE Microwave Section, May 1993.

[14] Howard Thomas. Operation of a Mach Zehnder EOM as a MMW sub-carrier bpsk modulator (symposium paper). In *IEICE Fall Convention Technical Report*. pages 502–503. IEICE, September 1993.

[15] Howard Thomas. Millimetre waves over optical fibre for broad band wireless communication (invited). In *OFC'94 Optical Fibre Communication*. Optical Society of America in co-operation with IEEE-MTT, February 1994.

[16] J G Proakis. *Digital Communications*. McGraw-Hill, second edition, 1989.

[17] Ematsu Moriyama. 2.6GHz multi-path characteristics measurement in a shielded building. In *Proceedings of 41th IEEE Vehicular Technology Conference*, May 1992.

[18] R Davies, Bensebti, M A Beach, and J P McGeehan. Wireless propagation measurements in indoor multipath environments at 1.7GHz and 60GHz for small cell systems. In *Proceedings of 41st IEEE Vehicular Technology Conference*, pages 589–593, June 1991.

[19] Barry J R. High-speed infrared communications fot wireless local-area networks. In *MTT-S'93 Wireless Communiaction Via Lightwave*, June 1993.

[20] D L Schilling et al. Spread spectrum for commercial communications. *IEEE Communications Magazine*, April 1991.

[21] Andrew J Viterbi. Wireless digital communication: A view based on three lessons learned. *IEEE Communications Magazine*, September 1991.

[22] R Pickholtz, L B Milstein, and D L Schilling. Spread spectrum for mobile communications. *IEEE Transactions on Vehicular Technology*, 40(2), May 1991.

[23] Dan J Hajela and Jawad A Salehi. Limits to the encoding and bounds on the performance of coherent ultra-short light pulse code-division multiple-access systems. *IEEE Transactions on Communications*, 40(2), February 1992.

[24] Kevin M Cuomo and Alan V Oppenheim. Synchronized chaotic circuits and systems for communications. RLE Technical Report 575, Research Laboratory of Electronics, Massachusetts Institute of Technology, Cambridge Massachusetts 02139-4307, November 1992.

[25] D L Schilling. Broad band spread spectrum multiple access for personal and cellular communications. In *Proceedings of 43rd IEEE Vehicular Technology Conference*, May 1993.

16 Appendices: Publications, Patents, Slides from OFC'94

The following is a list of publications and patents applied for during my stay at ATR. Also appended is a copy of the slides I presented at the OFC'94 Conference in San Jose which gives a graphical overview of my research activities at ATR.

References

[1] Howard Thomas and Nobuaki Imai. Millimetre waveband reflection type modulator. In *IEICE Spring Convention Technical Report*, volume 2, page 570. IEICE, March 1994.

[2] Howard Thomas. Millimetre waves over optical fibre for broad band wireless communication (invited). In *OFC'94 Optical Fibre Communication*. Optical Society of America in co-operation with IEEE-MTT, February 1994.

[3] Howard Thomas. All optical base-stations for MMW micro-cell radio. In *IEICE Technical Report Vol93, No 237, OQE93-87*, pages 33–38. IEICE Optics and Quantum Electronics Section, September 1993.

[4] Howard Thomas. Optical distribution of millimetre waves for mobile communications. In *PIMRC'93 Personal and Indoor Mobile Radio Conference*. IEICE in co-operation with IEEE, September 1993.

[5] Howard Thomas. Operation of a Mach Zehnder EOM as a MMW sub-carrier bpsk modulator (symposium paper). In *IEICE Fall Convention Technical Report*, pages 502–503. IEICE, September 1993.

[6] Hiroyo Ogawa, Howard Thomas, E Suematsu, S Banba, and H Kamitsuna. Fibre optic 50GHz FM sub-carrier transmission using HBT device. In *Abstracts 24th General Assembly of the International Union of Radio Science*, page 568, September 1993.

[7] Howard Thomas. Fibre optic link using an optical modulator as a millimetre wave sub-carrier bi-phase modulator. In *IEICE Technical Report Vol 93 No 78, MW93-29-38*, pages 13–20. IEICE Microwave Section, May 1993.

[8] Howard Thomas and Hiroyo Ogawa. Indoor millimetre wave PCN/LAN experiment based on direct MMW distribution over optical fibre and multi-path robust spread spectrum modulation. In *Proceedings of 43th IEEE Vehicular Technology Conference*, pages 236–240. IEEE Vehicular Technology Society, May 1993.

[9] Hiroyo Ogawa and Howard Thomas. Fibre optic 50GHz FM signal transmission experiment *[In Japanese]*. In *IEICE Spring Convention Technical Report*. IEICE, March 1993.

[10] Howard Thomas and Hiroyo Ogawa. Indoor millimetre wave distribution over fibre optic links. In *IEICE Fall Convention Technical Report*. IEICE, September 1992.

[11] Howard Thomas and Nobuaki Imai. Optical transmitter using a Mach Zehnder modulator to directly produce bi-phase modulated optical sub-carrier. Application for patent 196621, ATR Optical and Radio Laboratories, Kyoto, Japan, May 1993.

OFC'94: Symposium on Optical
Microwave Systems Using Fibre Optics

ATR

Millimetre waves over optical fibre for broadband wireless communications

Howard Thomas

Radio Systems Department

ATR Optical & Radio Research Laboratories
Kyoto, Japan

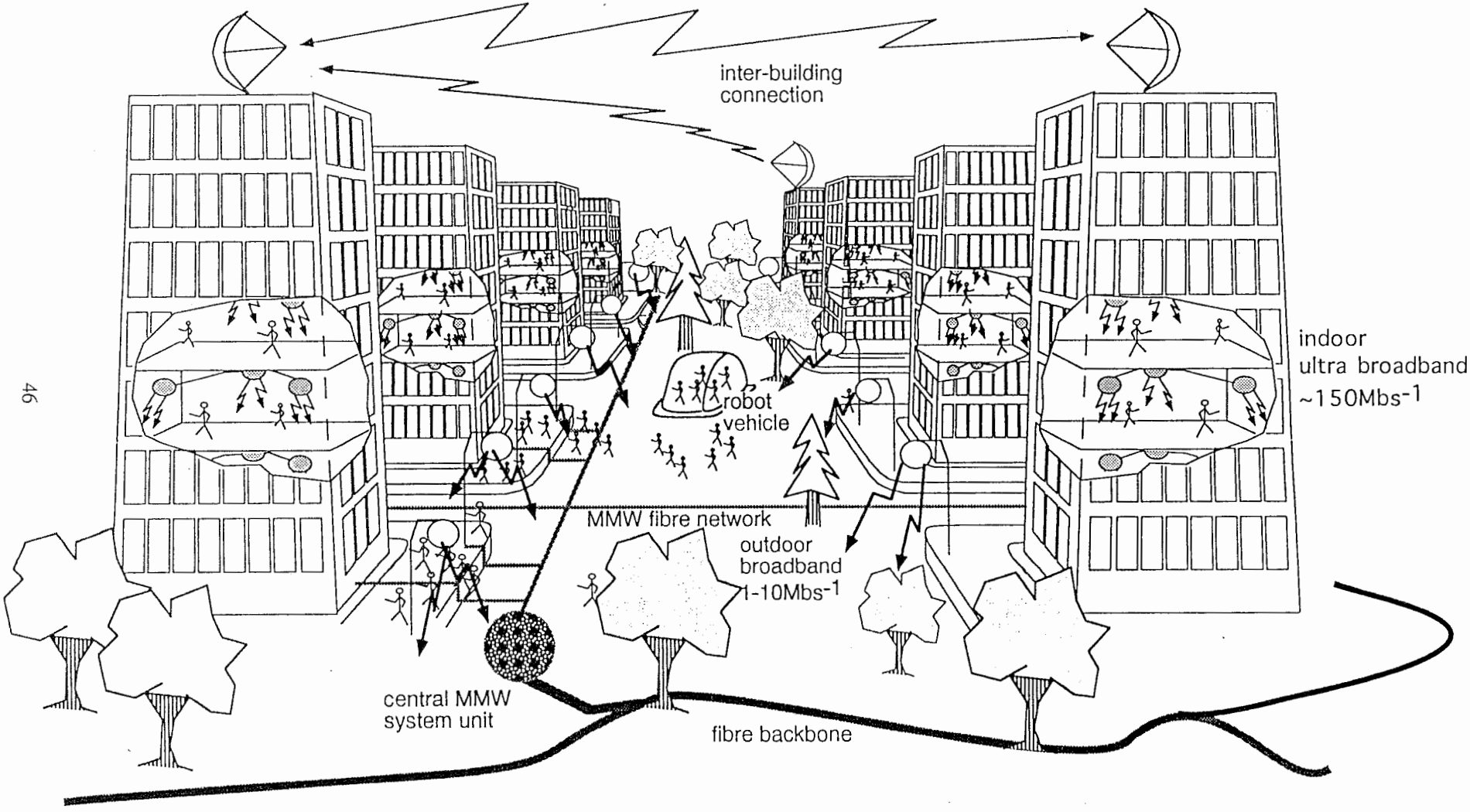
inter-building
connection
indoor
ultra broadband
~150Mbs-1
robot
vehicle
MMW fibre network
outdoor
broadband
1-10Mbs-1
central MMW
system unit
fibre backbone

Channel counter measures

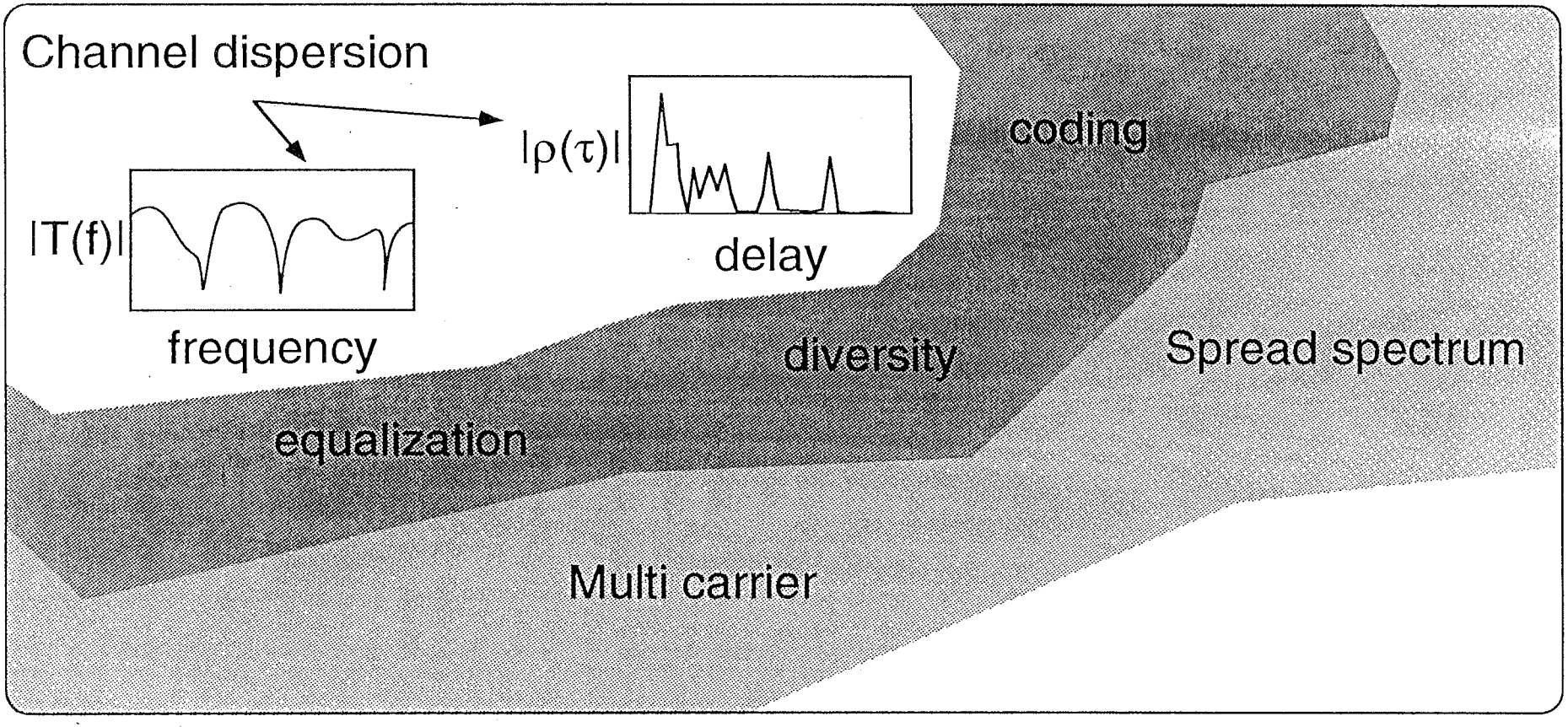

ATR Optical & Radio Research Laboratories
Kyoto, Japan

System requirements and means

ATR

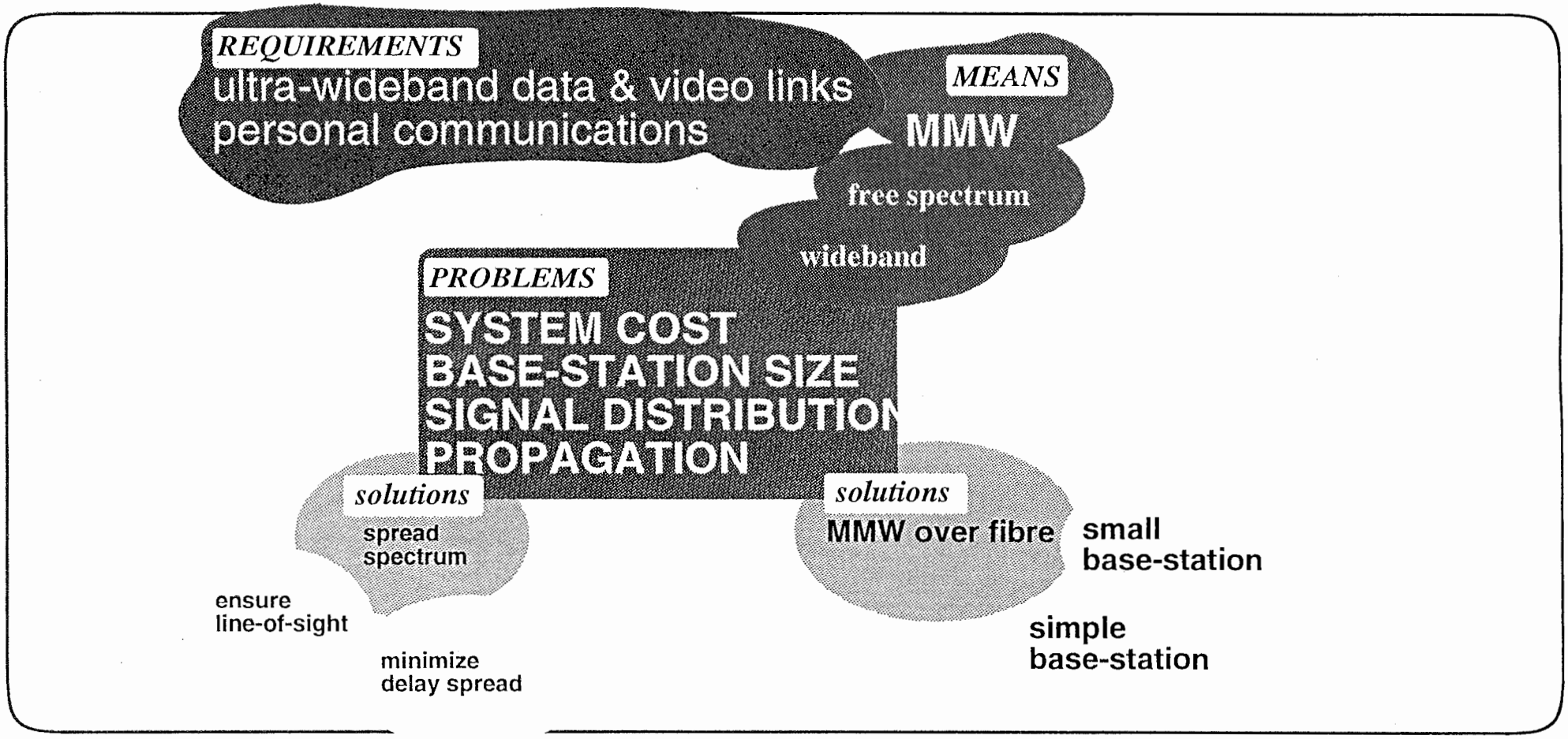

ATR Optical & Radio Research Laboratories
Kyoto, Japan

Fibre distribition of MMW access

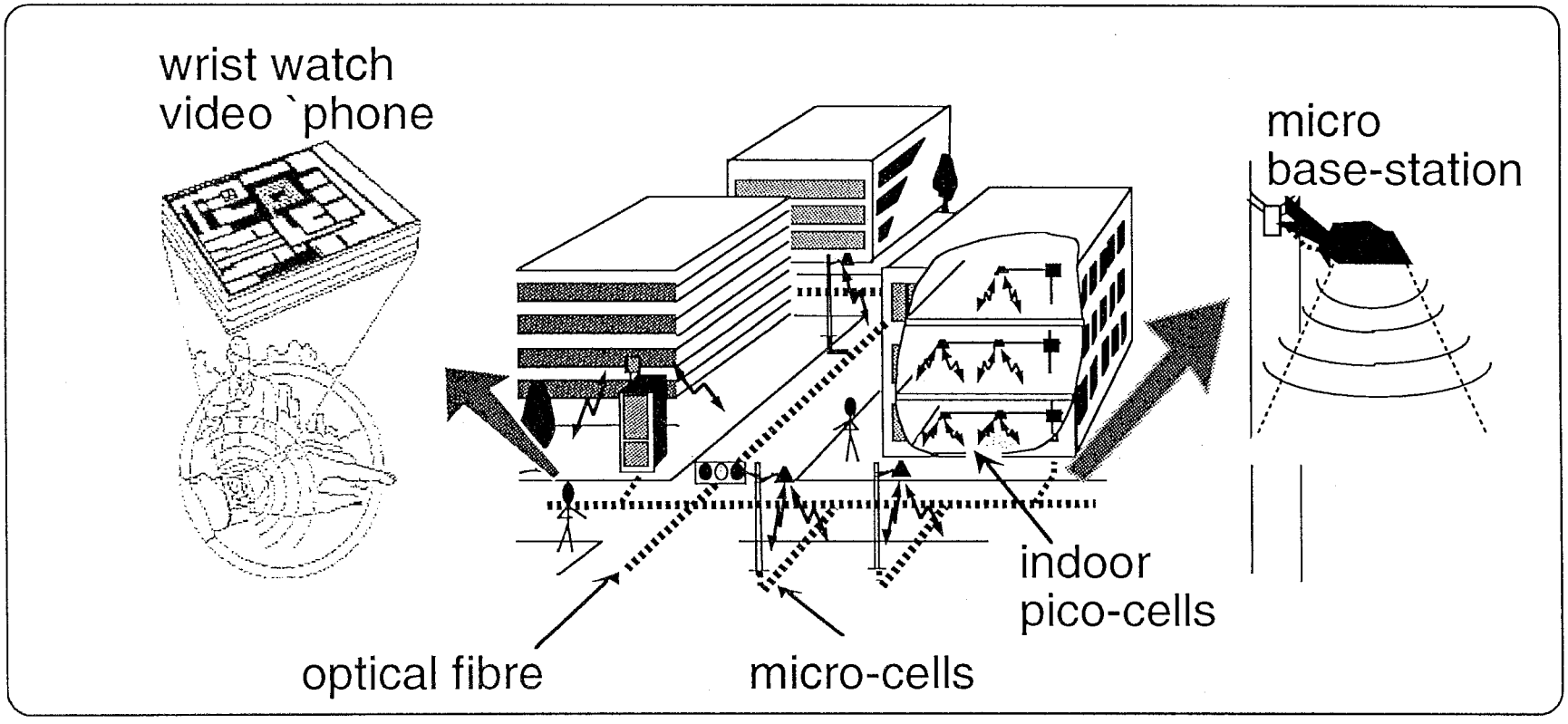

ATR Optical & Radio Research Laboratories
Kyoto, Japan

Millimetre wave pros & cons

ATR

	Radio	Millimetre wave	Optical
bandwidth	limited	very wide	very wide
propagation	long range	short range	short range
channel time dispersion	50-100ns (indoor)	about the same	smaller due to diffuse scattering
component	inexpensive	potential to be low with MMIC technology	potentially low
potential	no bandwidth	good, amps & coherent detection possible	good

ATR Optical & Radio Research Laboratories
Kyoto, Japan

Millimetre wave personal Radio
enabling technology

ATR

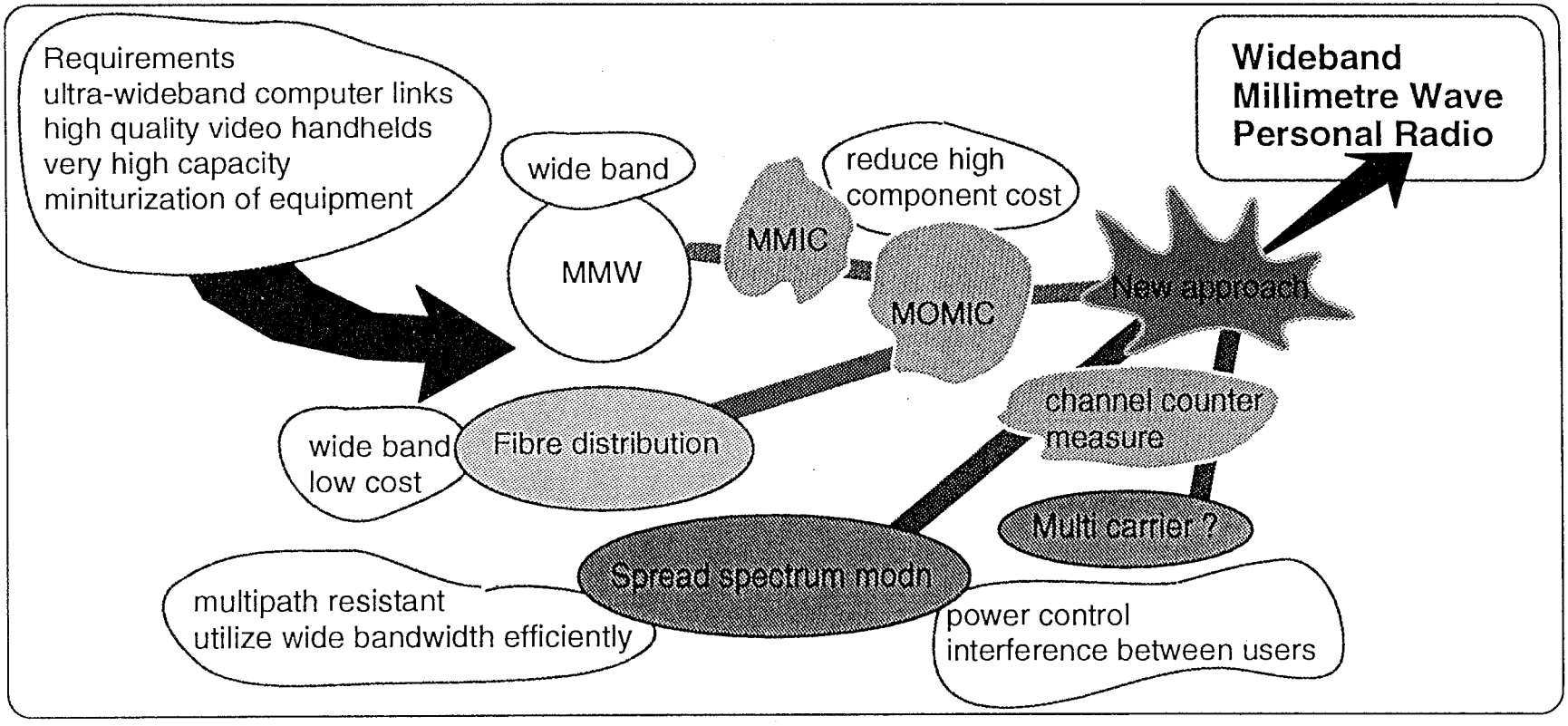

ATR Optical & Radio Research Laboratories
Kyoto, Japan

Direct millimetre wave transmission on fibre

ATR

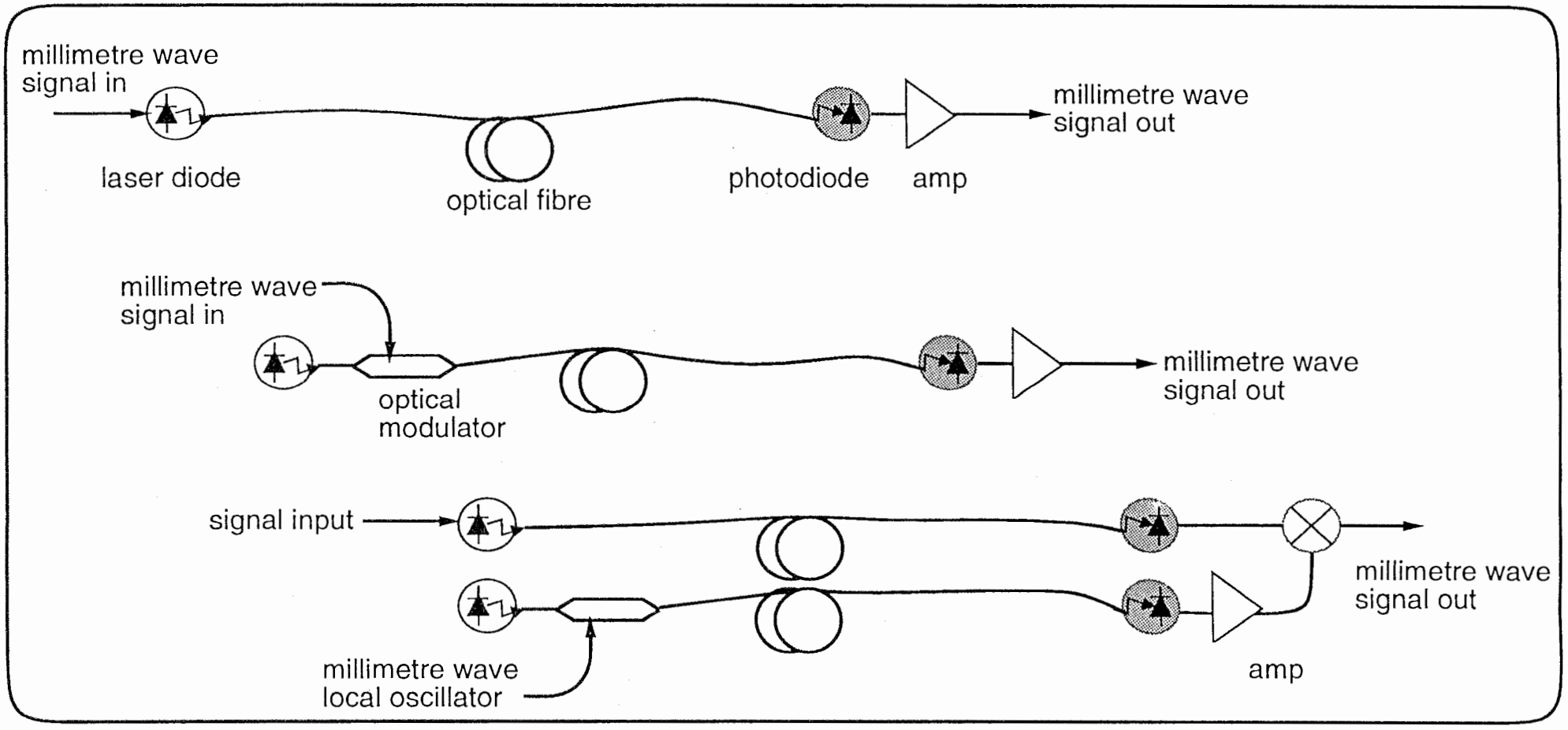

ATR Optical & Radio Research Laboratories
Kyoto, Japan

Indirect millimetre wave transmission on fibre

ATR

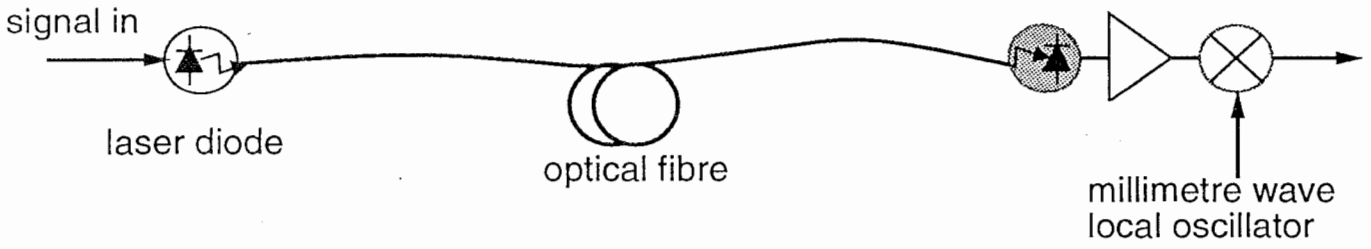

- low speed optical devices
- low link loss and high dynamic range
- requires millimeter wave local oscillator and mixer
- Therefore, greater cost occurs at the base-station

ATR Optical & Radio Research Laboratories
Kyoto, Japan

EOM as BPSK modulator

observed spectra
(PRBS input)

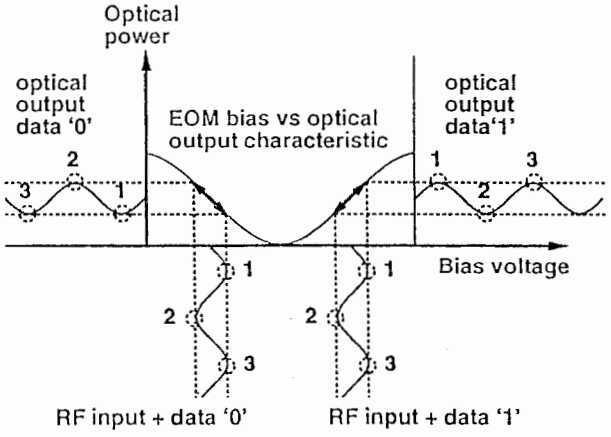

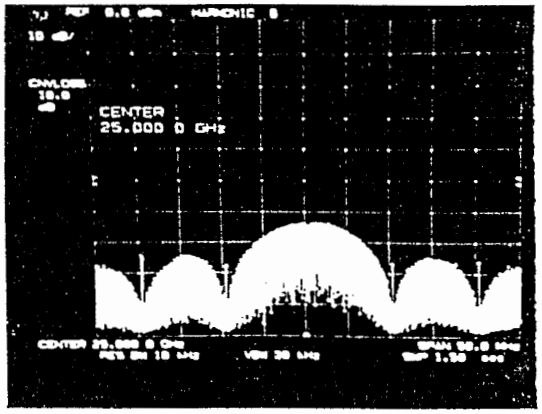

operational principle

ATR Optical & Radio Research Laboratories
Kyoto, Japan

EOM as doubling BPSK modulator

ATR

observed spectra
(PRBS input)

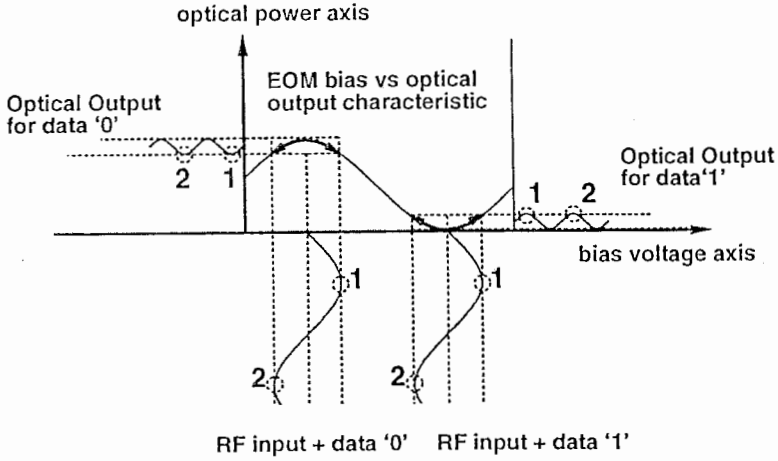

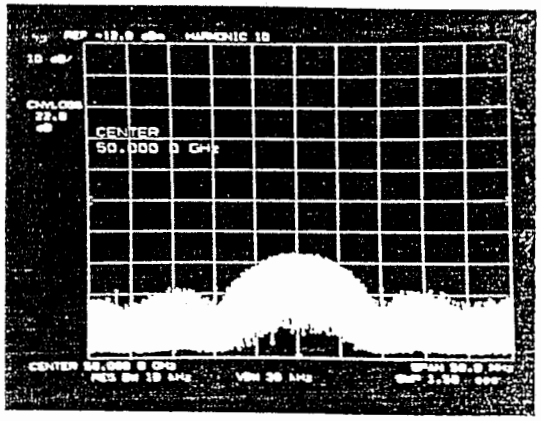

operational principle

ATR Optical & Radio Research Laboratories
Kyoto, Japan

EOM 1.4Gb/s BPSK spectrum

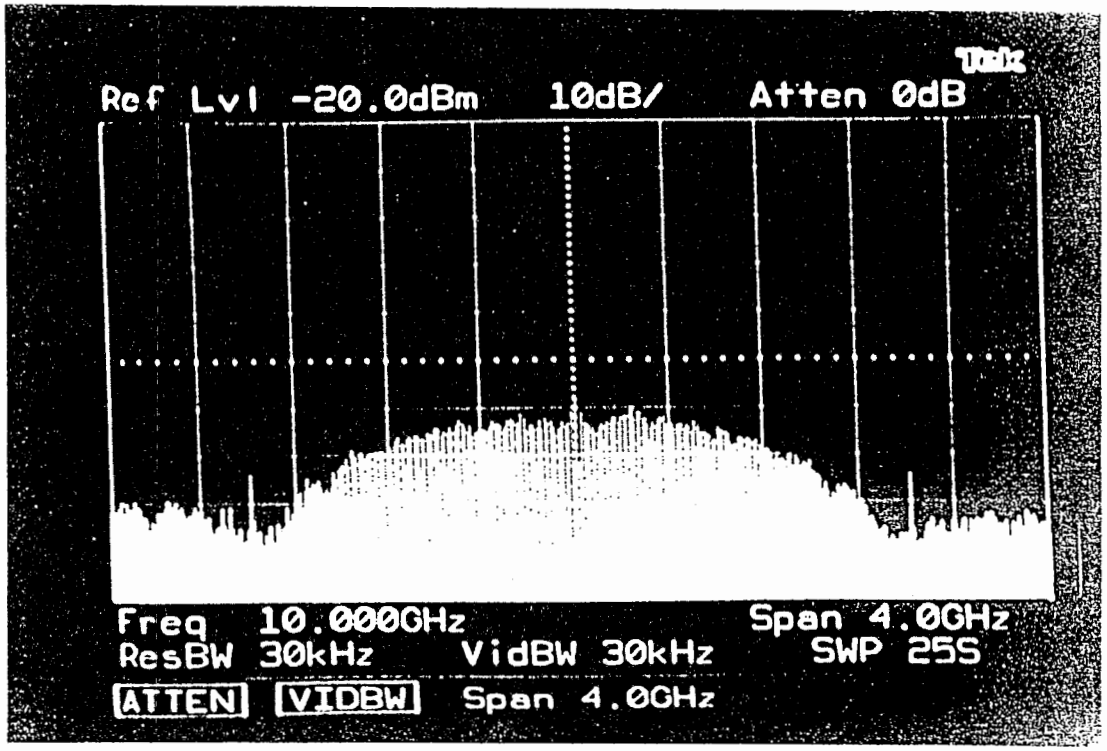

ATR Optical & Radio Research Laboratories
Kyoto, Japan

Comparison of EOM transmitters

ATR

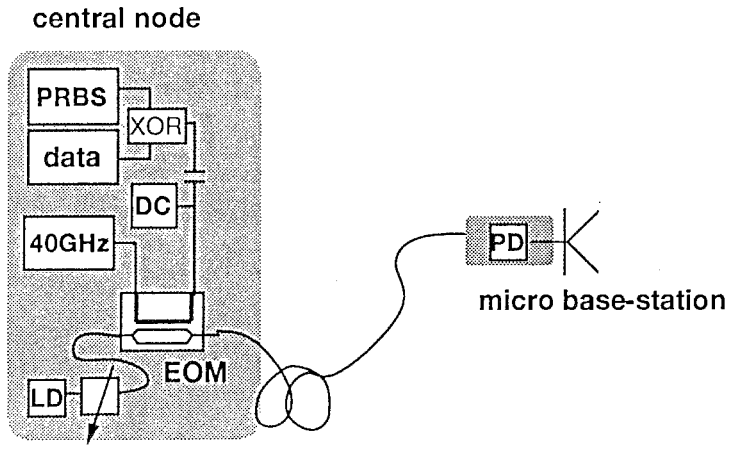

EOM as BPSK Modulator

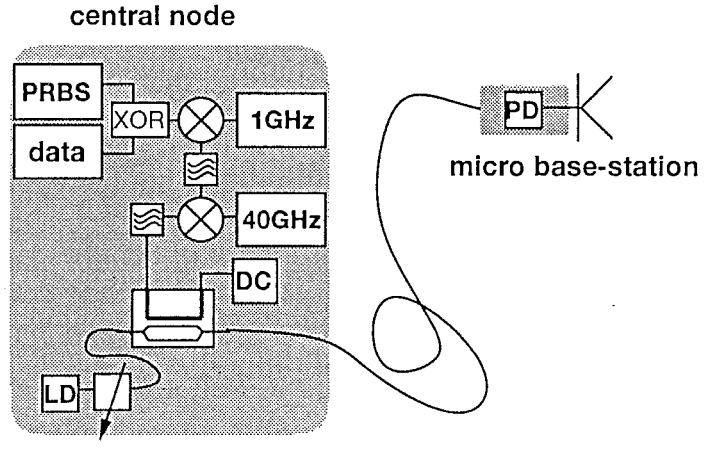

EOM as Linear Modulator

ATR Optical & Radio Research Laboratories
Kyoto, Japan

System Concept (CDMA)

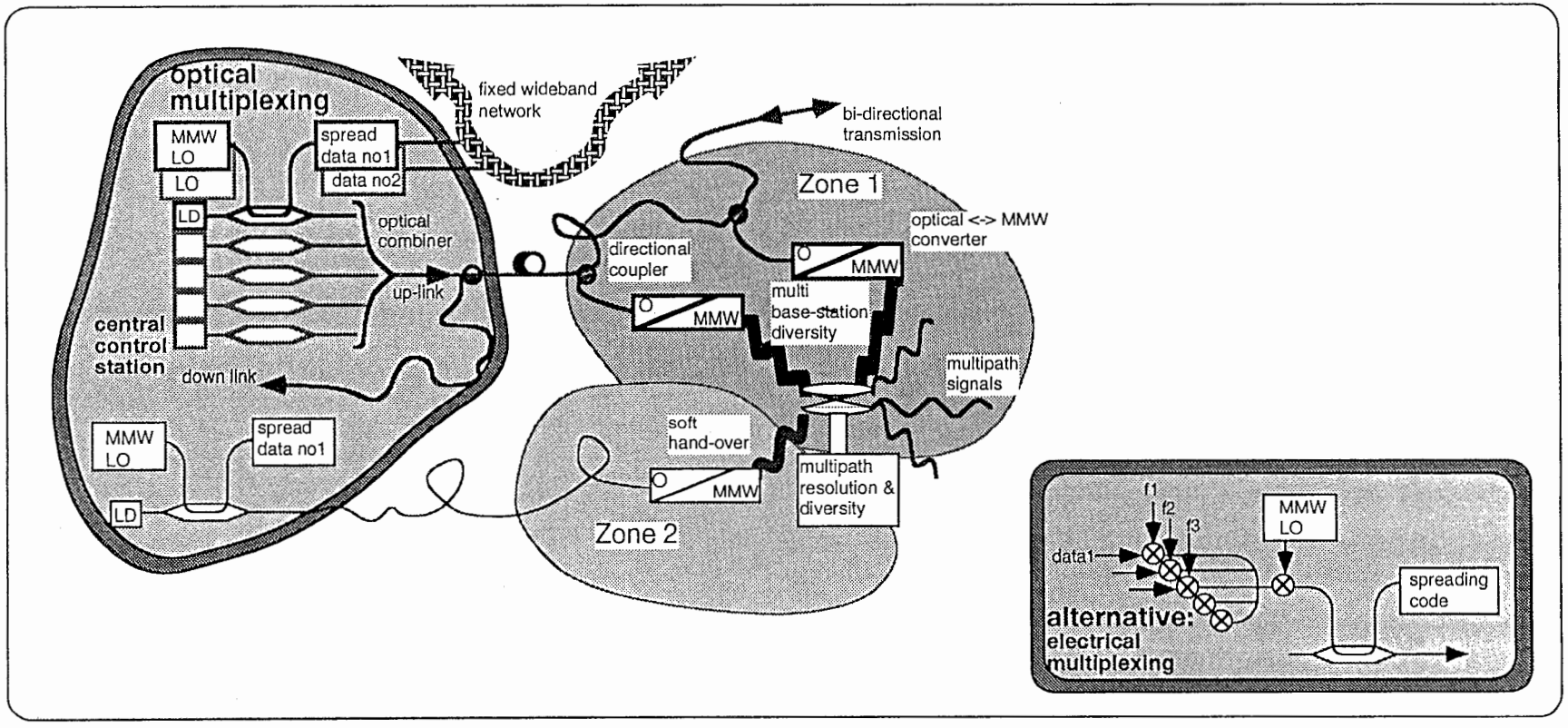

ATR Optical & Radio Research Laboratories
Kyoto, Japan

CDMA system concept

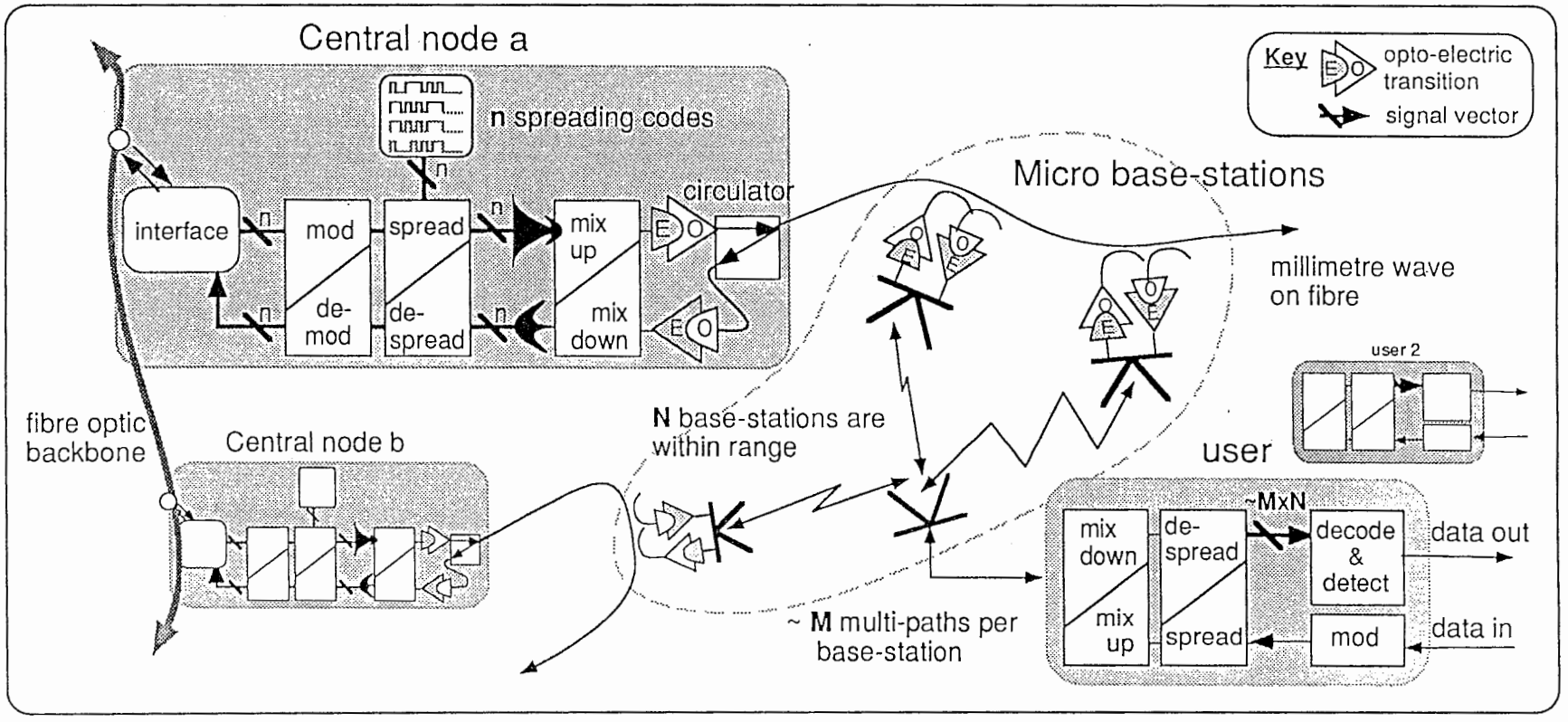

ATR Optical & Radio Research Laboratories
Kyoto, Japan

Millimetre wave-fibre optic LAN experiment

ATR

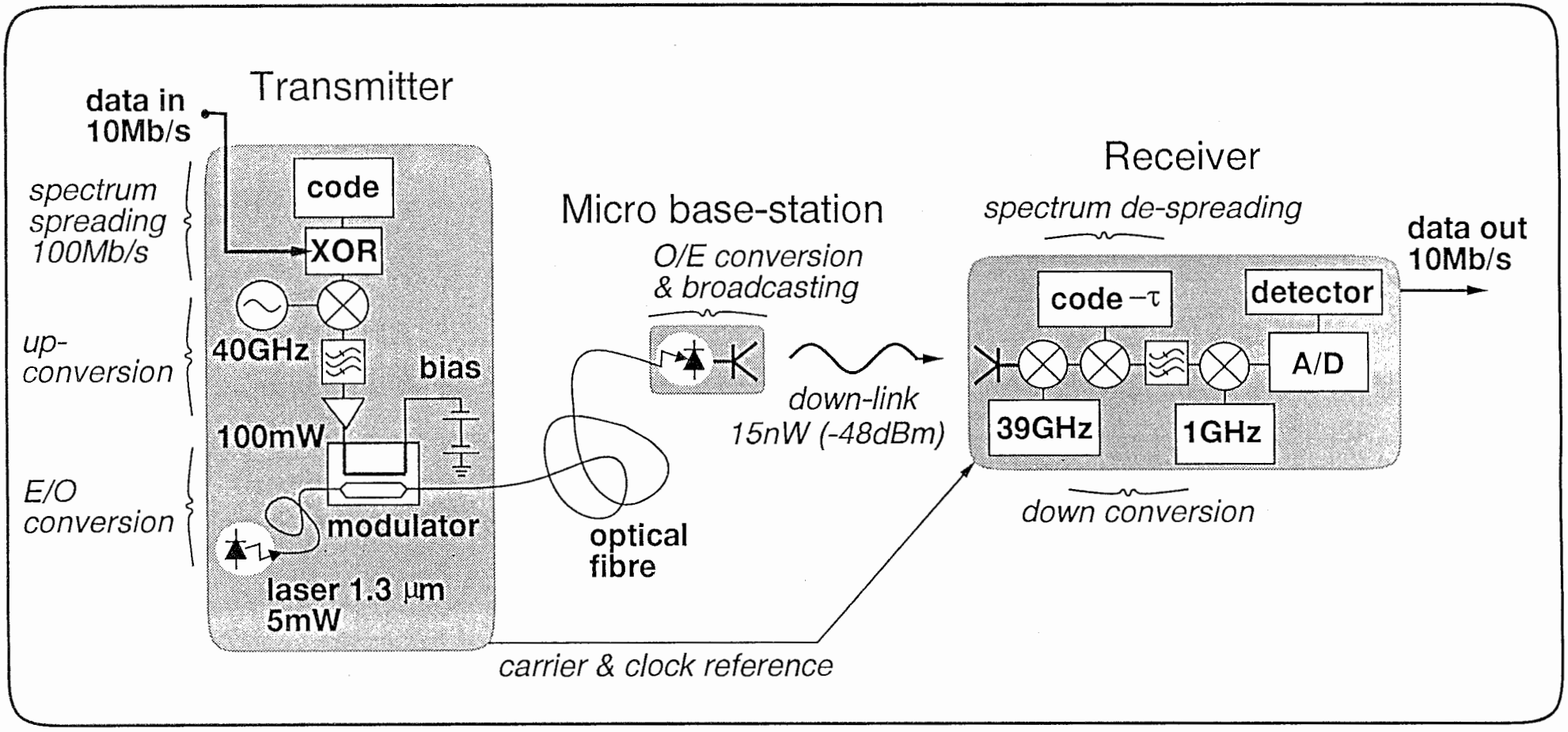

ATR Optical & Radio Research Laboratories
Kyoto, Japan

Millimetre wave-fibre optic LAN experiment

(direct optical sub-carrier BPSK modulation)

ATR

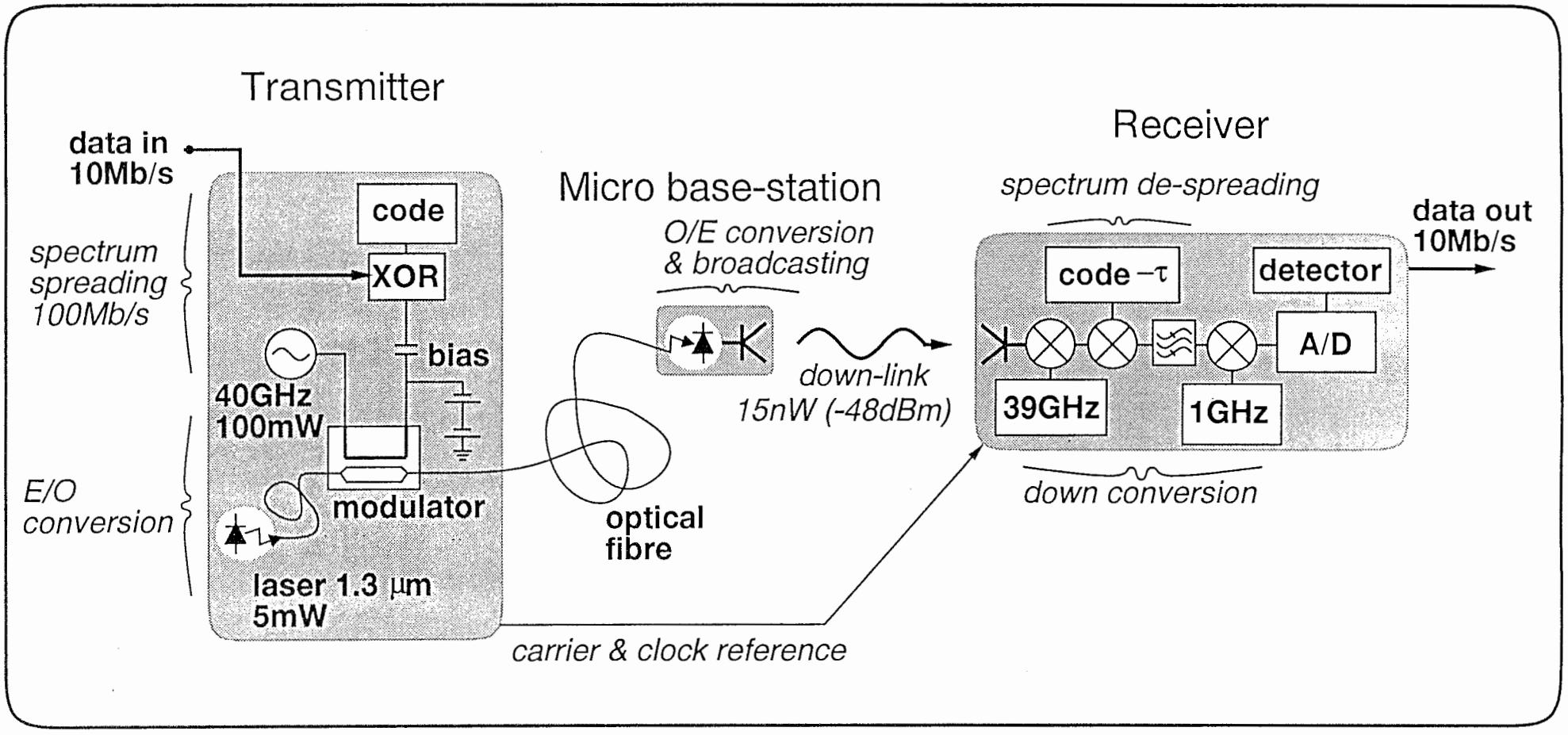

ATR Optical & Radio Research Laboratories
Kyoto, Japan

Experimental system schematic

ATR

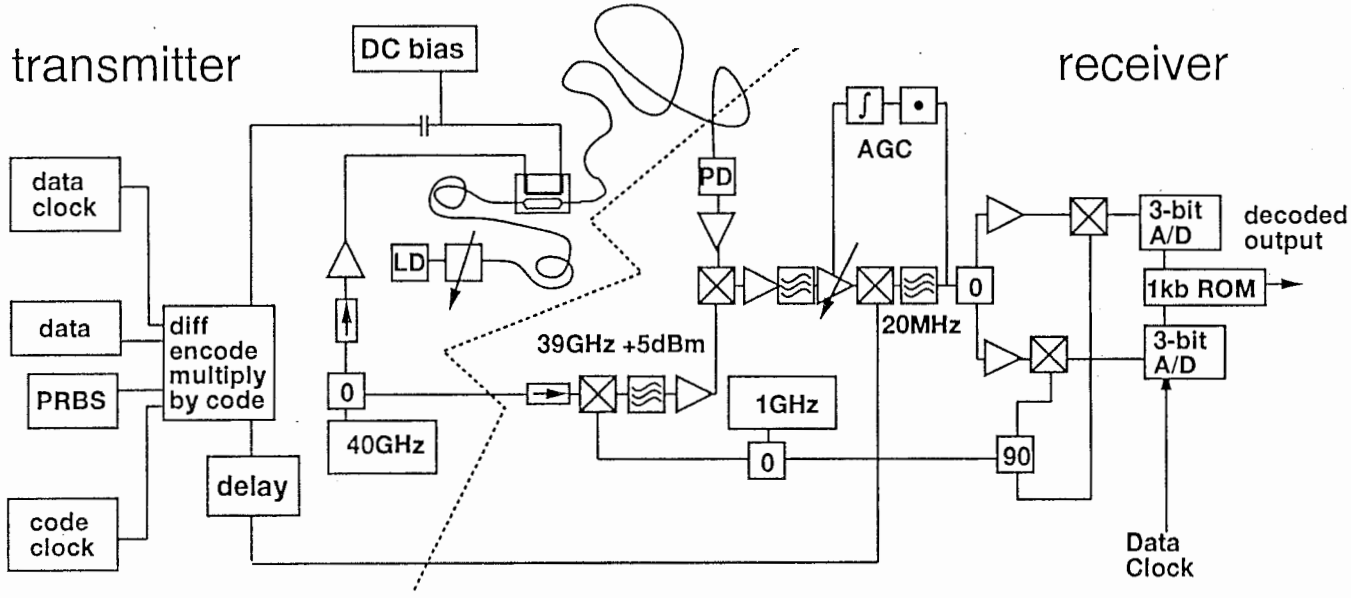

ATR Optical & Radio Research Laboratories
Kyoto, Japan

Comparison of BER performance

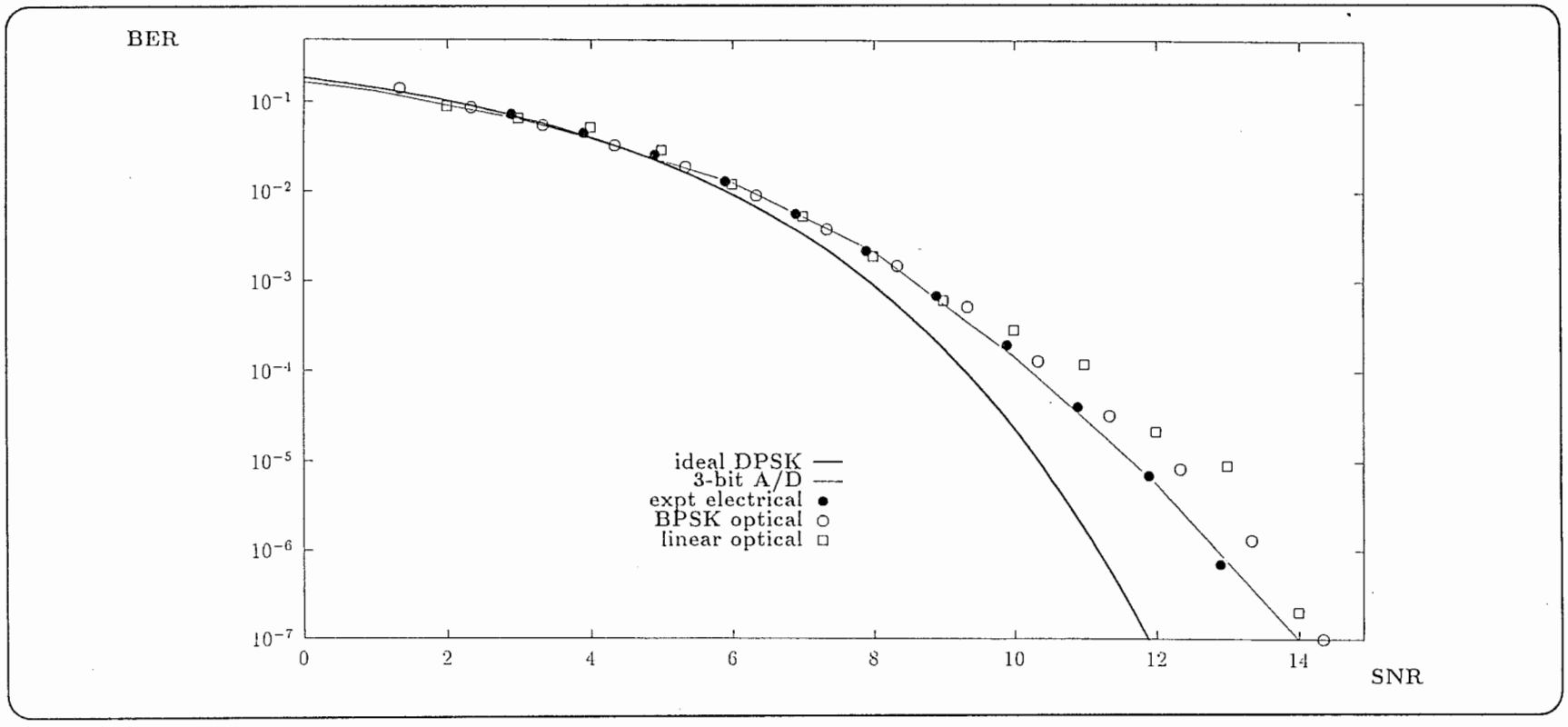

ATR Optical & Radio Research Laboratories
Kyoto, Japan

Reflection EOM link architecture

ATR

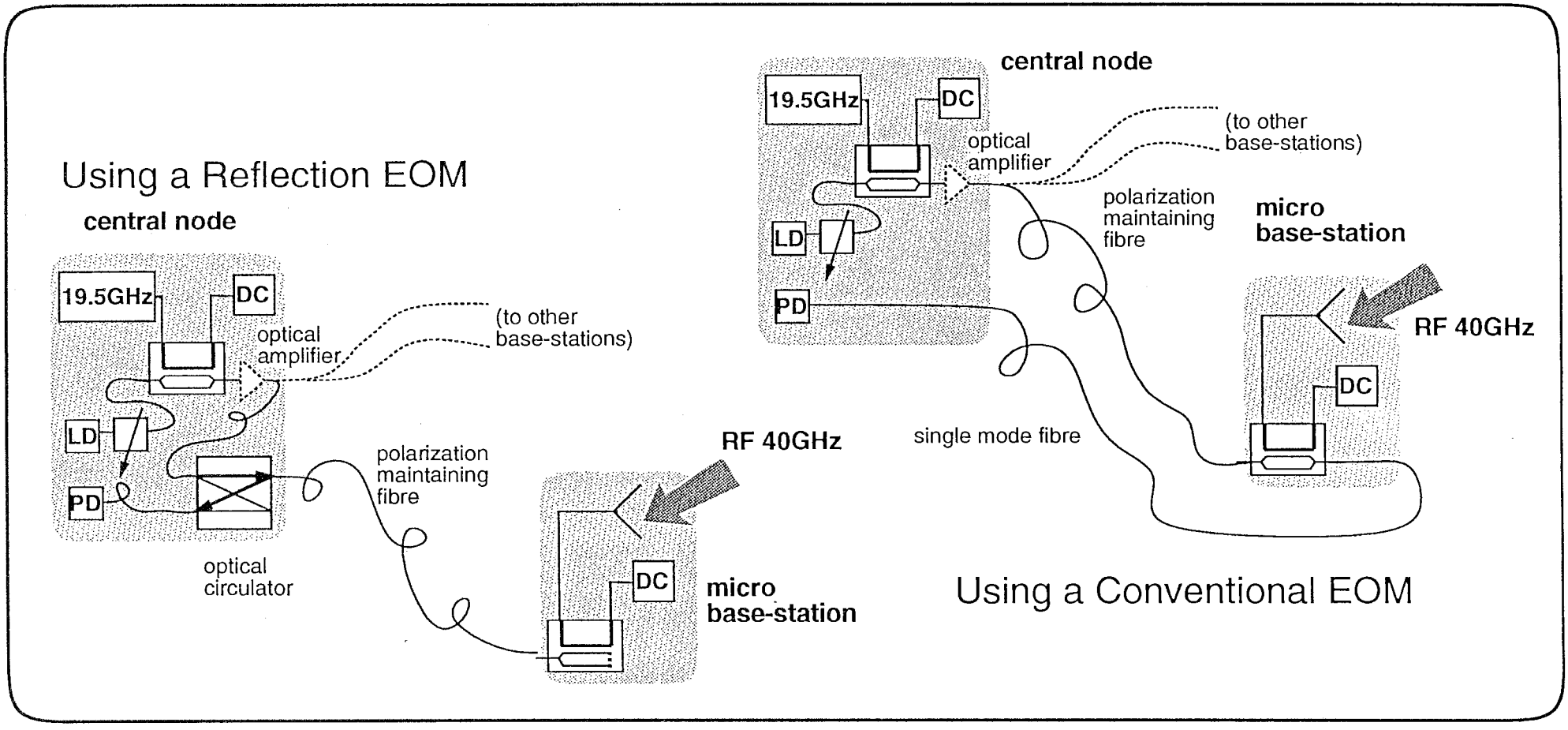

ATR Optical & Radio Research Laboratories
Kyoto, Japan

Concept of "all optical" up-link

(using reflection type modulator)

ATR

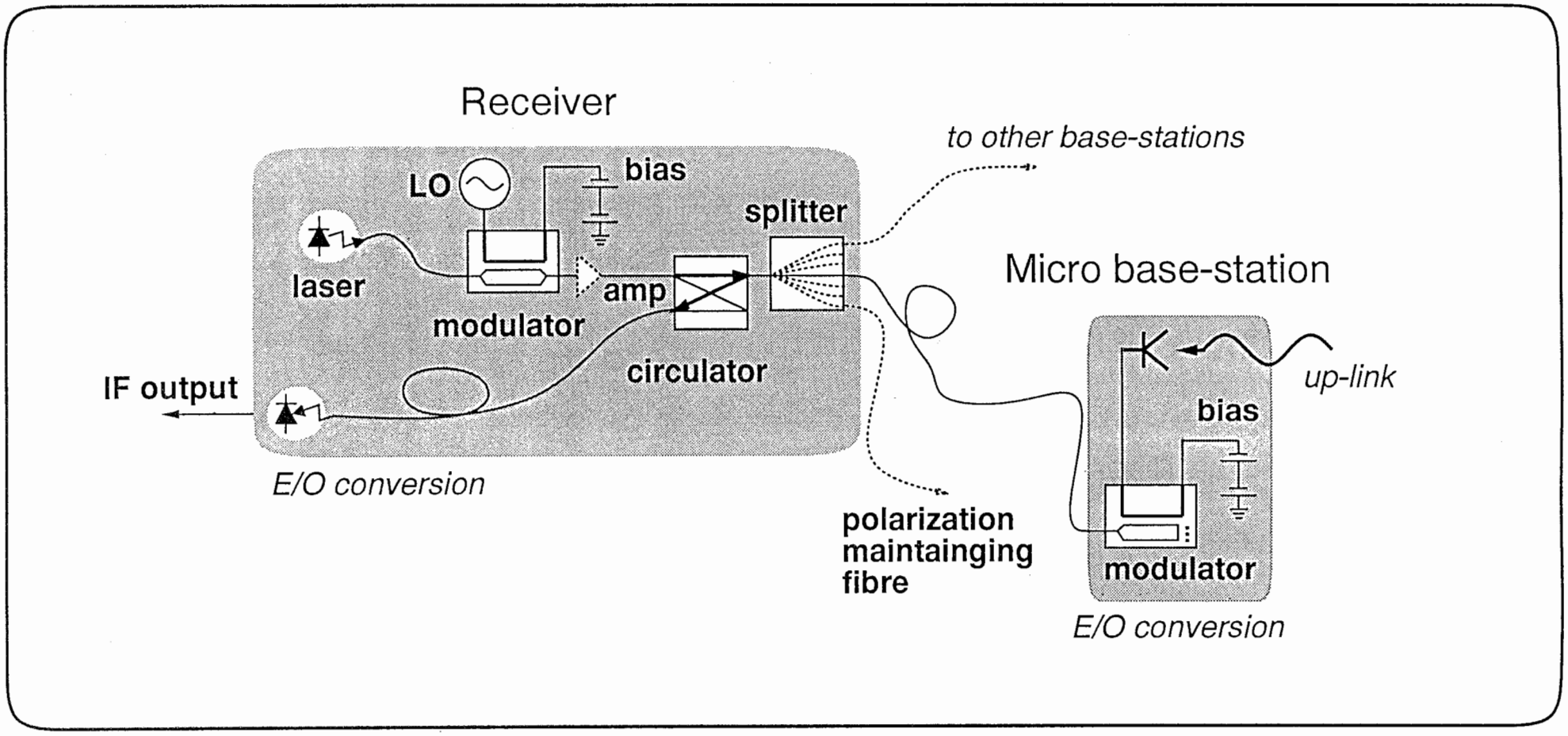

ATR Optical & Radio Research Laboratories
Kyoto, Japan

Dual EOM conversion loss

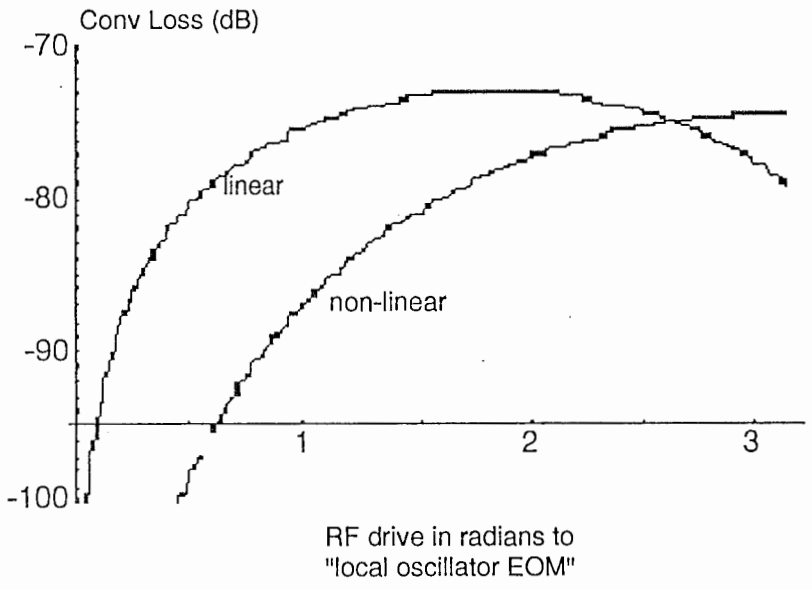

Comparison of dual-linear and non-linear EOM Configurations

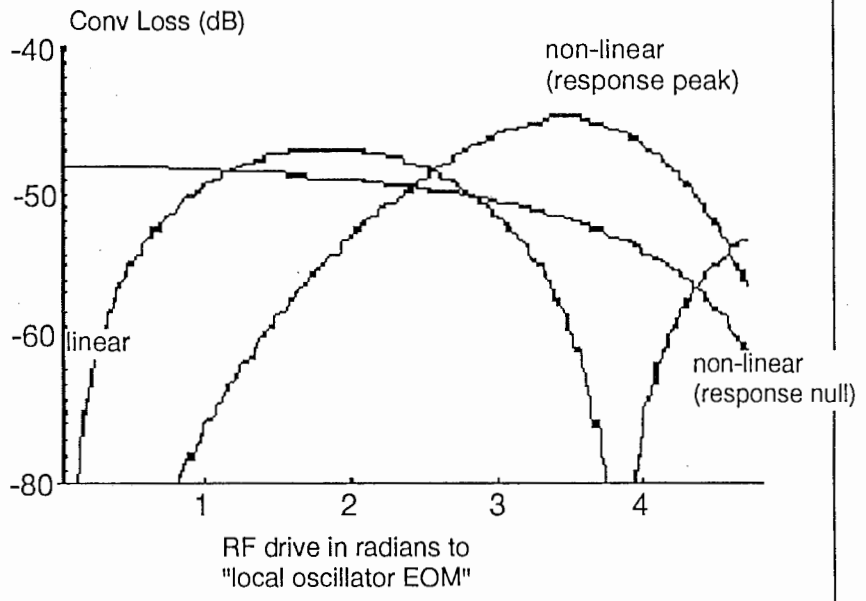

Comparison of dual-linear and non-linear EOM Configurations including optical amplifier

ATR Optical & Radio Research Laboratories
Kyoto, Japan

Concept of "all optical" up-link (2)

(using reflection type modulator)

ATR

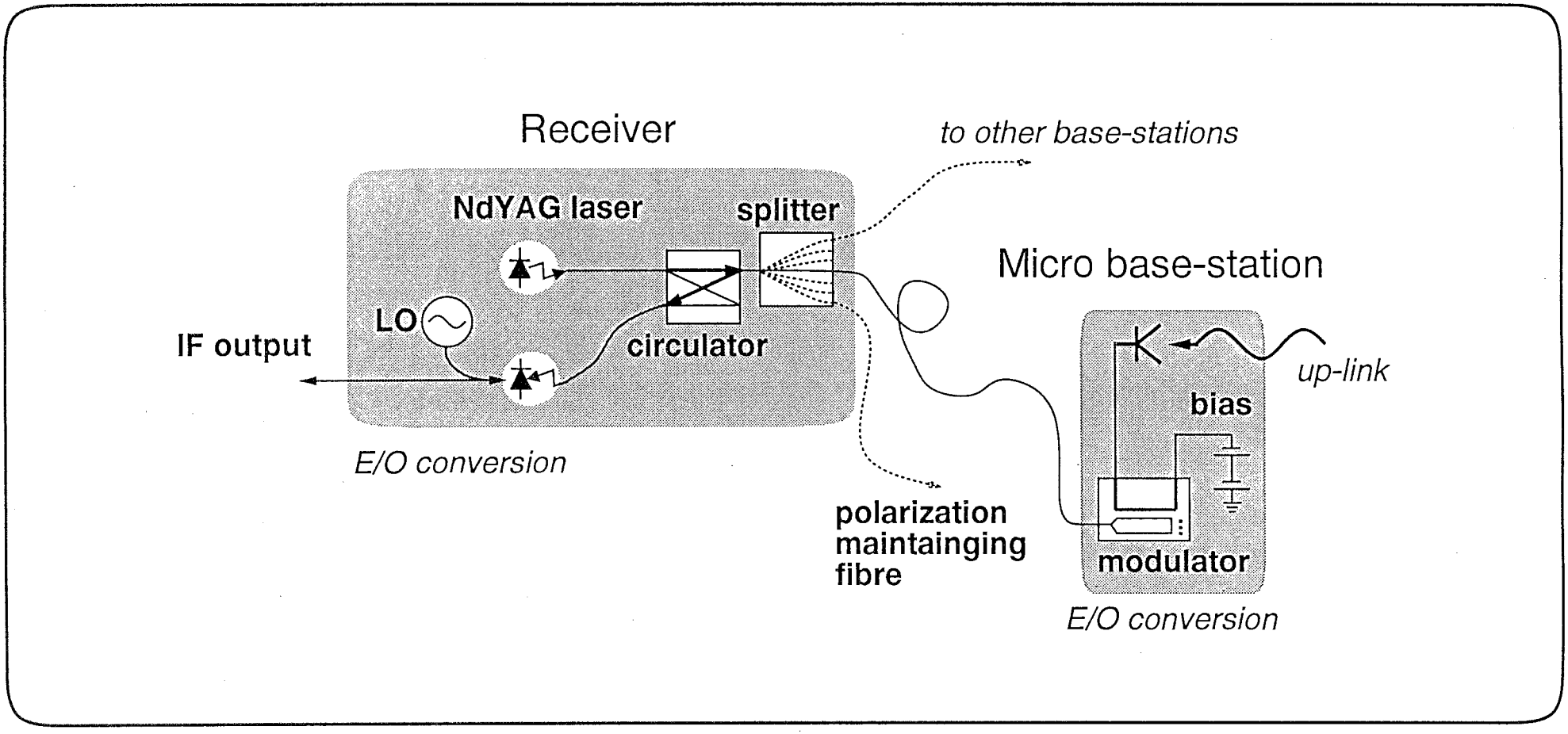

ATR Optical & Radio Research Laboratories
Kyoto, Japan

Concept of coherent "all optical" up-link (3)

(direct optical sub-carrier BPSK modulation)

ATR

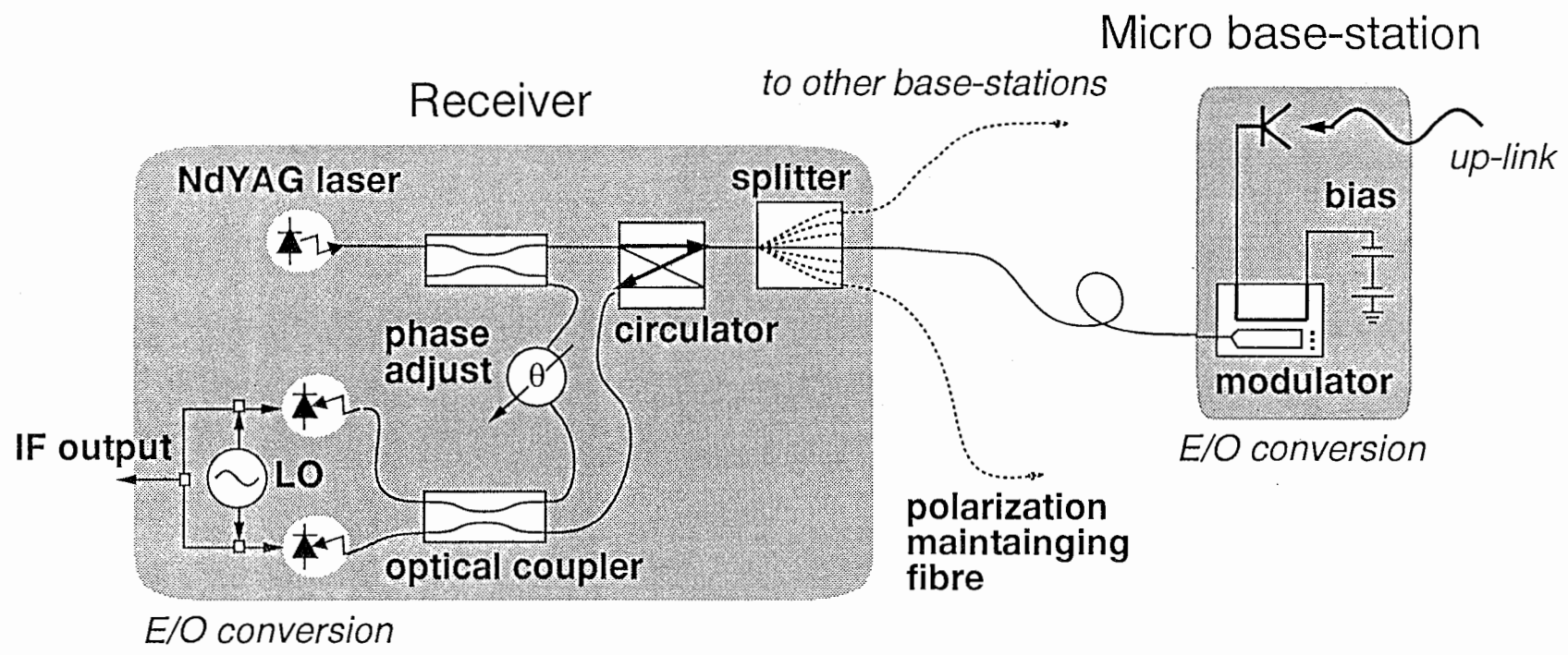

Possible configuration for homodyne amplitude detection up-link

ATR Optical & Radio Research Laboratories
Kyoto, Japan

Simplify, miniturize, lower cost

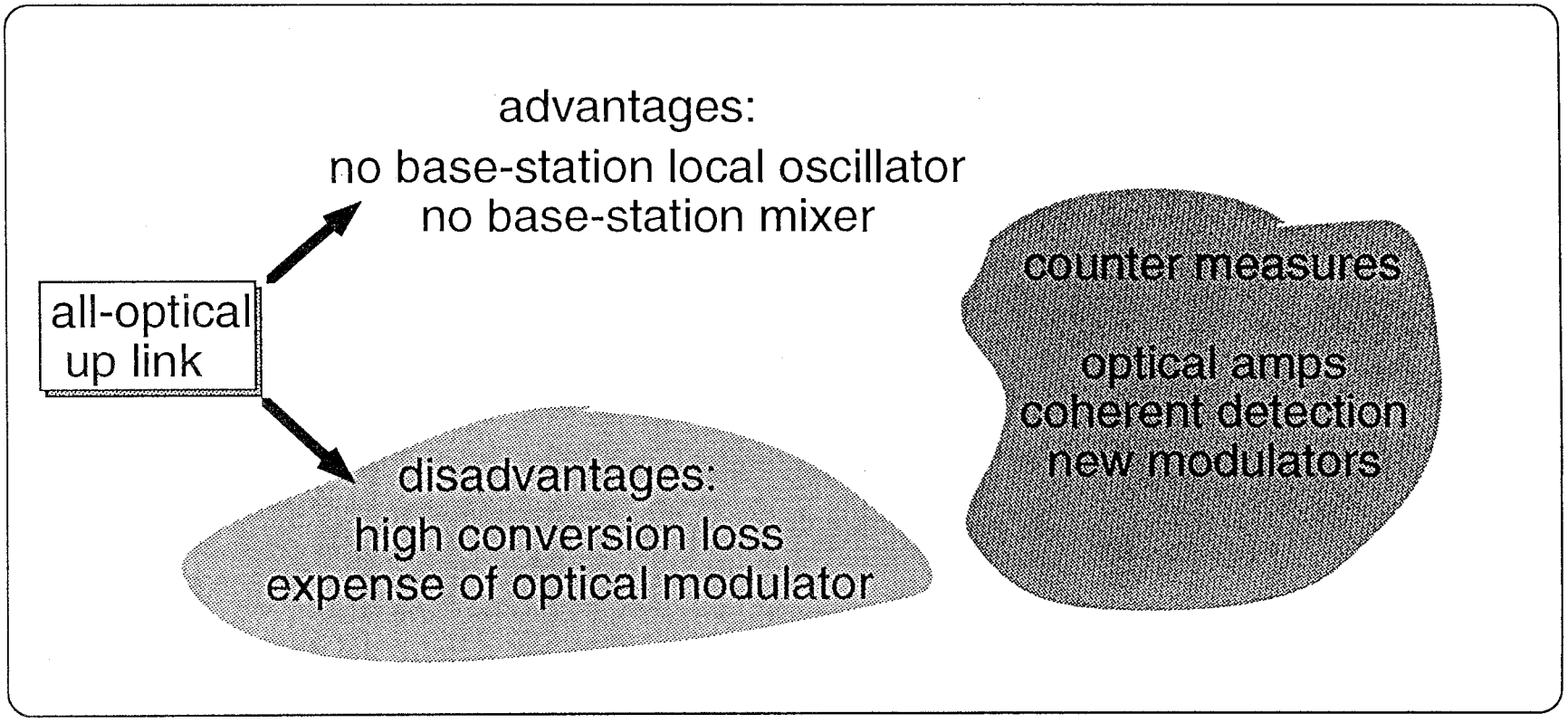

ATR Optical & Radio Research Laboratories
Kyoto, Japan

Cross section of EOM

ATR

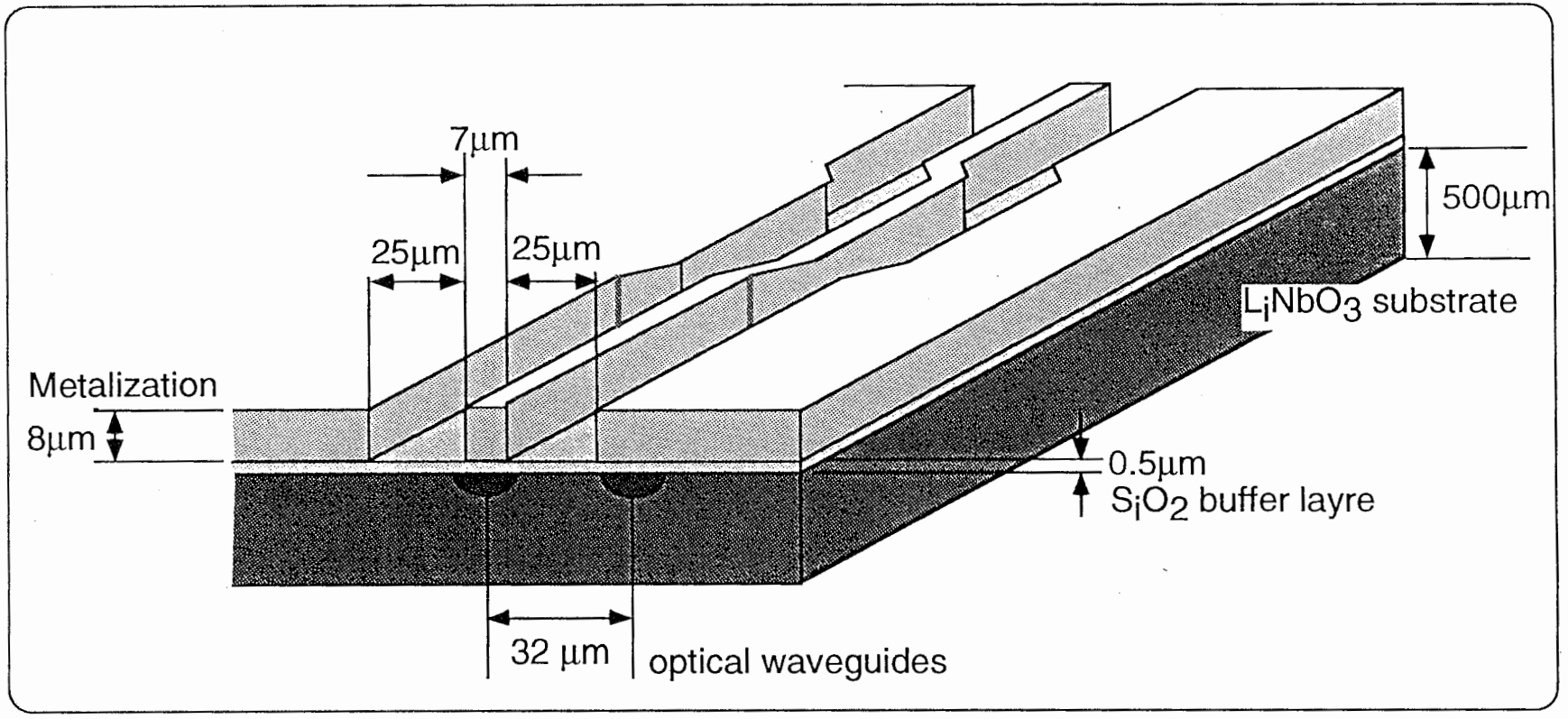

ATR Optical & Radio Research Laboratories
Kyoto, Japan

Reflection EOM electrode response

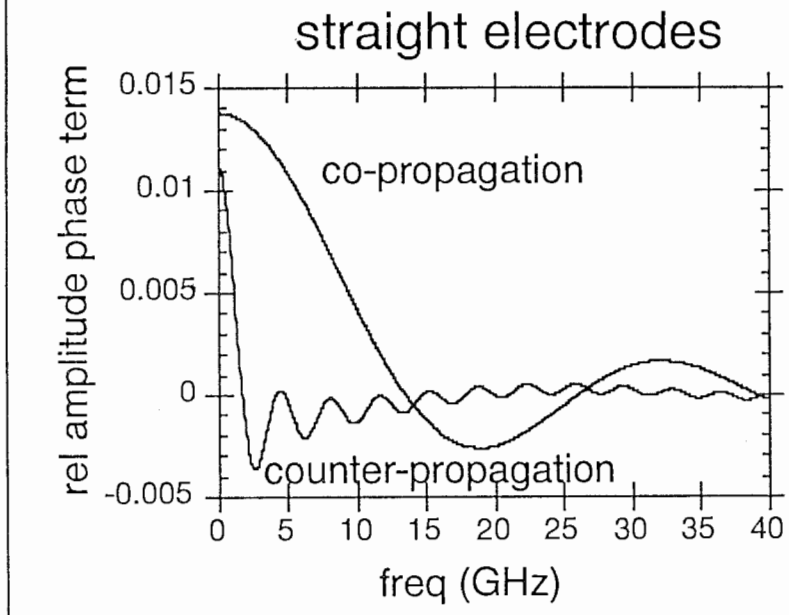

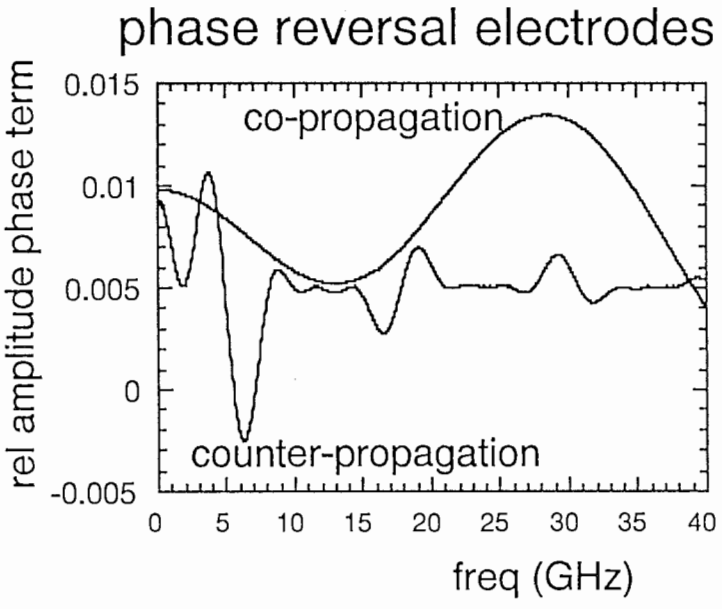

ATR Optical & Radio Research Laboratories
Kyoto, Japan

Reflection EOM result (straight electrode)

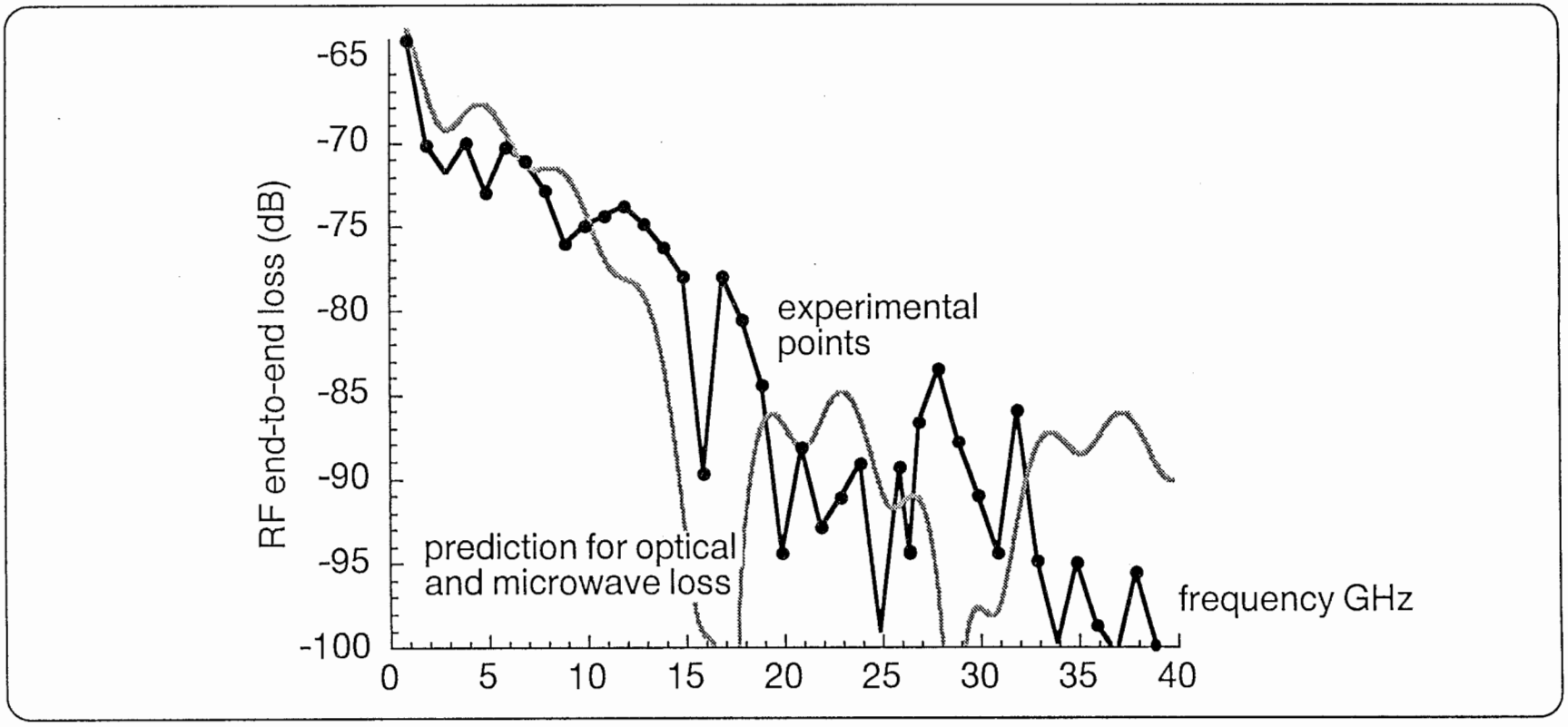

ATR Optical & Radio Research Laboratories
Kyoto, Japan

Phase reversal EOM result

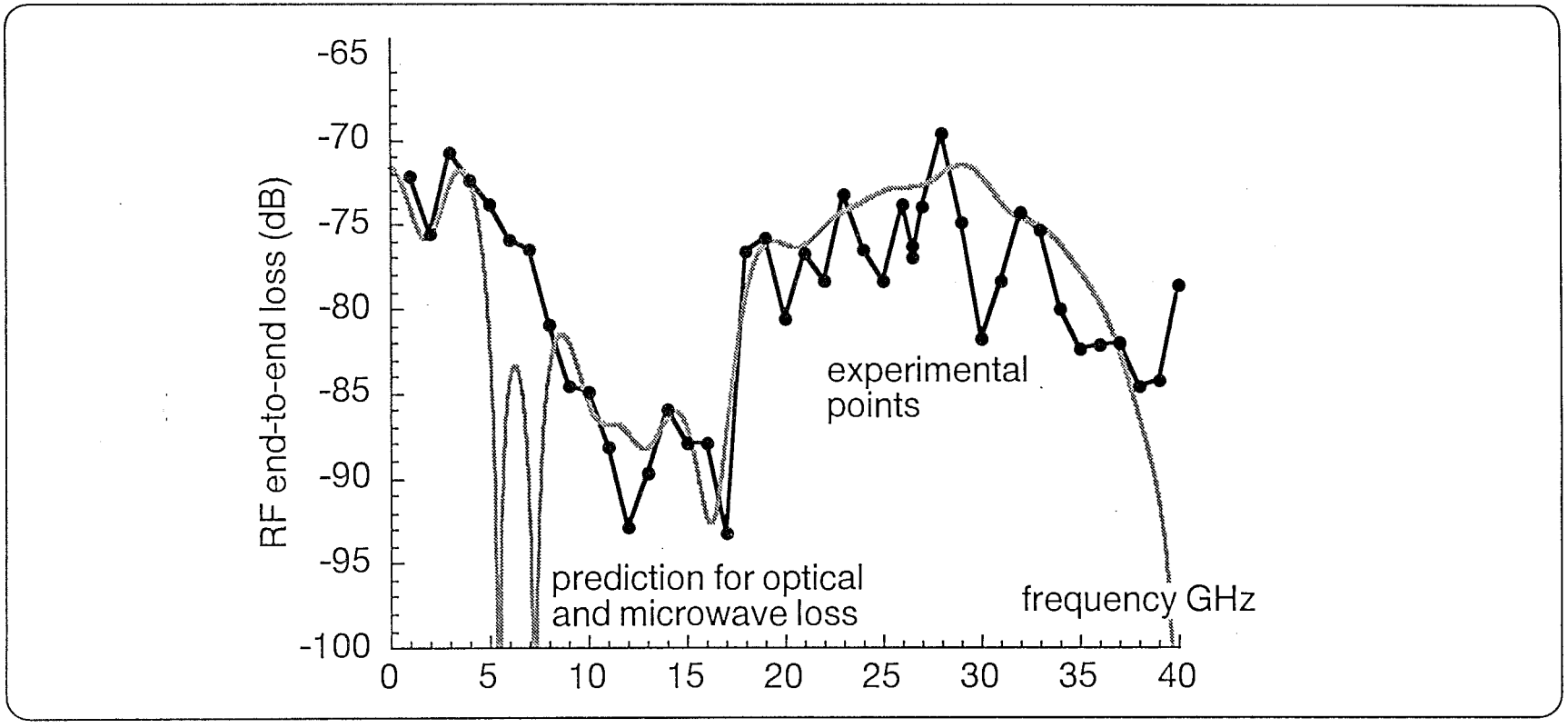

ATR Optical & Radio Research Laboratories
Kyoto, Japan

Comparison of EOM loss assumptions

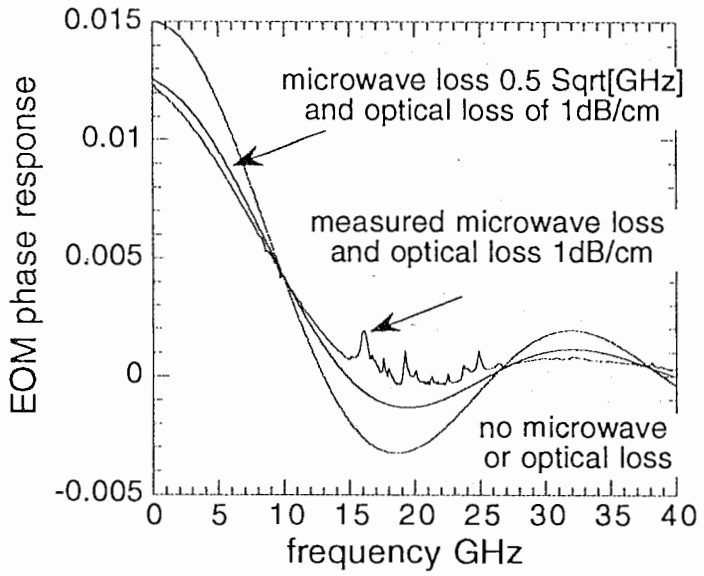

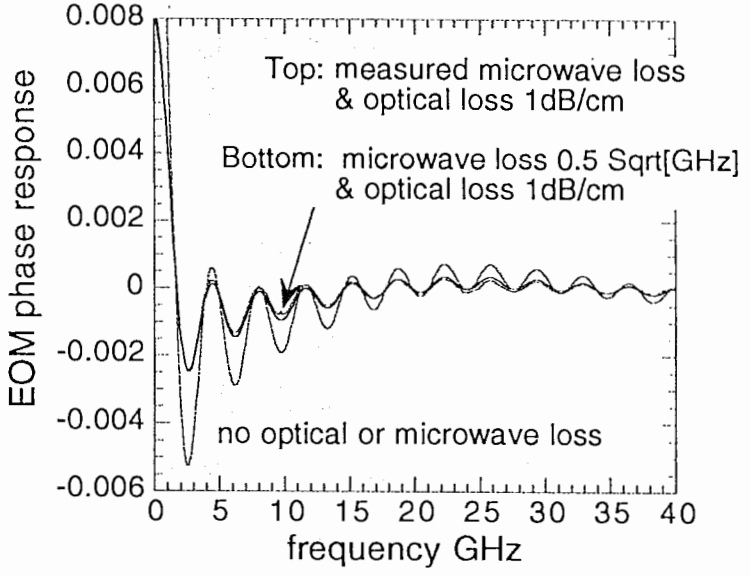

ATR Optical & Radio Research Laboratories
Kyoto, Japan

EOM future development

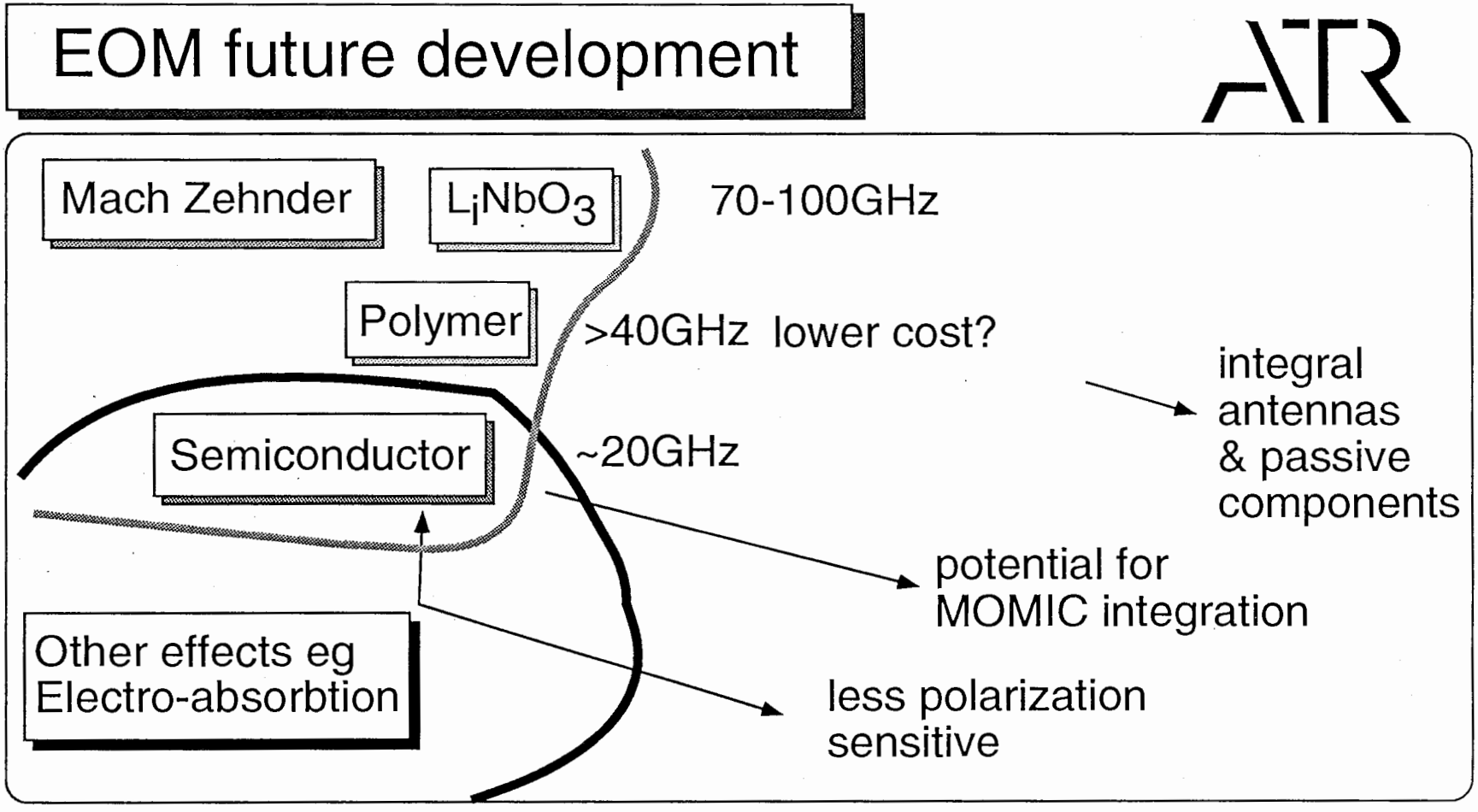

ATR Optical & Radio Research Laboratories
Kyoto, Japan

MMIC compatible optical detectors

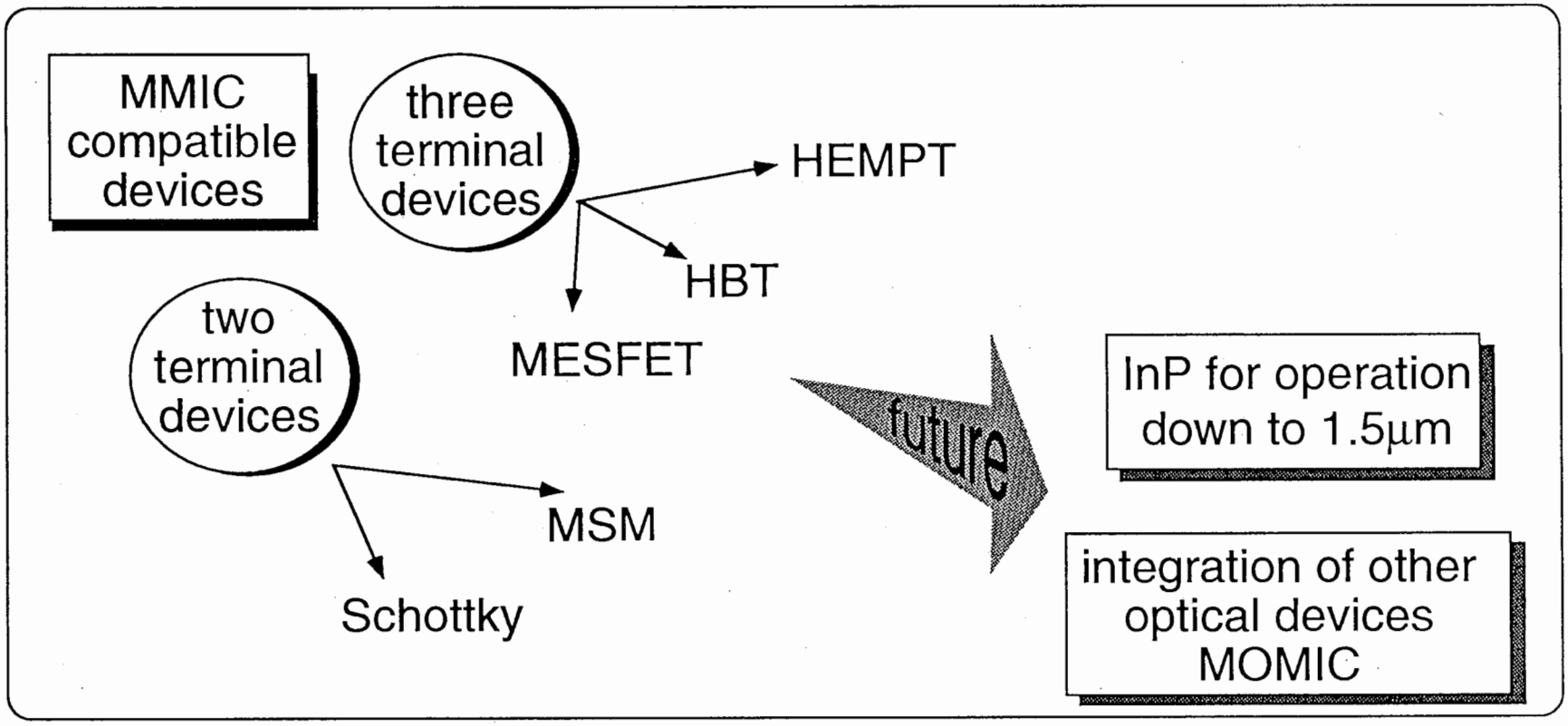

ATR Optical & Radio Research Laboratories
Kyoto, Japan

50GHz HBT experiment

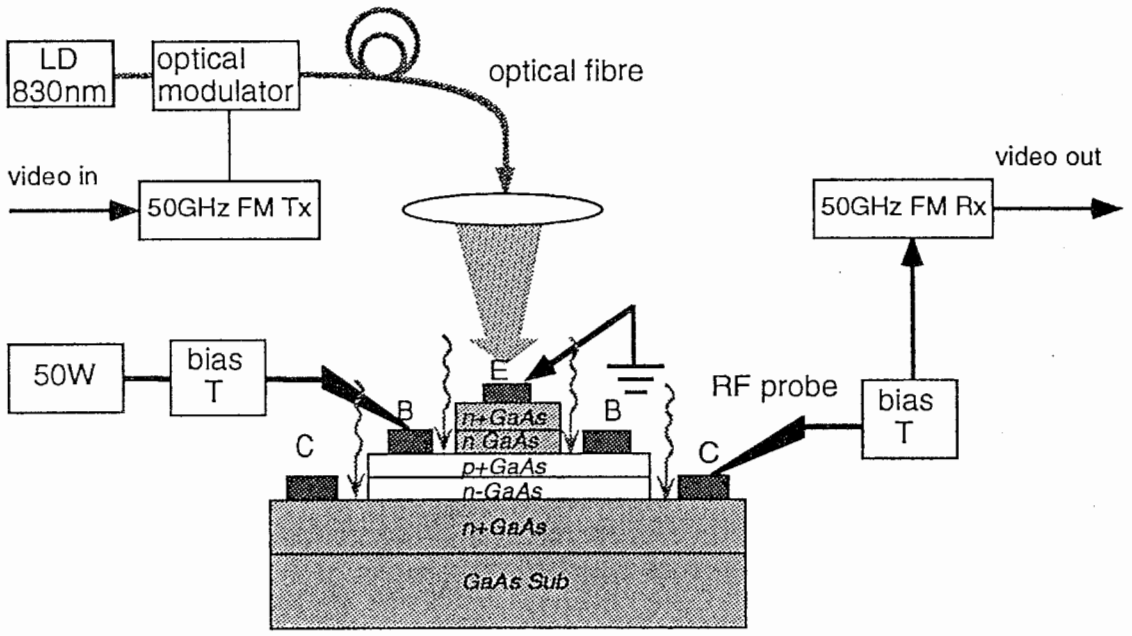

HBT(common emitter)

Result

45dB SNR (weighted)

-4dBm optical input

ATR Optical & Radio Research Laboratories
Kyoto, Japan

Conclusions

ATR

- Combined with size and cost reducing developing OMMIC and MOMIC technologies MMW over fibre could provide the key to realizing ultra wideband services.
- A 40GHz spread spectrum radio over fibre demonstrator was sucessfully realized.
- Base-station up-links can be realized over a single fibre with out a light source at the remote site using a reflection type modulator as a means to reduce base-station component count.
- 50GHz optical signals detected by HBT: a precursor to OMMICs

ATR Optical & Radio Research Laboratories
Kyoto, Japan